C1 Chemistry for the Production of Ultra-Clean Liquid Transportation Fuels and Hydrogen

Annual report

Research conducted October 1, 2003-September 30, 2004

U.S. Department of Energy Contract No. DE-FC26-02NT41594

Prepared by the Consortium for Fossil Fuel Science

Gerald P. Huffman, Director
University of Kentucky/CFFS
533 S. Limestone Street, Suite 107
Lexington, KY 40506-0043
Phone: (859) 257-4027
FAX: (859) 257-7215
E-mail: huffman@engr.uky.edu

Consortium for Fossil Fuel Science

University of Kentucky
West Virginia University
University of Pittsburgh
University of Utah
Auburn University

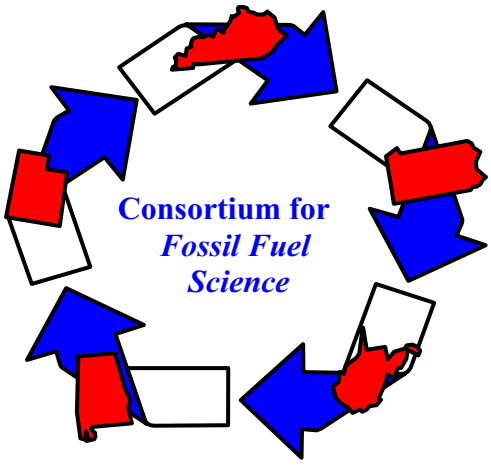

C1 Chemistry for the Production of Clean Liquid Transportation Fuels and Hydrogen

U.S. DOE Contract No. DE-FC26-02NT41594

ABSTRACT:
The Consortium for Fossil Fuel Science (CFFS) is a research consortium with participants from the University of Kentucky, University of Pittsburgh, West Virginia University, University of Utah, and Auburn University. The CFFS is conducting a research program to develop C1 chemistry technology for the production of clean transportation fuel from resources such as coal and natural gas, which are more plentiful domestically than petroleum. The processes under development will convert feedstocks containing one carbon atom per molecular unit into ultra clean liquid transportation fuels (gasoline, diesel, and jet fuel) and hydrogen, which many believe will be the transportation fuel of the future. Feedstocks include synthesis gas, a mixture of carbon monoxide and hydrogen produced by coal gasification, coalbed methane, light products produced by Fischer-Tropsch (FT) synthesis, methanol, and natural gas. Some highlights of the results obtained during the second year of the contract are summarized below.

Liquid fuels

1. Addition of acetylene during F-T synthesis, using either Co or Fe catalysts, decreases alpha values; increases branching of products; and produces oxygenates, primarily alcohols.
2. Heavy hydrocarbons are more readily removed from active catalyst sites during F-T synthesis in supercritical hexane (SCH), enhancing active site availability.
3. Hydroisomerization and hydrocracking are balanced using Pt-promoted tungstated zirconia and sulfated zirconia hybrid catalysts, increasing yields of jet and diesel fuels.
4. Metallic Co nanoparticles deposited on high surface area, mesoporous silica aerogel provide excellent F-T synthesis yields and selectivities towards the diesel fuel fraction, C10+.
5. An Fe-Cu-K catalyst supported on peat AC shows high initial F-T synthesis activity, but deactivates rapidly. Catalyst stability is improved significantly by addition of 6% molybdenum.
6. Reaction conditions have been optimized to convert syngas to C2-C4 light olefins using a hybrid catalyst consisting of a methanol synthesis catalyst and a methanol to olefin catalyst.

Hydrogen

1. Pt or Ni-Cu catalysts supported on stacked-cone nanotubes exhibit good activity for the dehydrogenation of cyclohexane or methylcyclohexane to pure hydrogen and aromatic liquids.
2. An alternating fluid-bed/fixed-bed reaction system is being developed for continuous catalytic dehydrogenation of light alkanes to pure hydrogen and carbon nanotubes.
3. A continuous reactor with online analysis for aqueous-phase reforming of ethylene glycol and polyethylene glycol is being constructed and tested.
4. Methanol reforming in supercritical water containing K compounds in a reactor made of Ni-Cu tubing yields a high-hydrogen content product gas (~98%).
5. A bimetallic Co-W carbide catalyst was used for steam reforming of methanol and showed nearly constant, high selectivity to hydrogen from 450 to 850 ºC.

These results should contribute to the eventual development of coal-based polygeneration plants that produce electricity, liquid transportation fuels, hydrogen, and chemicals.

Table of Contents

Executive Summary

Prepared by Gerald P. Huffman, Director, Consortium for Fossil Fuel Science
University of Kentucky, 107 Whalen Bldg., 533 S. Limestone St., Lexington, KY 40509
(859) 257-4027; huffman@engr.uky.edu

Introduction

The Consortium for Fossil Fuel Science (CFFS), a five university research consortium, is conducting a program of basic research aimed at developing innovative and economical technology for producing clean liquid transportation fuels and hydrogen from coal, natural gas, and other hydrocarbons by C1 chemistry. The research program is made up of thirteen separate but coordinated research projects being conducted at the five CFFS universities, all contributing towards achieving the goal of producing clean, economical transportation fuel from domestic resources. The current report briefly summarizes progress made toward those goals during the second year of this research contract. This Executive Summary briefly summarizes the principal results obtained during this period. The appended individual project reports provide more details and contain all the required elements of DOE research contract reports: an introduction, experimental procedures, results and discussion, conclusions, and references. Lists of all publications and presentations resulting from this research contract during this period are also given in these project reports.

Experimental

A discussion of experimental procedures is provided in each of the thirteen individual project reports that constitute the bulk of this report.

Results

Liquid fuels

Fischer-Tropsch mechanism studies using acetylene as a probe: F-T syntheses with acetylene as a probe were conducted over both cobalt and iron catalysts. For both catalysts, initiation of the reaction is the predominant action of acetylene, while hydrogenation is a favored reaction for co-fed ethylene. Acetylene is incorporated into F-T reactions much more effectively than are higher acetylenes, a finding similar to results reported with olefin addition. For iron catalysts hydrogenation is a favored reaction, while for cobalt, dimerization is favored. Additional results of adding acetylene include: (1) decreased alpha values, indicating that it serves mainly as a chain initiator; (2) increased branching of F-T products, possibly caused by 2-butene re-initiation; (3) production of oxygenates via hydroformylation for cobalt catalysts; and (4) production of oxygenates that follow the ASF distribution for iron catalysts. Alcohols are the major components of oxygenated products from F-T synthesis; the aldehyde/alcohol ratio increases with decreasing contact time, suggesting that alcohols are secondary products formed by hydrogenation of aldehydes.

Reaction pathway and kinetic modeling of F-T synthesis over an alumina supported cobalt catalyst in supercritical-hexane media: Heavy hydrocarbons are more readily removed from active catalyst sites during F-T synthesis in supercritical hexane (SCH) than in gas-phase F-T synthesis. The difference between the reaction medium in gas-phase and SCH F-T synthesis can result in modified active site chemical characteristics, enhancement in active site availability, and

different thermodynamic activities of the reacting species. Further experiments and model development should address each of the factors.

Diesel and jet fuel from Fischer-Tropsch wax: Using Pt-promoted tungstated zirconia and sulfated zirconia (PtWZr/SZr) hybrid catalysts, an appropriate balance of hydroisomerization and hydrocracking functions can be achieved to increase yields of jet and diesel fuels. The component ratio and hydrogen pressure are important factors in affecting reactivities and selectivities of the hybrid catalysts.

Aerogel supported catalysts for fischer-tropsch synthesis: Procedures have been developed to deposit metallic Co nanoparticles approximately 70 nm in diameter on high surface area, mesoporous silica aerogel. Both gas-phase and solution incorporation of cobalt or ruthenium precursors give rise to catalysts that are active towards F-T synthesis with single-pass CO conversions as high as 20% and selectivities towards the diesel fuel fraction, C10+, as high as 40%. "Redox targeting" of catalyst precursors appears to offer some benefit when compared with single stage incorporation. The use of zeolitic catalyst supports does not offer the advantage of substantially greater yields of diesel range fuels that would offset the greater cost of these catalyst supports than the probable cost of aerogels produced on an industrial scale.

Development of activated-carbon supported, molybdenum-promoted catalysts for diesel fuel synthesis: An Fe-Cu-K catalyst supported on peat AC shows high initial activity, but deactivates rapidly. Catalyst stability is improved significantly by addition molybdenum to produce Mo-Fe-Cu-K/AC with 6% Mo loading.

Carbon-support type affects both catalyst activity and selectivity. Pecan-shell and peat activated carbon supported catalysts are the most active and have better C5+ selectivity. The catalyst with the walnut-shell AC support has good C5+ selectivity, but is not as active as catalysts with peat and pecan-shell AC supports. The catalyst using a wood AC support is the least active and has the lowest C5+ selectivity. Good catalyst performance with peat and pecan-shell activated carbons may relate to their pore structures since both have significant mesopore and macropore volumes.

Value-added products

Production of light olefins and chemicals from syngas: Hybrid catalysts consisting of methanol synthesis catalyst C-79 and methanol to olefin (MTO) catalyst SAPO-34 were employed for the conversion of syngas to light olefins. The experimental results demonstrate that the CO conversions and C2-C4 light olefins selectivity can be significantly increased by employing the hybrid catalyst in a follow-bed reactor, as compared to using a mixed-bed configuration or either catalyst alone. Moderate increases in reaction pressure lead to higher C2-C4 olefins productivity, while higher syngas ratio (H_2/CO) decreases the olefins selectivity due to the enhanced hydrogenation. Low syngas flow rate also favors the increases in CO conversion.

Hydrogen

Hydrogen production by catalytic dehydrogenation of high hydrogen content liquids using Ni-Cu/SCNT catalysts: The results of catalytic partial dehydrogenation experiments to convert cyclohexane or methyl cyclohexane to hydrogen and benzene or toluene, respectively, were

reported in our six-month report and a recent publication. Using catalysts consisting of 0.25 to 1.0 wt% Pt supported on stacked-cone carbon nanotubes (SCNT), 100% conversion and selectivity was obtained at approximately 300 ºC and excellent time-on-stream (TOS) was observed. Catalytic partial dehydrogenation of cyclohexane using a more economical Ni-Cu/SCNT catalyst has now been attempted. Although the Ni-Cu catalyst shows 100% selectivity to hydrogen and benzene, its initial conversion is only about 75%, which declines to about 50% during 5-6 hours TOS. TEM indicates that much smaller Ni-Cu alloy particles need to be produced in order to increase the activity of the Ni-Cu/SCNT catalysts to a level comparable to that of the Pt/SCNT.

Catalytic production of hydrogen and carbon nanotubes from methane using a fluidized-bed reactor: Previously, we reported the development of alumina supported binary catalysts, (M-Fe)/Al_2O_3 (M=Pd, Mo, or Ni), that are very active for catalytic dehydrogenation of lower alkanes to produce pure hydrogen and carbon nanotubes (CNT). However, all experiments were done in a fixed-bed reactor. A new reactor has been developed in which the reactor can be operated both in fixed-bed mode and fluid-bed mode. The initial tests of this reactor for continuous methane dehydrogenation using a (0.5%Mo-4.5%Fe)/Al_2O_3 catalyst in the fluid-bed mode did not show any advantage for the methane dehydrogenation reaction. The fluid-bed mode is normally used to improve mass and heat transfer in a reactor. In our small fixed-bed reactor, there is no mass or heat transfer limitation and fluidizing the bed only causes more methane to pass without any reaction to produce hydrogen. In future tests, we will run this reactor under mixed-mode conditions in which the methane dehydrogenation reaction will occur at high efficiency in the fixed-bed mode and the fluid-bed mode will be used to carry out short maintenance cycle operations.

Production of hydrogen in supercritical water: Methanol reforming in supercritical water favors the formation of CH4, which is accompanied by a substantial loss of H_2. Factors favoring the methanation reaction include low steam-to-carbon ratio, high temperature, high residence time and high pressure. CH4 production can be reduced greatly by lowering the residence time so that the equilibrium is not reached. Methanation can also be reduced by the addition of small amounts of K2CO3 or KOH in the aqueous methanol feed. A reactor made of Ni-Cu tubing prevents the formation of CH4 even at higher pressures.

Hydrogen production by aqueous-phase reforming of ethylene glycol and polyethylene glycol: A continuous reactor with online analysis for aqueous-phase reforming of ethylene glycol and polyethylene glycol is currently being constructed and tested. Catalysts and operating conditions will be varied to obtain high conversion and selectivity to hydrogen with small amounts of by-products. Related feedstocks such as ethanol, 1-propanol, 1, 2-propanediol and glycerol may also be tested.

Methane and methanol reforming to produce hydrogen using Co-W carbide catalyst: A bimetallic Co-W carbide catalyst was used for dry reforming of methane and steam reforming of methanol. It was found that it required activation at a higher temperature (850 ºC) before it exhibited good reactivity for dry reforming of methane. After that, the catalyst maintained high reactivity and good stability over a long period, even at lower temperatures.

The same catalyst was used for steam reforming of methanol and showed nearly constant, high selectivity to hydrogen from 450 to 850 ºC.

Analytical characterization of catalysts and products

Spectroscopic characterization of C1 and H_2 chemistry catalysts: Mössbauer and XAFS spectroscopic methods have been used to characterize key elements in various catalyst formulations under development by Consortium researchers.

Mössbauer investigation of binary Fe-M (M = Mo, Ni, and Pd) supported on alumina used in the dehydrogenation of gaseous alkanes implies that austenitic Fe-M-C alloy particles bound to the alumina support by hercynite (FeAl2O4), are the active phase. Formation of cementite (Fe3C) and other metal carbide phases appear to be associated with catalyst deactivation.

Pt XAFS spectroscopy shows that the Pt speciation is quite different in Pt-Fe-Al_2O_3 catalysts than in catalysts prepared with Pt supported on stacked-cone carbon nanotubes, despite the observation that both types of catalyst are equally effective in converting cyclohexane to benzene. In the former case, the Pt is essentially all metallic, whereas in the latter case both metallic Pt and Pt oxide are observed.

Six Fe-containing silica aerogel (SA) catalyst samples prepared by Kim and Eyring at the University of Utah have been examined by iron XAFS and Mössbauer spectroscopies. The Fe is present as a mixture of hematite and ferrihydrite. The presence of K enhances the formation of ferrihydrite relative to hematite, whereas the presence of Al in the SA support material stabilizes hematite. Based on preliminary measurements, it appears that Mössbauer and XAFS spectroscopies will also be valuable for understanding the chemistry and activity of other novel catalyst systems consisting of SA impregnated using Fe, Co, and Ru-containing pentadienyl or cyclopentadienyl compounds.

Mössbauer and XAFS spectroscopy spectra obtained from Fe, Cr, K-based high temperature water-gas-shift (WGS) catalysts prior to reaction have established that it consists of substituted hematite, presumably (Fe,Cr)2O3. Surprisingly, the Cr XAFS spectrum showed the presence of Cr(VI) species, in addition to Cr2O3.

Science behind catalysis in C1 reactions: catalyst characterization and determination of active species: Investigations of Co-based catalysts have clearly shown the need for multi-technique characterization of the catalysts as used in our work. Co0 is the active catalysts in the F-T synthesis but its detection by XRD is often difficult if the particle size is less than 5 nm or if the concentration is less than 3%. However, by magnetic measurements, Co0 as well as CoO and Co_3O_4 are easily detected by their characteristic and different properties even in small quantities. Our investigations have shown that reduction of CoO and Co_3O_4 to Co^0 is often incomplete, which could affect the synthesis products and their distributions. These results have been reported to CFFS researchers using the catalysts for F-T synthesis.

Magnetic and XRD studies of Co- and Fe-based nanoparticles have shown that their properties are significantly different from those of their bulk counterparts.

Conclusions

The principal conclusions reached during the second year of this C1 chemistry research program are briefly summarized below.

Liquid fuels

1. The addition of acetylene as a probe molecule during F-T synthesis produces the following results: (1) decreased alpha values; (2) increased branching of F-T products; (3) production of oxygenates, principally alcohols, for both cobalt and iron catalysts.
2. Heavy hydrocarbons are more readily removed from active catalyst sites during F-T synthesis in supercritical hexane (SCH), enhancing active site availability.
3. Hydroisomerization and hydrocracking are balanced using Pt-promoted tungstated zirconia and sulfated zirconia hybrid catalysts, increasing yields of jet and diesel fuels.
4. Metallic Co nanoparticles deposited on high surface area, mesoporous silica aerogel provide excellent F-T synthesis yields and selectivities towards the diesel fuel fraction, C10+.
5. An Fe-Cu-K catalyst supported on peat AC shows high initial F-T synthesis activity, but deactivates rapidly. Catalyst stability is improved significantly by addition of 6% molybdenum.

Value-added products

1. Reaction conditions have been optimized to convert syngas to C2-C4 light olefins using a hybrid catalyst consisting of a methanol synthesis catalyst and a methanol to olefin catalyst.

Hydrogen

1. Catalysts consisting of Pt or Ni-Cu supported on stacked-cone nanotubes exhibit good activity for the dehydrogenation of cyclohexane or methylcyclohexane to pure hydrogen and benzene or toluene, respectively.
2. Work on development of a continuous reactor for catalytic dehydrogenation of light alkanes to produce pure hydrogen and carbon nanotubes indicates that an alternating fluid-bed/fixed-bed reaction system may be a promising approach.
3. A continuous reactor with online analysis for aqueous-phase reforming of ethylene glycol and polyethylene glycol is being constructed and tested.
4. Production of a high-hydrogen content product gas by methanol reforming in supercritical water is being investigated. The addition of small amounts of K_2CO_3 or KOH in the aqueous methanol feed and a reactor made of Ni-Cu tubing both improve this reaction significantly.
5. A bimetallic Co-W carbide catalyst was used for steam reforming of methanol and showed nearly constant, high selectivity to hydrogen from 450 to 850 ºC.

These results should contribute to the eventual development of coal-based polygeneration plants that produce electricity, liquid transportation fuels, hydrogen, and chemicals.

Fischer-Tropsch Mechanism Studies Using Acetylene as a Probe

Y. Zhang, L. Hou, J.W. Tierney and I. Wender
Chemical Engineering Department, University of Pittsburgh

Introduction

The Fischer-Tropsch (F-T) synthesis is a stepwise growth of hydrocarbon chains by addition of monomeric units, a postulation made by Fischer and Tropsch in the early days of their studies [1]. Unlike usual polymerization processes, the reaction proceeds by the addition of monomers formed in-situ from syngas. Due to the complexity of this process, many questions are still under debate; understanding the fundamental F-T chemistry is, therefore, extremely valuable with the present stimulus to invest in the FT process. In previous studies, we found that long chain alkynes are incorporated more easily than corresponding alkenes. It has been reported that ethylene is 10 to 40 times more easily incorporated into the F-T synthesis than are higher olefins.[2-5]. In this work acetylene is used as a probe molecule to study the mode of initiation of the F-T synthesis with consideration of possible differences in the pathways that occur with cobalt and iron catalysts.

Experimental

Supported cobalt catalysts were prepared by incipient-wetness impregnation of cobalt nitrate on alumina with a composition of Co(10wt%)/Al_2O_3(90wt%), followed by calcination at 300 ºC for 5 hours. Two types of iron catalysts: a precipitated iron catalyst with a composition of 100Fe/4.4Si/1.25K and a C-73 fused iron catalyst were obtained from Dr. B. Davis of the University of Kentucky.

The F-T reaction was carried out in a computer controlled fixed bed reactor (stainless-steel with i.d. 3/8 inches). Acetylene was introduced from a tank of premixed gas containing (mol): 1% acetylene, 10% Ar, 44% CO, 45% H_2. A thermocouple was inserted into the middle of the catalyst bed in the reactor which was loaded with 2.5 grams of a Co or an Fe catalyst. Co catalysts were activated by H_2 at a rate of 50 ml/min, with a temperature program ramping from room temperature to 350 ºC at 1 ºC /min, holding at 350 ºC for 10 hours. Fe catalysts were activated similarly but kept at 350 ºC for 5 hours and 450 ºC for 2 hours. After reduction, the temperature of the reactor was lowered to the reaction temperature. The F-T reaction was started by gradually increasing the CO and H_2 flow rate to avoid a temperature surge due to active sites present in the fresh catalysts. Liquid products were collected by a cold trap in an ice-water bath and analyzed by GC-MS. Wax products were collected by a hot trap at about 200 ºC. A stream of effluent gas was removed between the hot trap and the cold trap and sent through three sampling valves controlled by a computer and analyzed by two online GCs (HP6890 and HP5890).

Results and Discussion

Addition of acetylene to CO/H_2 on a cobalt catalyst

The F-T reactions were carried out on a cobalt catalyst at 180 ºC, 300psi with a CO to H_2 ratio of 1. Yields of hydrocarbon products from base (normal) reactions and F-T synthesis with acetylene are shown in Fig. 1(a). Addition of acetylene caused a significant increase in the rate of formation of C2+ hydrocarbons but had little influence on methane production.

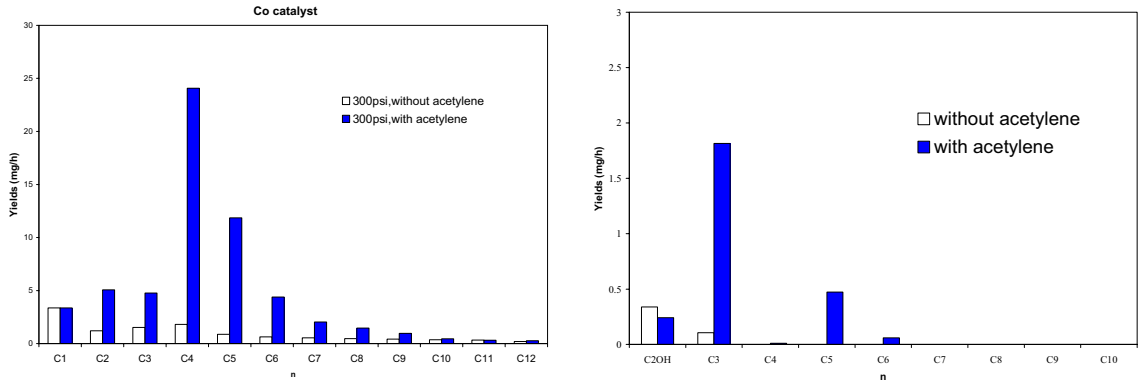

(a) (b)

Figure 1 Product distributions of incorporation of acetylene on a cobalt catalyst (a) hydrocarbons (b)oxygenates; 10Co/90Al, 300psi, 180C, $H_2/CO=1$, 1% acetylene

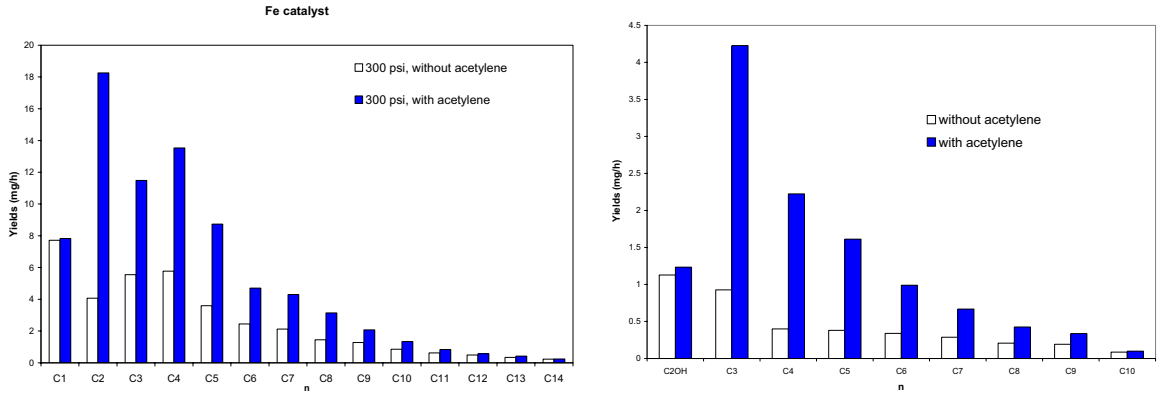

(a) (b)

Figure 2. Product distributions of incorporation of acetylene on an iron catalyst (a) hydrocarbons (b) oxygenates; 100Fe/4.4Si/1.25K, T=180 ºC, P=300psi, $H_2/CO=1$, 1% acetylene.

Products from both base case reactions and from F-T reactions with acetylene follow Anderson-Schulz-Flory (ASF) distribution; the presence of acetylene causes a decrease in alpha from 0.74 to 0.65. Figure 1 shows that the most significant products in the presence of acetylene over Co are C4 hydrocarbons, mostly 2-butene from acetylene dimerization. A sharp increase of C3 and C5 oxygenates is observed upon addition of acetylene. We have reported that incorporation of long chain alkynes into the F-T synthesis on cobalt catalysts produces oxygenates with one added carbon.[6] We postulated that aldehydes are primary products formed by a hydroformylation reaction, which are later hydrogenated to the corresponding alcohols. With acetylene, 1-pentanol is increased due to re-adsorption of C4 unsaturated hydrocarbons formed by acetylene dimerization.

Addition of acetylene to CO/H_2 on a precipitated iron catalyst

Effects of acetylene on the F-T reaction were investigated with an iron catalyst under the same reaction conditions as with cobalt catalysts. The yields of hydrocarbon products from F-T reactions in the absence and presence of acetylene on an iron catalyst are shown in Fig. 2. As found with cobalt catalysts, addition of acetylene with iron catalysts enhanced formation rates of C2+ products while the yield of methane was not changed. Unlike cobalt catalysts which show

great activity for dimerization, hydrogenation is the preferred reaction with iron catalysts. A striking difference between iron and cobalt catalysts is in the distribution of oxygenates which is not limited to addition of just add one carbon. With iron, oxygenates under either normal F-T synthesis or F-T synthesis with acetylene follow ASF distribution, just as with hydrocarbons. With iron catalysts, addition of acetylene results in an increase in oxygenates as well as hydrocarbons, an indication that oxygenate formation involves acetylene initiation of growing hydrocarbon chains. Increase in pressure leads to enhancement in production of oxygenated products. Only a small amount of oxygenated products of low molecular weight were produced on iron catalysts below 100psi; and 13% were formed below 300psi. At 700psi, oxygenates reach 23% of total products. The major components of oxygenated products with iron catalysts were alcohols and aldehydes.

Incorporation of acetylene on a fused iron catalyst

We carried out a few experiments on incorporation of acetylene at 180C and 700psi on a fused iron catalyst. Yields of hydrocarbons and oxygenates increased from 8 mg/h/g to 58 mg/h/g upon acetylene addition; but addition of acetylene did not lead to an obvious increase in selectivity to oxygenates. Hydrocarbons are the main products of acetylene initiated F-T reactions on the fused iron catalyst, but the fused iron catalyst tends to produce more oxygenates than the precipitated iron catalyst. About 30 wt % of the total products are oxygenates with the higher alpha value of 0.75.

Loktev et al. used 1% acetylene as the third reactant in CO hydrogenation over a fused iron catalyst at 150-190 C and high pressure (1500-3000 psi) [7]. Over 80% of their products were reported to be alcohols; both the reaction rate and selectivity to alcohols were increased in the presence of acetylene. These findings are likely due to the high pressures used in their work.

Conclusions

F-T syntheses with acetylene as a probe were conducted over both cobalt and iron catalysts. There are several interesting aspects of the results of incorporation of acetylene into F-T reactions. For iron and cobalt catalysts, initiation of the reaction is the predominant action of acetylene, while hydrogenation is a favored reaction for co-fed ethylene under F-T conditions. Acetylene is incorporated into F-T reactions much more effectively than are higher acetylenes, a finding similar to results reported with olefin addition. Selectivity to hydrogenation or dimerization of acetylene is strongly dependent on the catalyst rather than reaction conditions. For iron catalysts hydrogenation is a favored reaction, while for cobalt, dimerization is favored. Alpha values decreased upon addition of acetylene, indicating that acetylene serves mainly as a chain initiator. Addition of acetylene increases the degree of branching of F-T products, possibly caused by 2-butene re-initiation. Addition of acetylene to cobalt yields only oxygenates via hydroformylation. Addition of acetylene to iron yields a series of oxygenates which follow ASF distribution. Alcohols are the major components of oxygenated products from F-T synthesis; the aldehyde/ alcohol ratio increases with decrease in contact time. It appears that alcohols are secondary products formed by hydrogenation of aldehydes.

References

1. F. Fischer and H. Tropsch, Brennstoff-Chemie, 1926, 7, 97.
2. Schulz, H. and M. Claeys, Applied Catalysis, 1999, 186(1-2), 71.
3. B.H. Davis, Catalysis Today, 2003, 84(1-2), 83-98.

4. J. H. Boelee, J. M. G. Cüsters and K. Van Der Wiele, Applied Catalysis, 1989, 53, 1.
5. Robert T. Hanlon and Charles N. Satterfield, Energy & Fuels, 1988, 2, 196.
6. Y. Zhang, L. Hou, J.W. Tierney and I. Wender, Topics in Catalysis, in press.
7. S.M. Loktev, Journal of Catalysis, 1982, 17, 225.

Future Work

This work using acetylene as a probe for the F-T synthesis will be concluded during the next year. Preliminary work on the co-production of hydrogen and chemicals from methanol will be initiated.

Papers Presented or Published

1. Y. Zhang, L. Hou, J. W. Tierney and I. Wender, Acetylenes as Probes in the Fischer-Tropsch Reactions, ACS Annual Meeting, September, 2003, New York
2. Y. Zhang, L. Hou, J. W. Tierney and I. Wender, Fischer-Tropsch Mechanism Studies Using Acetylenic Molecules as Probes, Topics in Catalysis, submitted in January, 2004

Reaction pathway and kinetic modeling of Fischer-Tropsch synthesis over an alumina supported cobalt catalyst in supercritical-hexane media

Nimir O. Elbashir, Deborah B. Borough, Ram Gupta, Christopher B. Roberts
Department of Chemical Engineering, 230 Ross Hall, Auburn University, AL 36849

Introduction

In our previous reports we have addressed the advantages of applying supercritical fluids to Fischer-Tropsch synthesis (FTS) as a promising unconventional media that allows better control of hydrocarbon product distributions and selectivity. This enhanced performance as compared to conventional FTS operation is attributed to the in situ extraction of heavy hydrocarbons from the catalyst pores and the elimination of interphase transport limitations. Both of those factors promote reaction pathways toward the desired products. We have also measured the phase behavior and the critical properties of the reaction mixture in order to identify the single phase boundaries for the reaction (2004 Semi-annual Report). Tuning the reaction environment from liquid-like properties to vapor-like properties and vice versa, by either changing the reaction temperature or pressure, has resulted in an interesting phenomenon that involves deviations in hydrocarbon product distributions from the standard Anderson-Shultz-Flory (ASF) model (Fig. 1). This phenomenon is also accompanied by a high chain growth probability within the middle distillate hydrocarbon region.

This report covers an attempt to understand this phenomenon by proposing a chain-growth model in supercritical hexane FTS. The model attributes the deviation from the standard ASF model to the enhanced □-olefin incorporation within the middle hydrocarbon distillates products. The report also includes the development of a kinetic model for FTS reaction over a commercial 15% Co/ Al_2O_3 catalyst that will be used to predict CO consumption rates and CH_4 formation rates in both gas phase and supercritical fluid hexane (SCH) FTS. Our findings show that modifications to conventional FTS surface reaction model is needed to better predict the reaction behavior under supercritical phase conditions. The proposed modifications are in good agreement with the enhanced-olefin-incorporation model[1] for the chain growth mechanism in supercritical hexane FTS.

Experimental

Reaction system: The FTS reaction over a commercial 15% Co/Al_2O_3 (United Catalysts Co.) catalyst in supercritical hexane was carried out in our high-pressure FTS unit. This unit was described in detail in our previous reports and publications[1-3]. Three certified cylinders of different ratios of H_2 and CO (1:2, 1:1, 2:1) with a trace amount of N2 as an internal standard for chromatographic analysis were obtained from Air Gas Co. The flow rate of the syngas reactants was controlled by digital mass flow controllers. The hexanes solvent flow rate was controlled by an HPLC pump. The hexane/syngas molar ratio was fixed at 3/1 in all experiments. The combined stream entered the top of the downflow H.I.P reactor (1.27 cm×25.4cm of effective volume: 32 cm3) that was positioned in a temperature controller tube furnace controlled by an ATS temperature controller system. The pressure in the reaction zone was controlled by a back pressure regulator BPR (Tescom Inc.) located between the reactor and a hot trap. Methods for measuring the activity and selectivity using two gas chromatographs with FID and TCD columns were previously discussed in detail (2004 Semi-Annual Report).

Results and Discussion

Enhanced Incorporation of α-Olefin Model

Reaction Network. Fig. 2 shows our proposed reaction pathway for the FTS reaction in the supercritical phase. This model was developed based on the surface reaction kinetic model4 of FTS over cobalt-based catalytic systems. In the first stage, adsorption and disassociation of CO and H_2 take place on a cobalt catalyst active site. The removal of surface oxygen steps represented by the formation of water and CO2 is shown in the second stage. The postulation of oxygen removal was based on the modified Kellener and Bell[4] surface reaction model[5]. The hydrogenation of adsorbed carbon and the formation of oligomers are included in the third stage. The rate of alkyl (CH3.S) formation and termination to methane by hydrogenation of the monomers are included in the fourth and fifth stages. The corresponding rates for each of the reactions will be discussed later in this report. The scheme of chain growth mechanism work is illustrated by stage six and seven as shown in Fig. 2. The classical route of an alkyl group (R_n) propagation over an active site S consists of the primary reaction to produce olefins that can then re-adsorb to the same active site or another vacant S*, that has the same characteristics of S. Termination takes place whenever secondary reactions are favored yielding paraffins or isomers. The increased availability of S* is attributed to operation under near-critical and supercritical conditions that facilitates the incorporation of desorbed olefins into the chain growth process[6.]

Model Features and Assumptions. A typical product distribution for SCH-FTS over the alumina supported cobalt catalyst was used as representation for the enhanced olefin incorporation model (Figs. 3a and 3b). The model assumes that from the primary products only olefins have the capability of re-adsorbing and incorporating in the chain growth process. Paraffins are primary products of the synthesis and it can also be a product of olefins hydrogenation. We also neglected hydrogenolysis, isomerization, and oxygenation routes. Even though, such an assumption represents simplification to the complex routes of the FTS network, it agrees with our experimental observation for SCH-FTS (see 2004 Semi-annual Report and Elbashir and Roberts 2004[1]). As shown in Fig. 3b, the first point in the curve represents the methane selectivity (which we referred to as methanation). The light hydrocarbons (C2-C5) selectivity region is defined as the regular olefin incorporation range. Those hydrocarbons can participate in the propagation thereby decreasing their concentrations in the synthesis. Such a route will be particularly favored under high pressure operations[7]. Our approach introduces the enhanced olefin incorporation range as a unique contribution of the influence of the near-critical and supercritical solvent (hexane) on the FTS chain growth process. The incorporation of olefins from C7-Cb (where b represents the carbon number where the product distribution begins to follow the ASF model; see Fig. 3a) is attributed to the enhanced solubility of primary products in the single phase near-critical and supercritical which affects the adsorption/desorption equilibrium of those species. C6 hydrocarbons have not been included in the above range due to our inability to accurately measure the amounts of C6 hydrocarbons produced compared to those from the hexane solvent. The overall chain growth probability ($\alpha_{overall}$) under SCH-FTS is higher than that under gas-phase operation. The chain-growth probability within this region is very high (α_{md}>0.95). The last region in Fig. 3b follows the regular ASF distribution in the heavy hydrocarbon range. The rate of incorporation of those hydrocarbons in the chain growth process is much lower than the synthesis rate.

The overall scheme of the chain growth network mechanism in SCH-FTS is described in Fig. 3a. This sequence can either take place on the active site S or on the evacuated active site S*

on the cobalt catalyst surface. The methanation reaction or the hydrogenation of the monomer (building block, C1*) represents the first product in the chain growth sequence. Methane is the only saturated product and it's not a part of the general sequence of FTS chain growth process. Methane selectivity is neither predictable by the ASF model[8] nor the enhanced-olefin incorporation model over the cobalt catalyst. In the olefin incorporation range, re-adsorbed ethene is then rapidly converted to C2* that has similar characteristics of the building block C1* produced from the initial hydrogenation of adsorbed carbon molecules. As the C2* molecule competes strongly with H_2 for the catalyst active site, the re-adsorption sequence is more favored than the termination of the chain to ethane. This ability of lower alkenes (C2-C5) to re-adsorb and incorporate is mainly influenced by the characteristics of cobalt catalyst and less affected by the reaction medium[9]. The incorporation capability decreases with increasing carbon number while hydrogenation increases. In the enhanced olefin incorporation region, the incorporation mobility of the middle distillate olefins is enhanced in SCH-FTS. The tendency towards incorporation in the chain growth process by inserting into a growing chain of the middle distillate hydrocarbons decreases with carbon number. This trend suggests that either the termination rate to olefinic compounds or the re-adsorption rate to the active site must be higher than the termination rates to paraffin compounds in both the regular incorporation and enhanced incorporation ranges. This hypothesis is strongly supported by experimental findings of olefin/paraffin ratios and olefin selectivity in the supercritical phase compared to the conventional FTS operations[10-14]. However, in the heavy hydrocarbon range where the distribution follows the regular ASF mode, the hydrogenation rates to paraffinic compounds are much higher than termination rates to olefins or incorporation rates. As an example, only paraffinic compounds are measured in our products beyond C_{18}. These results are in a good agreement with previous experimental findings where even at high carbon number olefins can incorporate into the chain growth however they are more likely to hydrogenate than either initiate a new or insert in a growing chain[8].

Fig. 4 illustrates that the deviations from the ASF model were seen in both the distributions of olefinic and paraffinic compounds, especially in the middle distillate product range (enhanced olefin incorporation range). This is a surprising phenomenon since it is well known that while olefinic compound distributions deviate from the ASF model due to their incorporation into the chain growth process, paraffin compound distributions typically follow ASF model distribution[7]. We attributed this to the suppression of the termination routes by secondary reactions (specifically hydrogenation) of the primary products in the enhanced incorporation range due to the enhanced availability of re-adsorption sites in the supercritical phase. Thus, the paraffin compounds produced follow the same trend as that of the primary product of the synthesis (olefinic compounds), however with lower selectivity. This concurs with the chain growth scheme presented earlier in Fig. 3a. Nevertheless, at mild operation temperatures (260 °C) whereby the medium is of gas-like density both olefinic products and paraffinic products followed ASF with higher probability of olefinic products only in the light hydrocarbons range (see Fig. 5).

Kinetics of the Reaction in the Supercritical Phase. The illustration of the reaction routes (Fig. 2) and the description of the synthesis stages are discussed above. The derivation of the rate equations for each of the reactions proposed in Fig. 2 is carried out by using Langmuir–Hinshelwood–Hougen–Watson approach. The hydrogenation of surface carbon (the 1st reaction

in stage 3), was considered as the rate limiting step, while the other steps were assumed to be at quasi-equilibrium. After the establishment of steady state operation the rate of oxygen removal by water formation (the 2nd reaction in stage 2) was assumed to be equal to the rate of carbon hydrogenation according to the stoichiometric coefficient of the 3rd reaction in the first stage. Removal of oxygen by CO2 formation was neglected in the overall rate due to its very low selectivity over our cobalt catalyst (<2% in gas-phase reaction and <0.5% in SCH operation). The total concentration of the active sites (Ct) on the Co surface can be determined as the sum of vacant sites (Cv) and the occupied sites by the adsorbed species Cadi (eq 1).

$$C_t = C_v + \sum_{i=1}^{m} C_{ad_i.S} \quad (1)$$

$$\sum_{i=1}^{m} C_{ad_i.S} = C_{H.S} + C_{C.S} + C_{O.S} + C_{OC.S} \quad (2)$$

The occupied sites shown in eq. 2 do not include the active radicals (.CH. and .CH_2.) and water (OH) since they are not occupying a significant part of the active sites and their desorption rate is much higher than the other species[4,15]. Based on the previous assumptions, eq. 3 represents the fraction of the free active site (θs) and eq 4 the CO consumption rate (-rCO).

$$\theta_s = \frac{C_V}{C_t} = \frac{1}{1 + K_1 P_{H_2}^{1/2} + (K_2 + K_3) P_{CO}^{1/2} + K_4 P_{CO}} \quad (3)$$

$$-r_{CO} = \frac{k P_{CO}^{1/2} P_{H_2}^{1/2}}{[1 + K_1 P_{H_2}^{1/2} + (K_2 + K_3) P_{CO}^{1/2} + K_4 P_{CO}]^2} \quad (4)$$

where $k = k_{C_1} K_3 K_1 C_t^2$, $K_1 = \sqrt{K_{H_2}}$, $K_2 = \sqrt{\frac{K_c k_{c_1}}{k_{O_1}}}$, $K_3 = \sqrt{\frac{K_c k_{O_1}}{k_{C_1}}}$, $K_4 = K_{CO_1}$

CO consumption rate can also be calculated from the rate of monomer (CH_2.S) consumption. There are two possibilities for monomer consumption as illustrated in Fig 2; either by forming methyl species or by incorporating into a growing chain. As a result, the CO consumption rate can also be represented by eq 5.

$$-r_{CO} = k_{C_3} C_{H.S} C_{CH_2.S} + k_\alpha C_{CH_2.S} \sum_{n=1}^{\infty} C_{R_n.S} \quad (5)$$

For the elimination of the infinite sum in eq 5, we assumed that at steady state the initiation rate of the polymerization process should balance its termination rate[5,15]. Therefore, a mass balance around the methyl (CH_3.S or R1) initiation rate (3rd reaction in stage 3) and termination rate (to methane stage 4 or paraffins as included in stage 5) is sufficient for the determination of the infinite sum as seen in eq 6.

$$k_{C_3} C_{CH_2.S} C_{H.S} = k_t C_{H.S} \sum_{n=1}^{\infty} C_{R_n.S} \quad (6)$$

As a result, the concentration of both the monomer (CCH_2.S) and the methyl R1 (CCH_3.S) on the cobalt active site can be calculated from eqs. 4, 5, & 6. From stage 4, the rate of methane formation can then be calculated according to Eq.7 using the assumptions stated by Sarup and Wojcichowski10 in the low CO molecular coverage model.

$$r_{CH_4} = \frac{\phi_1 P_{H_2} \theta_s^2}{\left[\phi_2 \left(\left(1 + \phi_3 P_{CO}^{1/2} P_{H_2}^{-1/2}\right)^{1/2} - 1 \right)^{-1} + 1 \right]} \quad (7)$$

$$\phi_1 = \frac{C_t^2 K_H k_{c_3} k_{c_4}}{k_\alpha}, \ \phi_2 = \frac{K_4}{K_5 k_\alpha}, \ \phi_3 = \frac{K_6 k_{c_1} K_{cf}^{1/2}}{K_H^{1/2}}$$

where

Kcf represents the adsorption equilibrium constant for carbon and being defined with the rest of the constants as follows;

$$K_{cf} = \frac{k_{O1}}{k_{C1}}, \ K_5 = \frac{k_t}{2 k_\alpha}, \ K_6 = \frac{4 k_\alpha}{k_{C3} k_t}$$

The estimation of parameters appearing in eq 4 and 7 was calculated from the experimental data by minimizing a function of square of the absolute difference between the actual and predicted rates using the quasi-Newton method and a finite-difference gradient.

The performance of the 15% Co/Al_2O_3 catalyst measured by the rate of CO consumption in gas-phase FTS and SCH-FTS under different operating conditions is shown in Fig. 6 at 250 °C with a total pressure of 60 bar and a syngas partial pressure, Psyngas, of 15 bar at three different H_2/CO ratios. In the gas-phase experiments, a partial pressure of inert helium, P_{He}, of 45 bar was used as a pressurizing gas to achieve a total pressure of 60 bar. In the SCH experiments, the P_{syngas} was again 15 bar and the partial pressure of hexane solvent, Hexane, was 45 bar thereby yielding the same total pressure of 60 bar. The experiments in both gas-phase and SCH-FTS were conducted at a constant syngas flowrate of 100 sccm. Fig. 3 illustrates that increasing the H_2/CO molar feed ratio resulted in higher CO consumption rates at fixed reaction temperature in SCH operation. At low H_2/CO, an increase in reaction temperature from 240 °C to 250 °C results in only a slight increase in the CO consumption (data not shown), however, at a ratio of 2/1 a significant increase in the rate (>30%) is observed with this temperature increase (data not shown). The activity of the catalyst under SCH operation is higher than in the gas-phase at the same total pressure of 60 bar. The same result was observed in the absence of the helium pressurizing (diluent) gas whereby P_{syngas} was kept constant at 20 bar for both gas-phase and SCH operations (data not shown). However, the CO consumption rate in SCH is shown to be function of pressure that exhibits a maximum of 65 bar (data not shown). This trend is in agreement with our previous findings12 and is attributed to the fine balance between the effects of pressure on the bulk diffusion and the intra-particle pore diffusivity.

Fig. 7 presents the rate of methane formation as a function of the H_2/CO feed ratio at the conditions described above for both gas-phase and SCH FTS at 250 °C. An increase in H_2/CO ratio results in higher methane production rate in both gas-phase and SCH FTS. However, this rate in SCH is much lower than that in gas-phase and the difference between the two increases with increasing H_2 concentration. In addition to this phenomenon of the reduced methane formation under SCH conditions, it was also observed that SCH FTS resulted in higher olefin/paraffin ratio and shifts of product distributions towards the heavy hydrocarbons (data not shown) compared to gas-phase FTS at the previously specified conditions.

The kinetic model in eq 4 and eq 7 closely predict the CO consumption rates and CH_4 production in gas-phase operation as seen in Figs. 3&4. However, both of the models do a poor

job in the prediction of those rates under SCH operation. Higher methane formation rate than the actual was predicted by eq.7, while lower CO consumption rate was also predicted by eq 4 for the SCH FTS. The inconsistency of the kinetic model in predicting the SCH performance indicates that assumptions stated in developing this model for gas-phase operation is not sufficient to measure the performance under SCH operation. Two factors could contribute to the inability of this model to predict FTS performance under SCH conditions. First of all, the model relies on partial pressure (concentrations) of the reactants rather than their activities in the rate equations due to ideal gas assumptions made in previous model developments. Thermodynamic non-ideality must be incorporated into the model through use of activities rather than simply partial pressures to accurately predict the kinetic rates under SCH conditions. Secondly, this model does not included solvent effects on individual rate constants in the critical region and particularly for the initiation steps. The FTS reaction pathway (Fig.2) is modified (stage 6) to include enhanced olefin incorporation in chain growth process as a result of significant in-situ extraction in the SCH medium, especially for heavier hydrocarbons12. This modification accounts for the increased availability of active sites in the supercritical medium. This site (S*) is assumed to promote both adsorption of the reacting molecules (CO and H_2) and incorporation of primary products (□-olefins) into the chain growth process. It is also assumed that S* would have a higher coverage of active carbon than the regular site, S, and therefore it suppresses methane formation16. In addition the effective reaction order of higher hydrocarbon formation on S* is higher than the methane formation since the monomer involved on this site is likely a desorbed olefin close to the active site. The increased probability of covering S* by a monomer derived from the re-adsorbed α-olefin rather than an initiating monomer ($-CH_2-$) decreases the probability of methane formation.

Conclusions

While the role of enhanced in situ extraction of heavy products in SCH operation has not being quantified at this stage, it is clear that the removal of heavy hydrocarbons in the SCH would result in more active sites availability (S*). Moreover, including thermodynamic non-idealities into the rate expression will improve the model predictions under supercritical FTS operation. The difference between the reaction medium in gas-phase FTS and SCH FTS can result in modified active site chemical characteristics, enhancement in active site availability and different thermodynamic activities of the reacting species. Further model development should address each of the factors described above.

Future Work

1. We are currently investigating the role of the catalyst type and characteristics in the supercritical FTS reaction performance. We are investigating both iron-based catalytic systems and ruthenium-based catalytic systems in SCH-FTS. We will conduct a comparative study on the performance of those systems with the cobalt-based catalysts, specifically on the activity and deviations from the standard ASF model.
2. We will continue using our high-pressure reactor system to study the performance of Pd-based catalytic systems in hydrogenation and dehydrogenation reactions in supercritical CO2 environments. Our study will also include developing preparation techniques for nanoscale-Pd catalysts by deposition on conventional supports (silica and alumina), on carbon nanotubes, and the synthesis of highly porous polymer/Pd nanocomposite materials.

References

(1) Elbashir, N. O.; Roberts, C. B. Ind. Eng. Chem. Res. 2004, in press.
(2) Huang, X.; Elbashir, N. O.; Roberts, C. B. Ind. Eng. Chem. Res. 2004, 43, 6369.
(3) Elbashir, N. O.; Roberts, C. B. ACS Div. of Petr. Chem. Preprints 2004, 49, 422.
(4) Bell, A. T. Catal. Rev. - Sci. Eng. 1981, 23, 203.
(5) Uner, D. O. Ind. Eng. Chem. Res. 1998, 37, 2239.
(6) Elbashir, N. O.; Roberts, C. B. ACS Div. of Petr. Chem. Preprints 2004, 49, 157.
(7) Snel, R. J. Molecular Catalysis 1989, 53, 143.
(8) Puskas, I.; Hurlbut, R. S.; Pauls, R. E. J. Catal. 1993, 139, 591.
(9) Smith, D. F.; Hawk, C. O.; Golden, P. L. J. Am. Chem. Soc. 1930, 52, 3221.
(10) Bukur, D. B.; Lang, X.; Akgeman, A.; Feng, Z. Ind. Eng. Chem. Res. 1997, 36, 2580.
(11) Fan, L.; Fujimoto, K. Appl. Catal. A: Gen. 1999, 186, 343.
(12) Huang, X.; Roberts, C. B. Fuel Proc. Technol. 2003, 83, 81.
(13) Jacobs, G.; et al. Fuel 2003, 82, 1251.
(14) Fan, L.; Yokota, K.; Fujimoto, K. AIChE Journal 1992, 38, 1639.
(15) Sarup, B.; Wojciechowski, B. W. Can. J. Chem. Eng. 1989, 67, 62.
(16) Bertole, C. J.; Mims, C. A.; Kiss, G. J. Catal. 2002, 210, 84.

Publications during 2003-2004

1. Elbashir N. O.; Roberts C. B. "Enhanced Incorporations of □-olefins in the Fischer-Tropsch Synthesis Chain-Growth Process over an Alumina Supported Cobalt Catalyst in Near-Critical and Supercritical Hexane Medium Industrial & Engineering Chemistry Research." In press (2004).
2. Elbashir N. O.; Roberts C. B. Reaction Pathway and Kinetic Modeling of Fischer-Tropsch synthesis over an Alumina Supported Cobalt Catalyst in Supercritical-Hexane Petr. Chem. Div. Prep. 49(2) (2004)157-160.
3. Huang X.; Elbashir N. O.; Roberts C. B. Supercritical Solvent Effects on Hydrocarbon Product Distributions in Fischer-Tropsch Synthesis over an Alumina Supported Cobalt Catalyst Industrial & Engineering Chemistry Research. 43 (2004) 6369-6381.
4. Elbashir N. O.; C. B. Roberts "Selective Control of Hydrocarbon Product Distributions in Supercritical Phase Fischer-Tropsch Synthesis" Petr. Chem. Div. Prep. (2004) 422-425.
5. P. Dutta; N. O. Elbashir; A. Manivannan; M. S. Seehra, C. B. Roberts "Characterization of Fischer-Tropsch Cobalt-based Catalytic Systems (Co/SiO2 and Co/Al_2O_3) by X-ray Diffraction and Magnetic Measurements" Catalysis Letters. In press (2004).
6. Elbashir N. O.; P. Dutta; A. Manivannan; M. S. Seehra, C. B. Roberts "Impact of cobalt catalyst characteristics in conventional gas and supercritical phase Fischer-Tropsch synthesis" submitted to Applied Catalysis, A: General (2004).

Presentations during 2003-2004

1. Elbashir N. O.; C. B. Roberts "Selective Control of hydrocarbon Product Distribution in Supercritical phase Fischer-Tropsch Synthesis" ACS 228th National Meeting, August 22-26 (2004) Philadelphia, Pennsylvania.
2. Elbashir N. O. ; D. Boroughs, ; R. Gupta; C. B. Roberts "Impact of Cobalt-based Catalyst Characteristics on Conventional Gas-Phase and Supercritical Phase Fischer-Tropsch

Synthesis Performance" Consortium of Fossil Fuel Science (CFFS) 18th Annual Technical Meeting, August 1-4 (2004) Stonewall Resort, West Virginia.
3. Elbashir N. O.; C. B. Roberts "Kinetics Model of Fischer-Tropsch synthesis over Alumina Supported Cobalt Catalysts in Supercritical-Hexane Medium" Fischer-Tropsch: Material, Theories, and Practice 227th ACS National Meeting · March 28 - April 1 (2004) Anaheim, California.
4. Elbashir N. O.; X. Huang; D. Boroughs; C. B. Roberts "Enhanced Hydrocarbon Chain-Growth in Supercritical Phase Fischer-Tropsch Synthesis: Experiments and Modeling" [546] - Reactions in Near Critical and Supercritical Fluids American Institute of Chemical Engineers (AIChE) Annual Meeting, November, 16-21 (2003) San Francisco, California.
5. Elbashir N. O.; D. Boroughs; C. B. Roberts; P. Dutta; A. Manivannan; M. S. Seehra "Influence of Cobalt Based Catalysts Characteristics on Fischer-Tropsch Synthesis in Conventional Gas-Phase Media and Supercritical Phase Media " Poster Session: Kinetics, Catalysis, and Reaction Engineering, American Institute of Chemical Engineers (AIChE) 2004 Annual Meeting, November, 7-12 (2004) Austin, Texas.

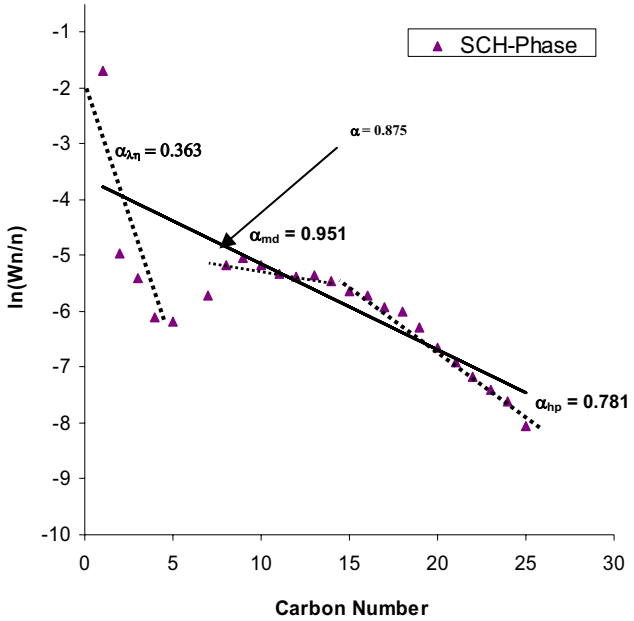

Fig. 1 Hydrocarbon product distribution from SCH-FTS at 65 bar T= 250 °C, syngas flowrate = 50 sccm/ g-cat, hexane flowrate =1.0 mL/min, and H_2/CO feed ratio = 2.

1) Reactant dissociation and chemisorption on the active site (S)

$$H_2 + 2S \overset{K_H}{\Leftrightarrow} 2H.S$$

$$CO + S \overset{K_{CO_1}}{\Leftrightarrow} CO.S$$

$$CO.S + S \overset{K_{CO2}}{\Leftrightarrow} C.S + O.S$$

(2) Oxygen removal

$$O.S + H.S \overset{K_{O_1}}{\Leftrightarrow} OH.S + S$$

$$OH.S + H.S \overset{K_{O_2}}{\Rightarrow} H_2O + 2S$$

$$CO.S + O.S \overset{K_{O_3}}{\Rightarrow} CO_2 + 2S$$

(3) Monomer formation

$$C.S + H.S \overset{K_{C_1}}{\Leftrightarrow} CH.S + S$$

$$CH.S + H.S \overset{K_{C_2}}{\Leftrightarrow} CH_2.S + S$$

$$CH_2.S + H.S \overset{K_{C_3}}{\Leftrightarrow} S + CH_3.S$$

(4) Termination to methane

$$CH_3.S + H.S \overset{K_{C_4}}{\Rightarrow} CH_4 + 2S$$

(5) Chain growth & termination sequences

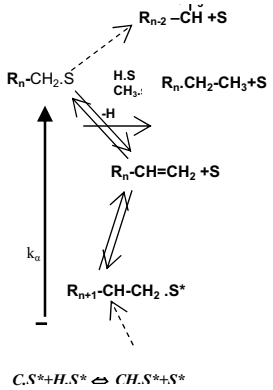

(6) Enhanced activity & olefin incorporation in SCH

Fig. 2 FTS reaction network including the enhanced activity and olefin incorporation sites.

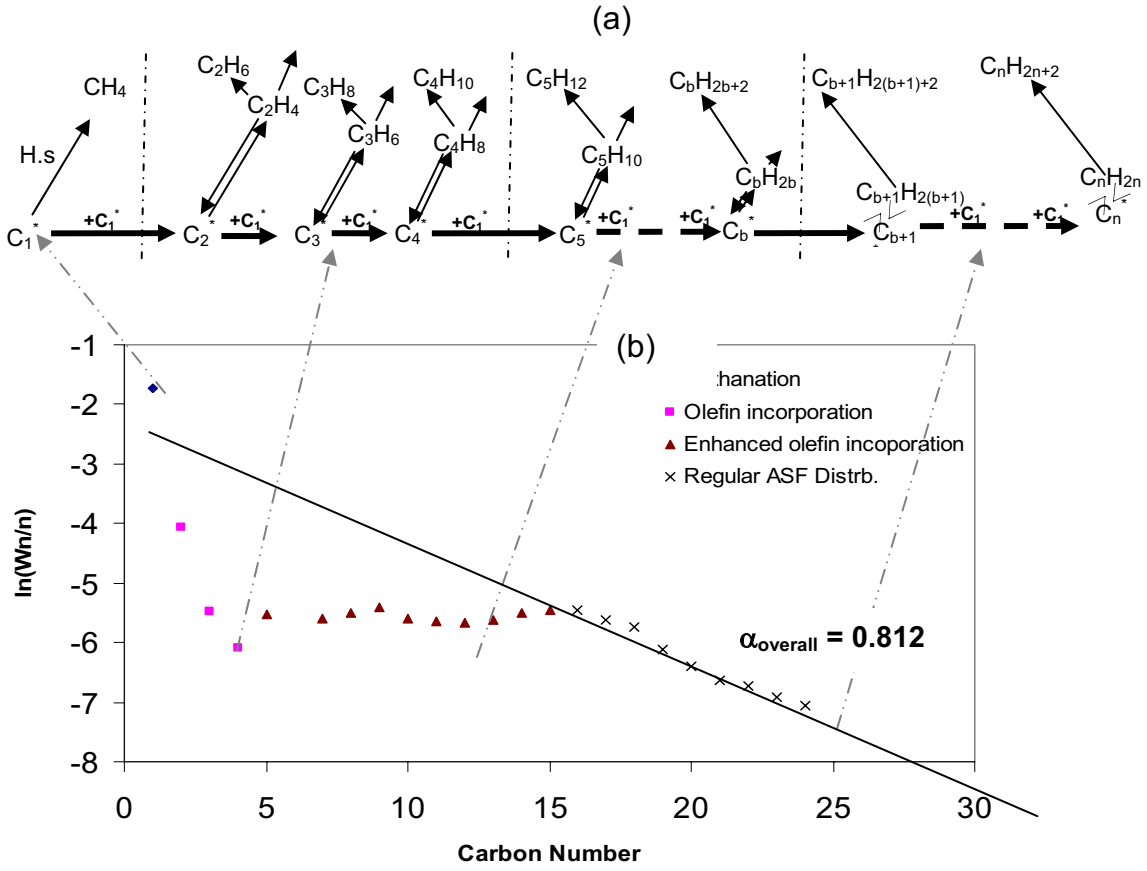

Fig. 3 (a) Description of the chain growth process in the enhanced-olefin-incorporation model in SCH-FTS starting with methanation and ending with the heaviest hydrocarbon detected under the specific reaction conditions. (b) Typical product distribution curve in SCH-FTS including all regions defined in the chain growth process above.

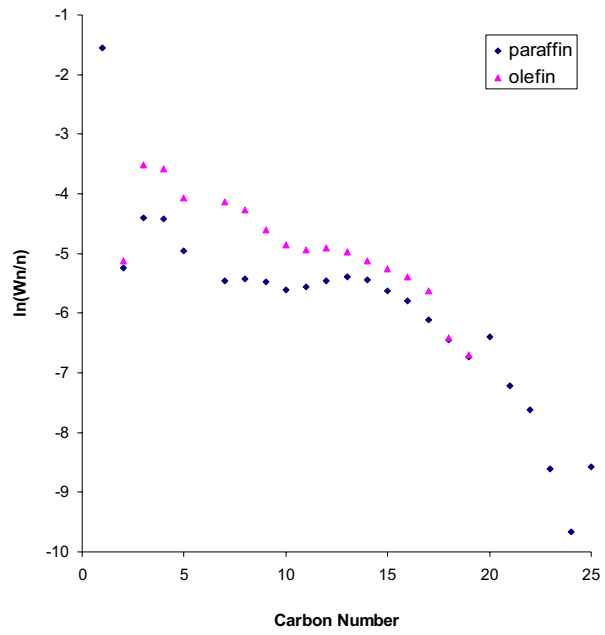

Fig. 4 Distributions of olefinic and paraffinic compounds in SCH-FTS at 250 °C and 65 bar with syngas flowrate of 50 sccm/g-cat, hexane flowrate of 1.0 mL/min, and H_2/CO feed ratio of 2.

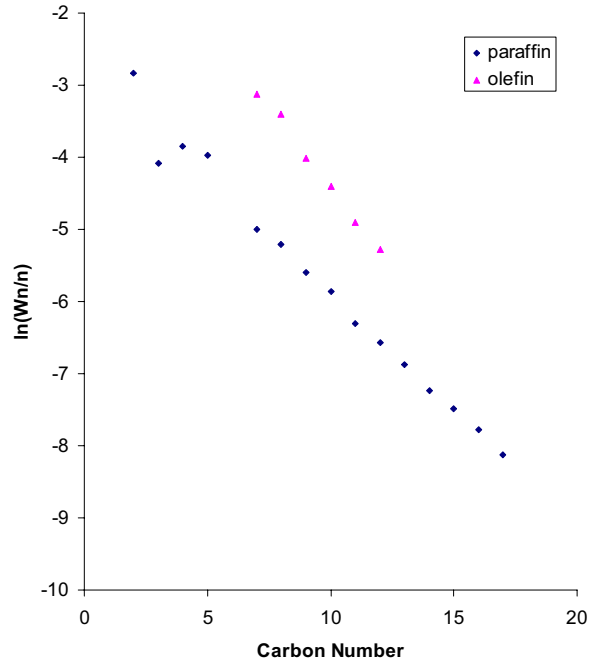

Fig. 5 Distributions of olefinic and paraffinic compounds in SCH-FTS at 260 °C, and 65 bar with syngas flowrate of 50 sccm/g-cat, hexane flowrate of 1.0 mL/min, and H_2/CO feed ratio of 2.

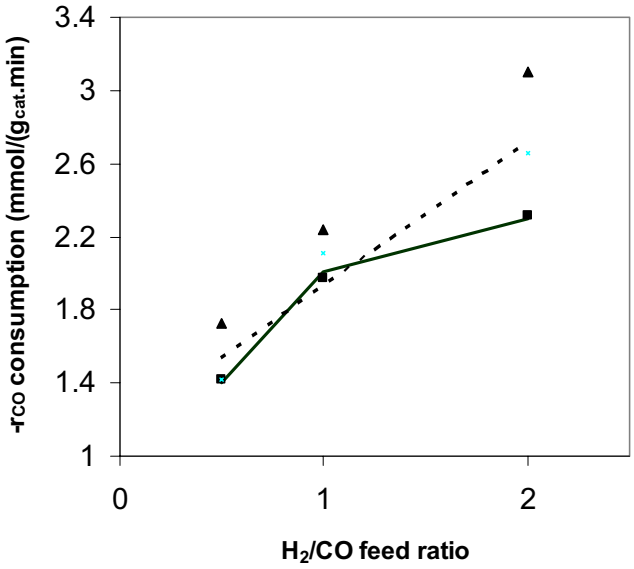

Fig.6 CO consumption rate in gas-phase (squares) and SCH phase (triangles) as a function H_2/CO ratio at 250 °C. Total pressure is 60 bar (P_{syngas} = 15 bar) and syngas flow rate 100 sccm/min. The solid line represents the predicted rate in gas-phase while the dotted line represents the predicted rate in SCH FTS operation by using the estimated parameters in eq 4 (k = 0631, K1= 0.007, K2= 0.51, K3 = 0.098, K4 = 6.64×10-5).

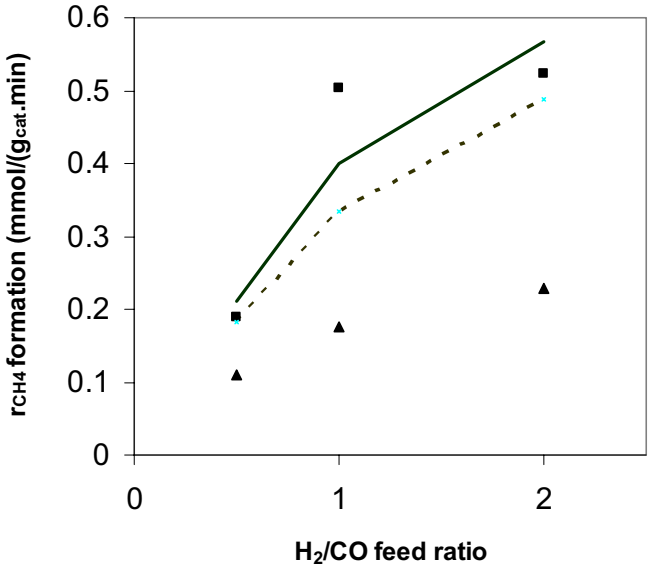

Fig.7 CH4 formation rate in gas-phase (squares) and SCH phase (triangles) as a function H_2/CO ratio at 250 °C. Total pressure is 60 bar (P_{syngas} = 15 bar) and syngas flow rate 100 sccm/min. The solid line represents the predicted rate in gas-phase while the dotted line represents the predicted rate in SCH operation by using the estimated parameters of eq. 7 ($\phi 1 \theta s2$ = 0.0306, $\phi 2$ = 303, $\phi 3$ = 0.045).

Diesel and Jet Fuel from Fischer-Tropsch Wax

Z. Zhou, Y. Zhang, J.W. Tierney and I. Wender
Chemical Engineering Department, University of Pittsburgh

Introduction

Premium fuel products produced from synthesis gas via the Fischer-Tropsch (F-T) process can be used as blending agents to upgrade transportation fuels made from petroleum. Because of the sequential chain-growth mechanism involved in F-T reactions, it is not possible to obtain products with a specific molecular weight range. F-T products are always mixtures of light and heavy hydrocarbons. The heavy products (F-T waxes) must be cracked and isomerized to obtain desired transportation fuels.[1] Previous applications of the F-T synthesis convert F-T waxes to desired fuel fractions, such as diesel fuel by using proprietary zeolite-based catalysts which have low reactivities and operate at about 350-500°C.[2] In the present work, we aim at obtaining a readily available, active catalyst system which can be configured to convert F-T waxes into clean high octane gasoline, jet fuel or high cetane diesel at about 200°C and 100-300 psi hydrogen pressure. The catalyst systems studied are based on anion-modified zirconia catalysts which have demonstrated high reactivities in the conversion of the long-chain alkanes in FT waxes. Sulfated zirconia (SZr) is a strong cracking catalyst and tungstated zirconia (W-Zr) has high selectivity for isomerization in converting long-chain alkanes. [3] The difference can be explained in part by a higher hydrogen transfer rate over the surface of WZr.[4] Pt is generally used as a promoter to keep the catalysts stable and active. Zirconia catalysts with Pt loading are termed as PtSZr and PtWZr respectively. While SZr and WZr have been studied individually,[5] There are few reported studies on combinations of these two types of catalysts, which we have termed as hybrid catalysts. We studied hybrid catalysts consisting PtWZr and SZr to convert long-chain paraffins in FT waxes into middle distillate fuels (jet and diesel). Hydrogen pressure is important in determining product distributions. Catalyst characterization tests were also carried out.[4]

Experimental

Catalyst preparation:

PtWZr was prepared by incipient wetness impregnation of WZr (12.5 wt%W) prepared from samples of Magnesium Elektron, Ltd. (MEL) with $Pt(NH_3)_4Cl_2 \cdot H_2O$ (Strem Chemicals) to achieve a desired Pt loading of 0.5 wt%. These were then calcined at 600°C in air. SZr (9 wt% SO3) was prepared from samples of Magnesium Elektron, Inc (MEI). Hybrid zirconia catalysts (PtWZr/SZr) with various weight ratios were prepared by mechanical mixing PtWZr with SZr followed by calcination at 550ºC for 3 hours.

Experimental procedures:

Catalytic tests were carried out in a 27 ml autoclave reaction system using n-C36 as a model compound for an FT wax. In a typical reaction, 0.2 g of the catalyst was activated at 500°C and then added to the reactor, which had been pre-dried overnight. The initial hydrogen pressure was set at room temperature before heating the reactor to 200°C. The reactor was shaken horizontally at 180 rpm during reaction to mix the contents. A computer was used to record the reaction pressure, temperature and time during the run. The reaction was ended at the desired time by quickly cooling the reactor with ice water. Products in the gas phase were discharged into a collector and analyzed using an HP-6890 gas chromatography with a TCD detector. Liquid products in the reactor were collected in vials. When waxy products remained in the reactor,

appropriate amounts of CS2 were used to dissolve them for analysis. Liquid samples were injected into an HP-5890 gas chromatograph with an FID detector. We used GC analysis results of the reaction products to calculate conversions and selectivities. Peaks after n-C9, up to and including n-C20 are termed as middle distillates.

Results and Discussion

At given reaction conditions, PtSZr and PtWZr catalysts have different product distributions in converting n-C36. Neither of the pure catalysts gives a high yield of middle distillates. With PtWZr/SZr hybrid catalyst, the production of middle distillates is significantly increased. The product distribution using PtWZr/SZr with 1:1 component ratio is shown in Figure 1. We tested and compared various catalysts at 200°C, a 25-minute reaction time and a 4:1 reactant/catalyst ratio. Component ratio affects the performance of a PtWZr/SZr hybrid catalyst (Figure 2). The curves of both conversion and yield of middle distillates demonstrate an interaction within the hybrid catalyst system.

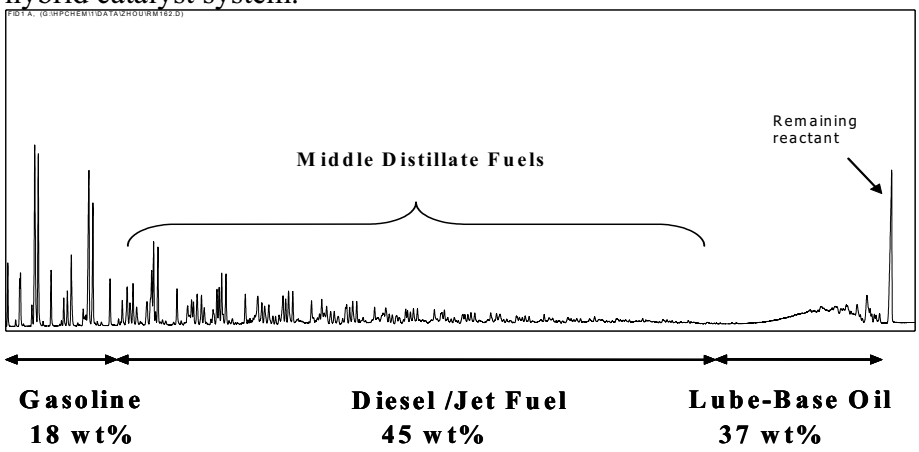

Conversion 90wt%; Reaction conditions: 200 ºC, H_2 pressure = 300 psig, Catalyst/n-C36=1:4, 25min

Figure 1. Increased yield of middle distillates using PtWZr/SZr(1:1) hybrid catalyst

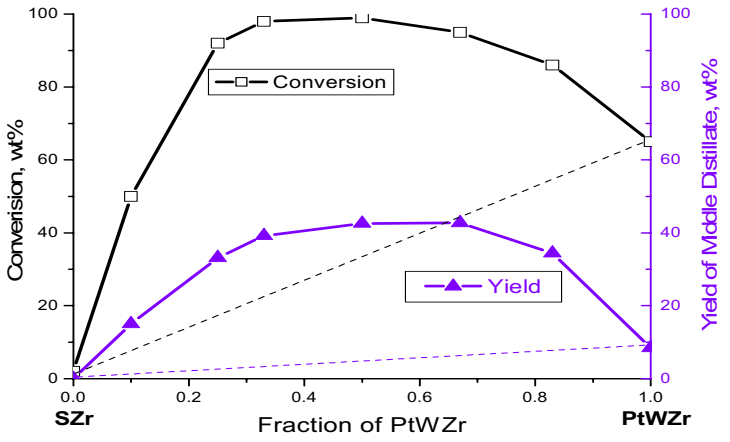

Figure 2. Component ratio affects conversion and yield of middle distillates with PtWZr/SZr (300psi H_2 pressure)

The reactivity of PtWZr increases and the reactivity of PtSZr decreases at low hydrogen pressures. Hybrid catalysts consisting of PtWZr and SZr components are greatly affected by

hydrogen pressure. The performance of PtWZr/SZr under a lower hydrogen pressure (100 psi) is shown in Figure 3.

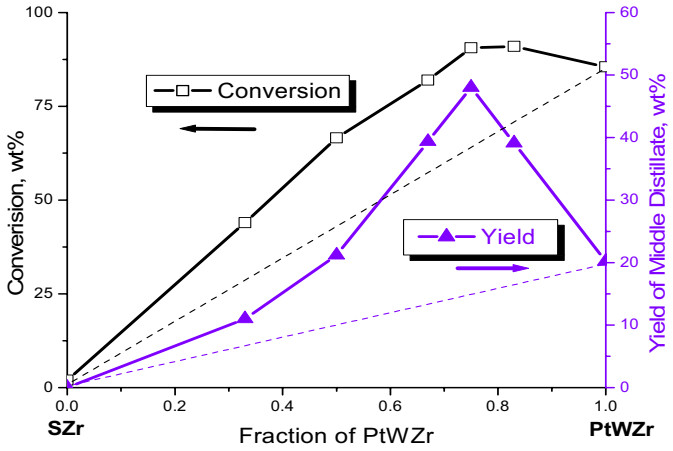

Figure 3. Performance of PtWZr/SZr under lower hydrogen pressure (100psi)

The SZr component is more sensitive to hydrogen pressure than is PtWZr in the hybrid system. At low hydrogen pressure, the decreased contribution of the SZr component exceeds the increase in PtWZr activity. The performance of the hybrid catalysts is better at 300 psi than at 100 psi. Characterization tests (SEM, XRD, BET and TPD) show that the hybrid catalysts prepared in this research are mechanical mixtures of the two components.

Conclusions

There are active interactions between the components in hybrid catalysts consisting of Pt-promoted tungstated zirconia and sulfated zirconia (PtWZr/SZr) in converting long-chain alkanes in a FT wax. Using PtWZr/SZr hybrid catalysts, an appropriate balance of hydroisomerization and hydrocracking functions can be achieved to increase yields of jet and diesel fuels. The component ratio and hydrogen pressure are important factors in affecting reactivities and selectivities of the hybrid catalysts.

References:

(1) Sie, S. T.; Senden, M. M. G.; Van Wechem, H. M. H. Catalysis Today 1991, 8, 371-394.
(2) Dry, M. E. Catalysis Today 1990, 6, 183-206.
(3) Iglesia, E.; Barton, D. G.; Biscardi, J. A.; Gines, M. J. L.; Soled, S. L. Catalysis Today 1997, 38, 339-360.
(4) Barton, D. G.; Soled, S. L.; Meitzner, G. D.; Fuentes, G. A.; Iglesia, E. Journal of Catalysis 1999, 181, 57-72.
(5) Arata, K. Advances in Catalysis 1990, 37, 165-212.

Future Work

This work is very promising in converting F-T wax to diesel and jet fuels. Although continuation of this work is highly desirable, our efforts during the next year will be concerned with the production and storage of hydrogen.

Papers Presented or Published

Z. Zhou, Y. Zhang, J. W. Tierney, I. Wender, "Producing Fuels from Fischer-Tropsch Process", Petroleum Technology Quarterly, Vol. 9 (1), P. 137-144, 2004

Z. Zhou, Y. Zhang, J.W. Tierney, I. Wender, "Hybrid Zirconia Catalysts for Conversion of Fischer-Tropsch Waxy Products to Transportation Fuels", Fuel Process Technology, Vol. 83, p.67-80, 2003

Presentation, "Anion-modified Zirconia Catalysts for Producing Clean Transportation Fuels from Fischer-Tropsch Wax", 42nd Pittsburgh-Cleveland Catalysis Society Symposium, Carnegie Mellon University, Pittsburgh, August 2004

Presentation, "Novel Catalysts for Producing Clean Transportation Fuels from Fischer-Tropsch Wax", Chemical Engineering Symposium, University of Pittsburgh, Pittsburgh, April 2004

Presentation, "Novel Catalysts for Hydroisomerization and Hydrocracking of Fischer-Tropsch Wax", AIChE National Meeting, New Orleans, Louisiana, April 2003 Presentation, "Environmentally Benign Catalysts for Producing Fuels", Particle Engineering Research Center, University of Florida, Gainesville, Florida, January 2003

Aerogel Supported Catalysts for Fischer-Tropsch Synthesis

Brian C. Dunn, Paul Cole, Dae-Jung Kim, Daniel Covington, Matthew C. Webster, Zhiru Ma, Ronald J. Pugmire, Greg Turpin, Yifan Shi, Richard D. Ernst, and Edward M. Eyring
Department of Chemistry, University of Utah, Salt Lake City, UT 84112

Introduction

CFFS sponsored research at the University of Utah in the 10/01/03 – 9/30/04 fiscal year was focused on synthesizing and characterizing improved catalysts for converting syngas to transportation fuels. Three research teams under the leadership of Professors Rick Ernst, Ted Eyring, and Ron Pugmire collaborated closely in this research. Toward the end of the fiscal year the three research teams consisted of the following personnel: Prof. Richard Ernst, Mr. Greg Turpin (graduate student), Mr. Yifan Shi (graduate student), Mr. Paul Cole (GC/MS technician); Prof. Edward M. Eyring, Dr. Brian C. Dunn (postdoc), Dr. Dae-Jung Kim (postdoc), Mr. Richard Gates (undergraduate research assistant), Mr. Matthew Webster (undergraduate research assistant); Prof. Ronald J. Pugmire, and Dr. Zhiru Ma (postdoc). All of these people collaborated in making and characterizing new heterogeneous catalysts that facilitate the reaction of carbon monoxide with hydrogen to produce hydrocarbons in the diesel fuel/kerosene range. This is called Fischer-Tropsch chemistry that was discovered in Germany about eighty years ago.1 The major advance at Utah during the 2003-2004 fiscal year was success in doping, by two complementary techniques, high surface area silica aerogels with nanoscale cobalt and ruthenium metal particles that have catalytic activity for the production of Fischer-Tropsch alkanes as well as alkenes.

Experimental Procedure

The first step in the experimental work at Utah is the synthesis of high porosity, high surface area silica supports for heterogeneous catalysts.2 A liquid sol is prepared by first mixing liquid tetraethoxysilane (TEOS) with ethanol. A solution of ethanol, water and ammonium hydroxide is added to this mixture and stirred to homogeneity. The mixture is poured into polypropylene cylindrical forms, and it gels in about five minutes. The gel is subsequently aged under ambient conditions for 14 days and then is bathed in absolute ethanol (with four repetitions) to replace all the water and ethanol inside the gel with pure ethanol. This is a branch point in the catalyst preparation.

If an ethanolic solution of cobalt(II) nitrate is loaded into the gel, one can fill an autoclave with the impregnated gel and the ethanolic cobalt(II) nitrate solution. (WARNING: care must be taken to exclude oxygen thus preventing an explosion. Purging of oxygen is accomplished by introducing 200 psi N2 ten times.) The autoclave is then heated under pressure to 1800 psi and 300 °C to exceed the critical point of ethanol (Pc = 926 psi, T_c = 243 °C). After one hour under supercritical fluid conditions, the gas pressure is vented to the atmosphere. This procedure for removing ethanol from the gel circumvents formation of capillary forces that would otherwise collapse the gel if a gas-liquid interface were permitted to exist inside the gel.3. This sort of supercritical drying produces a very low density cobalt doped aerogel that retains the original shape and size of the gel cast earlier in the polypropylene cylindrical form. The catalyst is then crushed, sieved for size, and the cobalt(II) in the gel is reduced to metallic cobalt in a stream of H_2 at 500 °C maintained for four hours. Several different physical methods have shown that

cobalt metal nanoparticles approximately 70 nm in diameter are scattered fairly uniformly through the resulting highly porous silica matrix.

Once aerogels have been synthesized, impregnated, crushed, and reduced in hydrogen gas at elevated temperatures, the next important experimental step is to verify their effectiveness as heterogeneous catalysts for Fischer-Tropsch production of hydrocarbons from syngas. A laboratory-scale packed bed reactor charged with 250 mg of catalyst is used in reaction product studies. Reactant gases and an argon internal standard are introduced into the reactor by three mass flow controllers. Iron carbonyl impurities in the CO reactant stream are removed by passing the CO through a tube containing PbO_2/Al_2O_3. The H_2:CO mole ratio is maintained at 2:1. The gas hourly space velocity of reactants is maintained either at ~500 hr-1 or ~250 hr-1 depending on catalyst activity requirements. A backpressure regulator maintains pressure inside the reactor at ~100 psi. Product gases are identified and quantified by gas chromatography (TCD and FID detectors) and by gas chromatography/mass spectrometry (GC/MS). Over the course of the 2003-2004 fiscal year it became clear that the GC/MS instrumentation (borrowed from the Henk Meuzelaar lab) yielded little information about reaction products of the Fischer-Tropsch reaction when used on-line that could not be deduced from GC measurements. An exception to this generalization is Paul Cole's deduction from GC/MS spectra of the presence of significant amounts of olefins in the reaction products under certain propitious reaction conditions. Arguably, the olefins could have been detected by GC without a mass spectrometric analyzer if the GC operator had been looking for unsaturated products.

Some of the "Results" that will be described below were obtained by CFFS collaborators at other universities. Their "Experimental Procedures" will not be described in this present annual report, but their results will be given and integrated into the story emerging from the experimental work done at Utah.

Results and Discussion

Silica Aerogel Catalyst Supports

One of the most exciting discoveries made in the CFFS sponsored research at Utah during 2003-2004 was the successful impregnation of silica aerogels from the gas phase using organometallic compounds of iron, cobalt, and/or ruthenium designed and synthesized in the Ernst lab. This discovery gave rise to an invention disclosure submitted to the University of Utah Technology Transfer office by Professor Ernst.

One of the most compelling attractions of impregnation from the gas phase is the possibility of introducing more than one catalytic element into the metallic nanoparticles scattered through the porous silica aerogel matrix. There is a growing body of experimental evidence4 that bimetallic or even polymetallic nanoparticles can be more effective catalysts for reactions such as Fischer-Tropsch synthesis of hydrocarbons than nanoparticles containing only one metallic element. Getting two or more metals into nanoparticles in silica aerogels from the gas phase appears to be more feasible than impregnation from a liquid solution.

In fact, a "redox targeting" approach has been developed, in which one metal is incorporated and oxidized, after which a second metal is introduced as a complex which can undergo a redox reaction with the first metal oxide, leading to a selective co-incorporation. As an example, once ruthenium has been deposited in an aerogel, it can be converted to a supported oxide. Exposure of the supported oxide to highly reducing cobaltocene vapor should lead to a redox reaction, and the generation of a cationic cobaltocene ion adjacent to the now-reduced ruthenium oxide. Notably, a 2%Ru/2%Co catalyst prepared in this manner has been found to be of comparable

activity to a 6% ruthenium catalyst. While ruthenium is well known5 to serve as an effective activator for cobalt catalysts, this example shows that cobalt can also be used to activate ruthenium; specifically, one sees that the added 2% cobalt serves as the equivalent of 4% ruthenium. When a less reducing cobalt complex, (cyclooctadiene)(cyclooctenyl)cobalt, was employed in place of cobaltocene, one still observed enhancement of the catalyst activity, but not nearly to the degree found for the latter, supporting the proposition that a redox-related targeting process was involved for cobaltocene, and was responsible for the higher activity.

There are two kinds of information arising from the CFFS studies of silica aerogel supported heterogeneous catalysts for Fischer-Tropsch chemistry. The first kind of information is that concerning the morphology and other physical characteristics of cobalt or ruthenium metal nanoparticle catalysts mounted on/in a high porosity glass with a prodigious surface area per gram of materials. The second kind of information is the identification and quantitation of hydrocarbon product molecules emerging from a packed-bed reactor loaded with catalysts that differ systematically in the amount and size of metal nanoparticles loaded on the silica aerogel support.

Transmission electron microscopy (TEM) images made by Shah and Huffman at Kentucky have shown that cobalt metal nanoparticles are larger than the mesopores of the silica aerogel network thus precluding sintering at elevated temperatures. This is good news for a prospective heterogeneous catalyst. The downside is that the 75 nm diameter cobalt metal spheres in a 6% cobalt loaded catalyst are about 10 times larger than those nanoparticles that have been found to be most active catalytically in other heterogeneously catalyzed reactions. Smaller metal nanoparticles would mean more exposed surface area per unit weight of metal available to catalyze reactions. The cobalt particles were well separated and uniformly distributed throughout the aerogel support for the solution impregnated catalysts. TEM and STEM studies of the gas-phase derived ruthenium catalysts revealed that at low loadings, one obtained well-dispersed, rather uniformly small and spherical particles, without evidence of any surface segregation. At higher loadings, one observes a mixture of these small, spherical particles together with much larger, needle-shaped particles.

The state of the cobalt prior to reduction was determined using temperature programmed reduction (TPR). With lower loadings of cobalt, two reduction steps were observed below 500 ºC which indicates the presence of Co_3O_4 which was reduced to CoO, and then to metallic cobalt.6 With higher mass loadings of cobalt, a third reduction step was observed at 700 ºC which was not seen in the other samples. This likely indicates the formation of cobalt silicate compounds which are very difficult to reduce.

The surface area, pore volume, and pore size distribution were determined with nitrogen adsorption. The surface area of all catalysts was ~800 m2 / g with pore volumes around 4 mL / g. Measurements of bulk density indicate that the pore volume is 6.2 mL / g which corresponds to a pore fraction of 96%. The difference in the results from the two methods of determining pore volume can be attributed to failure of N2 to condense in micropores during the nitrogen adsorption determination.7

Activity and selectivity results for nine catalysts are presented in Table 1. The catalysts using Co(NO3)2 as precursor were prepared by solution loading and all others were prepared by gas-phase incorporation. All catalysts showed Fischer-Tropsch activity with production of hydrocarbons up to C16. The space velocity during the catalytic tests was 2-fold higher for the gas-phase incorporated catalysts which decreases the apparent CO conversion when compared with the solution loaded samples. The CO conversion was directly related to the amount of

active metal, either Co or Ru, as expected. The amount of hydrocarbons produced as olefins was not expected. The 6% Ru and 10% Ru each yielded around 30% of C10-C14 hydrocarbons as the olefinic species. This is likely due to the large mass transport within a catalyst particle that is possible because of the mesoporous nature of the aerogel support. Another notable result is that the 6% Ru and 2% Ru/2% Co from Ru(dmp)2/Co(Cp)2 had very similar activities (dmp = 2,4-dimethylpentadienyl). This indicates that the two step "redox targeting" has been successful in creating a more effective catalyst than would be obtained from a single metal loading step. Further support for the "redox targeting" scenario comes from the observation of higher reactivity observed for a 10% cobalt catalyst produced via a two (rather than one) step incorporation procedure.

Table 1. Fischer-Tropsch activity and selectivity for silica aerogel supported catalysts.

Catalyst	Precursor	CO Conversion %[a]	C10+ Selectivity %	Average Olefin Fraction %
2% Co	Co(NO3)2	5	30	40
6% Co	Co(NO3)2	20	43	7
10% Co	Co(NO3)2	22	49	7
6% Ru	Ru(dmp)2[b]	6	29	31
10% Ru	Ru(dmp)2	10	27	27
10% Co	Co(cod)2[c]	6	16	4
10% Co (5+5)	Co(cod)2/Co(Cp)2d	10	16	4
2% Ru/2% Co	Ru(dmp)2/Co(cod)2	4	14	15
2% Ru/2% Co	Ru(dmp)2/Co(Cp)2	7	14	5

[a]Temperature was 265 ºC, space velocity was 250 hr-1 for Co(NO3)2 loaded, 500 hr-1 for others.
[b]Ru (dmp)2 is bis(2,4-dimethylpentadienyl)ruthenium.
[c]Co(cod)2 is (cyclooctadiene)(cyclooctenyl)cobalt.
[d]Co(Cp)2 is bis(cyclopentadienyl)cobalt.

Chris Roberts' group at Auburn has also studied the 10% Ru on silica aerogel catalyst under supercritical conditions with hexane as solvent (44 bar total, 30 bar hexane, 2:1 H_2/CO), at 230 and 250 ºC. Under some conditions, conversions exceeding 65% were achieved, with detectable products nearly up to the C30 range. The chain growth probability (□) values were observed to range from ca. 0.73-0.83; notably, after 49 hours of run time at 250 ºC, the □ value increased from 0.73 to 0.83. Olefin selectivities could be as high as 35-50% for mid-range products in runs at 230 ºC.

Collaborative studies with other groups in the Consortium have provided important insight into the metal-aerogel support interactions. The initial, presumably single-site, metal species obtained via gas phase incorporation using metal pentadienyl sources are typically pyrophoric, revealing a very weak metal-support interaction. TEM studies carried out by Shah and Huffman of subsequently reduced ruthenium catalysts show substantial agglomeration, which is not

surprising based on observations with other supports. However, agglomeration is even observed for cobalt oxide species prior to any reduction, based upon the observations by Seehra and Dutta of the lack of any ESR signal despite clear sample paramagnetism. Additionally, attempts by Huggins and Huffman to obtain Mössbauer spectra of the iron-derived species have been unsuccessful at room temperature. These studies together provide a compelling case that the coordination environment(s) available on aerogel supports are rather ineffective towards metals. This conclusion has recently been bolstered by the observation that at least the initial aerogel-supported ruthenium complex reacts directly with hydrogen. This could lead to distinctly different catalyst sites than would be obtained by a two step oxidation/reduction regime.
Solid state NMR studies have also provided some noteworthy results. Interestingly, 13C NMR studies of aerogel-supported Fe(C5Me5) units, derived by reaction of Fe(C5Me5)(pentadienyl) complexes with aerogel surface hydroxyl groups, indicate that two unique coordination environments are available. It is not yet clear whether the more air-sensitive aerogel-supported Fe(C5H5) analogues also reside in multiple coordination environments. Based on solid state 13C NMR powder pattern experiments, both ferrocene and ruthenocene exhibit rapid tumbling within the aerogel structure on a time scale equivalent to that observed in liquid and gaseous states. As a result of this motion, the metal complexes would be widely distributed throughout the aerogel pores. Hence, when reduction occurs one might expect that the reduced metal particles would also be somewhat dispersed. This assumption is supported by TEM data from the University of Kentucky wherein the images indicate reasonable metal dispersion as well as relatively small particle size.
The fact that more than one coordination environment might be available to the aerogel-bound organometallic species suggests that XAFS/XANES studies could be very complicated. However, at least for ferrocene- and cobaltocene-derived samples, the Huffman group was able to obtain clean spectra which were entirely different from ones obtained from iron or cobalt oxide samples. Quite strong, well-defined M-C peaks were observed, reflecting very regular (symmetric) M-C coordination in each case. Oxidation of these samples led to spectra with clearly defined M-O peaks, but relatively weak M-M peaks, reflecting a high degree of sample dispersal. More recently, XAFS/XANES data for a variety of analogous ruthenium samples have also been obtained, and are being analyzed.

Zeolitic Catalyst Supports

MCM-41 and SBA-15 are two types of mesoporous silica which possess an ordered, periodic structure much like a zeolite. This regular structure is vastly different from the random, amorphous nature of the silica aerogel, however, the pore sizes of both types fall into the mesoporous (2-50 nm) regime. SBA-15 and MCM-41 have a narrow pore size distribution which may influence the Fischer-Tropsch product selectivity. The question addressed by the study described below is the following: Does the regular structure of a zeolite material have the usual advantage of molecular sieves of producing a narrower range of product molecule chain lengths in a Fischer-Tropsch synthesis than has been observed to date with silica aerogel supports?

Eight cobalt catalysts supported on structured mesoporous silica were prepared to investigate the effects of pore structure, impregnation method, solvating agent, and cobalt loading on carbon monoxide conversion and hydrocarbon selectivity. Furthermore, we modified the mesoporous silica via a silylation method to yield highly reducible cobalt oxide which may improve Fisher-Tropsch synthesis activity. The Fisher-Tropsch synthesis results are listed in

Table 2. The 3CAT sample shows higher C5+ selectivity and chain growth probability than the 1CAT sample. TPR indicates that the 1CAT sample had a reduction peak at 890 ºC which was not observed in the 3CAT sample, indicating the 1CAT sample had more irreducible cobalt oxides than the 3CAT sample. The average pore sizes of the 1CAT and 3CAT samples were 2.65 nm and 8.08 nm, respectively. Accordingly, differences in the irreducible cobalt oxides and pore size may lead to differences in C5+ selectivity and chain growth probability.

Table 2. Fischer-Tropsch synthesis results of cobalt loaded structured mesoporous silica catalysts.

Sample	Silica	Precursor	Co Loading	Loading Method[a]	CO Conversion %	C5+ Selectivity %	α^c
1CAT	MCM-41	$Co(NO_3)_2$	6	IW	17	46	0.82
2CAT	SBA-15	$Co(NO_3)_2$	3	IW	8	66	0.87
3CAT	SBA-15	$Co(NO_3)_2$	6	IW	18	72	0.90
4CAT	SBA-15	$Co(NO_3)_2$	20	IW	36	62	0.77
5CAT	SBA-15	$Co(ac)_2$[b]	6	PS	5	40	0.85
6CAT	SBA-15	$Co(Cp)_2$	6	GP	8	48	0.82
7CAT	SBA-15	$Co(NO_3)_2$	6	IW	2	6	0.74
8CAT	Silylated SBA-15	$Co(Cp)_2$	6	GP	9	79	0.88

[a]IW is incipient wetness; PS is post synthesis; GP is gas phase.
[b]Co(ac)2 is cobalt acetate.
[c]α denotes chain length probability calculated from the Anderson-Schultz-Flory distribution.

The increase in cobalt loading gives rise to increases in carbon monoxide conversion, but at cobalt loading over 6 wt%, C5+ selectivity and chain growth probability decrease. The nitrogen adsorption results showed that BET area and pore volume were significantly decreased by the increase in cobalt loading. This suggests that the pores of highly loaded cobalt 4CAT have been blocked and some cobalt oxides may exist on the outer surface of the support. The decrease in C5+ selectivity and chain growth probability with the increase of cobalt loading may be attributed to the significant change of pore structure and cobalt oxides on the outer surface.

The 3CAT sample shows the highest carbon monoxide conversion, C5+ selectivity and chain growth probability among the samples (3CAT, 5CAT, 6CAT) obtained by three different impregnation methods, incipient wetness, post synthesis and gas phase deposition. The three samples showed similar values in BET surface area and pore volume. TPR of cobalt oxides in the 30 ºC to 450 ºC range for the three samples, however, was very different. The 3CAT sample had much higher reduction of cobalt oxides than the other samples and overall reduction of cobalt oxides on the 3CAT sample was complete at lower temperature than the 5CAT and 6CAT samples. The differences in extent and temperature of reduction may contribute to the differences between the three samples in carbon monoxide conversion, C5+ selectivity, and chain growth probability.

The 3CAT sample shows higher values in carbon monoxide conversion, C5+ selectivity and chain growth probability than the 7CAT sample. The 3CAT sample was prepared from ethanol while the 7CAT sample was prepared from butanol with all other parameters remaining identical. This result indicates that the Fischer-Tropsch synthesis activity is influenced by the solvating agent of the cobalt precursor, and use of ethanol as solvent gives rise to the lowest amount of irreducible cobalt oxides.

In this study, we used hexamethyldisilazane as the agent for silylation of SBA-15. The 8CAT sample with silylation shows much higher values of carbon monoxide conversion, C5+ selectivity, and chain growth probability than the 6CAT sample without silylation. This result indicates that silylation strongly reduces the number of interacting silanol groups and gives more easily reducible cobalt oxides on the surface of the SBA-15.

The major conclusion of the zeolitic catalyst support study are that the regular structure of the support does not yield a narrower distribution of diesel range Fischer-Tropsch hydrocarbons, but distinct advantages in hydrocarbon yield arise from silylation of the zeolitic catalyst support.

Conclusions

High surface area, mesoporous silica aerogel can serve as a support for both cobalt and ruthenium based heterogeneous catalysts. Cobalt exists as discrete nanoparticles about 70 nm in diameter that are larger than the average pore size. The incorporation of Co(NO3)2 into the preparation scheme does not significantly alter the morphological properties of the silica aerogel support as indicated by measurements of surface area, pore size, and pore volume. The supercritical ethanol processing conditions required to synthesize the catalysts results in transformation of the $Co(NO_3)_2$ into Co_3O_4 which can be reduced in hydrogen to CoO and which can be further reduced to metallic cobalt. Higher mass loadings of cobalt result in formation of cobalt silicates that do not reduce at temperatures less than 700 ºC. Both gas-phase and solution incorporation of cobalt or ruthenium precursors give rise to catalysts which are active towards Fischer-Tropsch synthesis with single-pass CO conversions as high as 20% and selectivities towards the diesel fuel fraction, C10+, as high as 40%. Significant amounts of olefins that were produced with certain catalysts may be a direct result of the mesoporosity of the aerogel support. "Redox targeting" of catalyst precursors appears to offer some benefit when compared with single stage incorporation. The use of zeolitic catalyst supports does not offer the advantage of substantially greater yields of diesel range fuels that would offset the greater cost of these catalyst supports than the probable cost of aerogels produced on an industrial scale.

Papers Published or Presented

1. Dunn, B. C.; Covington, D. J.; Cole, P.; Pugmire, R. J.; Meuzelaar, H. L. C.; Ernst, R. D.; Heider, E. C.; Eyring, E. M., "Silica Xerogel Supported Cobalt Metal Fischer-Tropsch Catalysts for Syngas to Diesel Range Fuel Conversion," Energy & Fuels, 2004, 18, 1519-1521.
2. Dunn, B. C.; Cole, P.; Covington, D. J.; Webster, M. C.; Pugmire, R. J.; Ernst, R. D.; Eyring, E. M.; Shah, N.; Huffman, G. P., "Silica Aerogel Supported Catalysts for Fischer-Tropsch Synthesis," Applied Catalysis A, in press.

3. Dunn, B. C.; Cole, P.; Turpin, G. C.; Ma, Z.; Pugmire, R. J.; Ernst, R. D.; Eyring, E. M.; Shah, N.; Huffman, G. P., "Silica Aerogel Supported Catalysts for Fischer-Tropsch Synthesis," 227th ACS National Meeting, March 28 - April 1, 2004, Anaheim, CA.

4. Ma, Z.; Dunn, B. C.; Turpin, G. C.; Cole, P.; Eyring, E. M.; Ernst, R. D.; Pugmire, R. J. "Solid State NMR Investigation of Fischer-Tropsch Catalysts," 45th Experimental Nuclear Magnetic Resonance Conference (ENC), April 18 - 23, 2004, Pacific Grove, CA.
5. Eyring, E. M.; Dunn, B. C.; Cole, P.; Turpin, G. C.; Ma, Z.; Pugmire, R. J.; Ernst, R. D.; Shah, N.; Huffman, G. P. "Silica Aerogel Supported Catalysts for Fischer-Tropsch Synthesis," Joint Regional Meeting of the Northwest and Rocky Mountain Sections of the American Chemical Society, June 6-9, 2004, Logan, UT.
6. Dunn, B. C.; Turpin, G. C.; Cole, P.; Webster, M. C.; Ma, Z.; Pugmire, R. J.; Ernst, R. D.; Eyring, E. M.; Shah, N.; Huffman, G. P., "Cobalt and Ruthenium Fischer-Tropsch Catalysts Supported on Silica Aerogel," 228th ACS National Meeting, August 22-26, Philadelphia, PA.

Future Work

Using similar preparation methods as those described above, high surface area, mesoporous catalysts for the water-gas shift (WGS) reaction will be synthesized, characterized, and evaluated for catalytic activity. Catalysts supported on silica are not active towards WGS, but Cu, Pd, or Au supported on ceria have been shown to be effective.8,9 Ceria aerogel will be synthesized in an analogous fashion to the silica aerogel described above starting with cerium(IV) methoxyethoxide in place of TEOS. Incorporation of catalytic metals from both the gas-phase and from solution will be explored. The pure ceria aerogels can only be catalytically effective at lower temperatures (150 – 250 ºC) due to the tendency of ceria aerogel to densify above 300 ºC and lose the bulk of its surface area and pore volume. To circumvent this limitation, volatile and very hydrolytically-sensitive cerium(IV) alkoxides can be deposited on preformed silica aerogel frameworks. The silica will lead to thermally stable structures while the catalytic metals on the ceria layer will promote the WGS reaction.

References

(1) Fischer, F.; Tropsch, H. Brennst. Chem. 1923, 4, 276-285.
(2) Husing, N.; Schubert, U. Angew. Chem. Int. Ed. 1998, 37, 22-45.
(3) Casula, M. F.; Corrias, A.; Pashina, G. J. Sol-Gel Sci. and Tech. 2003, 26, 667-670.
(4) Guczi, L.; Borko, L.; Schay, Z.; Bazin, D.; Mizukami, F. Catalysis Today 2001, 65, 51-57.
(5) Price, J. G.; Glasser, D.; Hildebrandt, D.; Coville, N. J. Studies in Surface Science and Catalysis 1997, 107, 243-248.
(6) Jacobs, G.; Das, T. K.; Zhang, Y.; Li, J.; Racoillet, G.; Davis, B. H. Appl. Catal. A 2002, 233, 263-281.
(7) Scherer, G. W. Advances in Colloid and Interface Science 1998, 76-77, 321-339.
(8) Fu, Q.; Saltsburg, H.; Flytzani-Stephanopoulos, M. Science 2003, 301, 935-938.
(9) Qi, X.; Flytzani-Stephanopoulos, M. Ind. Eng. Chem. Res. 2004, 43, 3055-3062.

DEVELOPMENT OF ACTIVATED-CARBON-SUPPORTED, MOLYBDENUM-PROMOTED CATALYSTS FOR DIESEL FUEL SYNTHESIS

Wenping Ma, Edwin L. Kugler, Huifang Shao, James Wright and Dady B. Dadyburjor
Department of Chemical Engineering,West Virginia University, Morgantown, WV 26505

INTRODUCTION

It is well known that the Fischer-Tropsch synthesis (FTS) provides an alternative way to convert coal indirectly to transportation fuels. The traditional industrial catalysts used for this reaction are precipitated iron and silica-supported cobalt catalysts, which are used commercially in South Africa and Malaysia [1-2]. These two types of Fischer-Tropsch catalysts produce a broad-range of hydrocarbons, which need to be further treated to yield liquid diesel fuels. In order to simplify conventional FTS technology and to lower the capital cost of the diesel fuels, selective FTS catalysts have been suggested, on which medium-molecular weight hydrocarbons (mainly diesel fuels) are expected to be directly formed from syngas [3-4]. Hydrocarbon chain growth can be limited over iron and cobalt catalysts supported on activated carbon (AC) and on carbon nanotube supports, indicating that carbon material may be a good choice for limiting hydrocarbon chain length to a certain range.

We have been working on AC-supported Mo catalysts since 1991. Mo-Ni-K/AC catalysts have been successfully used for synthesis of high-molecular-weight alcohols [5, 6]. These studies also demonstrated that AC-supported catalysts are able to produce hydrocarbons with limited carbon numbers, e.g. less than C6. In the current work, we focus on molybdenum-promoted AC-supported iron catalysts for the synthesis of liquid hydrocarbons. The effects of molybdenum on catalyst activity, selectivity and stability have been determined. In addition, we have studied the effect activated-carbon type on the stability and selectivity of Mo-Fe catalysts for synthesis of diesel fuels.

EXPERIMENTAL

Catalyst Synthesis. Four types of activated carbon were used as catalyst supports: one from peat, one from pecan shells, one from walnut shells and the last from generic wood. Activated carbon from peat was supplied by Sigma-Aldrich; AC from wood by Norit, and the AC's from pecan and walnut shells were provided by the US Department of Agriculture. All four AC's were washed in hot, distilled water, calcined at 500 ºC for 2 h in flowing N2, and ground to 20-40 mesh. Table 1 lists surface area and pore volume properties of the carbon supports. Supported Fe-Cu-K catalysts with or without Mo were prepared using sequential incipient wetness impregnation. If Mo was required, then an appropriate amount of aqueous ammonium molybdate solution was impregnated first onto the AC support. The material was then dried in air at 90-100 ºC overnight. An aqueous solution containing ferric nitrate and cupric nitrate corresponding to final iron and copper contents on the catalyst of 15.7 wt% and 0.8 wt%, respectively, was impregnated onto either fresh support or the Mo/C sample, again followed by drying in air at the same temperature overnight. Potassium nitrate solution (corresponding to 0.9 wt% K) was the last additive to be put onto the sample, again followed by drying in air at 90-100 ºC overnight.

Catalyst Testing in a Fixed-bed Reactor. Catalysts were tested in a computer-controlled fixed-bed-reactor system. A detailed description has been published previously [7]. For the current

study, reaction gases were pre-mixed syngas ($H_2/CO = 0.9$) containing 5% He as an internal standard, high-purity hydrogen and high-purity helium. After leaving the reactor, the exit gases passed through a product trap to recover liquid hydrocarbons. The uncondensed gases went to either a bubble flow meter or a GC for online analysis. The runs in this study lasted for 72-400 hours on stream.
Typically, 1.0 g (20-40 mesh) of catalyst was placed into the reactor. To minimize axial temperature gradients, the catalyst was diluted with 4.0 g of quartz chips of the same size. The catalyst reduction conditions were 400 ºC, 76 psig, and 3 Nl/g-cat/h for 12 h by H_2, and reaction conditions were 310-320 ºC, 300 psig, 3 Nl/g-cat/h, and $H_2/CO = 0.9$.

Product Analysis. Inlet and outlet gases were analyzed on-line by gas chromatography (GC) using a HayeSep DB column for fixed gases and a DB-5 column for hydrocarbons. The organic-liquid phase (C4-C34 hydrocarbons) was analyzed by GC using an MXT-5 capillary column; the water-phase product was analyzed by GC using a Porapak-Q packed column. The alcohols in the water phase were quantified using tert-amyl alcohol as an internal standard.

RESULTS AND DISCUSSION

Effect of Mo loading on catalyst activity, stability and selectivity. Supported Fe-Cu-K catalysts were prepared with 0, 6 and 12wt % Mo to evaluate the effects of Mo loading. The support was activated carbon from peat. The effect of catalyst composition on CO conversion is shown in Figure 1. A catalyst without molybdenum deactivated rapidly. CO conversion dropped from 97 to 51 % during a 72-hour test at 320 ºC. A catalyst containing 6% Mo in addition to 15.7% Fe, 0.8% Cu and 0.9% K showed just the opposite effect. Its CO conversion activity increased from 60 to 90% over the first 72 hours at 320 ºC and then remained stable for the next 72 hours. After 144 hours on-stream, the temperature was lowered 310 ºC with the result that CO conversion decreased slowly with time. Conversion after 312 h was 76%. Reaction temperature was increased to 320 ºC to see if the catalyst regained its prior activity. Increasing the temperature reversed deactivation and caused an increase in CO conversion from 312 to 360 hours-on-stream. Finally the catalyst was cooled to 310 ºC with the result that it returned to 76% conversion as observed after 312 hours. In case of 12% Mo with 15.7% Fe, 0.8% Cu and 0.9% K, the catalyst began with 64% CO conversion and decreased slowly to 55% conversion after 143 hours. Decreasing the temperature to 310 ºC caused the CO conversion to drop to 40% and to continue the slow deactivation observed at the higher temperature.

Changes of CH4 and C5+ selectivity with time-on-stream are shown in Figure 2a-b. Adding Mo to a Fe-Cu-K/ Peat AC catalyst affected primarily CH_4 selectivity. The catalyst with 0% Mo produced 6 - 8% CH4 during 72 hours of testing at 320 ºC. Catalysts with Mo showed 11 – 14% CH4 selectivity at the same temperature. All three catalysts tested showed C5+ selectivity of approximately 50%. However, the liquid-product yield of the Mo-Fe-Cu-K catalyst with 6% Mo was the highest since it had the highest (and most stable) conversion.

Representative hydrocarbon distributions for the Mo-Fe-Cu-K/Peat AC catalysts are shown in Figure 3. The hydrocarbon distribution up to C34 can be described by single □using the Anderson-Schulz-Flory distribution law (Wn/n = □n-1(1-□)2). The chain-growth probability, □is similar for all three catalysts. This suggests that hydrocarbon chain growth was primarily influence by Fe-Cu-K and the carbon support. The Mo promoter affected catalyst stability.

Effect of Activated-Carbon Source on Catalyst Performance. The catalyst composition was fixed at 6.0% Mo, 15.7t% Fe, 0.8% Cu and 0.9% K to study the effect of carbon-support type on

catalyst performance. Figure 4 shows CO conversion with time-on-stream for catalysts on four different activated-carbon supports. The activated carbons were produced from peat, pecan shells, walnut shells and wood. Catalysts using the peat and pecan-shell activated carbons were tested at both 310 and 320 ºC, whereas the catalysts supported on wood and walnut-shell activated carbons were tested at 320 ºC only. Catalyst size (1.0 g) and process conditions (300 psig, 3 Nl-g-cat/h and $H_2/CO = 0.9$) were maintained the same during the test periods.

All four catalysts exhibit instabilities at the start of the test runs. The CO conversion activity with peat and pecan-shell AC increases with time over the first 72 hours, before reaching constant activity. In contrast, the CO conversion activity with wood and walnut-shell charcoal decreases for the first 48 hours. After 48 hours on stream, the activity of the walnut-shell AC supported catalyst shows an increase in activity. The wood AC supported catalyst continues to deactivate slowly. Because all four tests are run at the same reaction conditions, it can be concluded that the catalyst using wood AC is the least active, while the catalysts using peat and pecan-shell AC are the most active. The temperature was lowered to 310 ºC with both the peat and pecan-shell AC catalysts. Dropping the temperature causes both catalysts to deactivate slowly.

Changes of CH_4 and C5+ selectivity with time-on-stream catalysts with the four carbon supports are shown in Figure 5a-b. At 320 ºC, methane selectivity with the walnut and pecan-shell AC supports is nearly the same (13-15%) at steady state. Methane selectivity with the wood-AC support is lower than with pecan and walnut-shell AC. Methane selectivity is the lowest for the peat-AC support between 30 and 90h (10-11.6%), but increases with time reaching 14 % at 120 h. When the reaction temperature is lowered to 310 ºC, methane selectivity on both the peat and pecan-shell AC supports are similar, decreasing to about 11.8 %. Effect of carbon-support type on C5+ selectivity is different from methane selectivity. At 320 ºC, C5+ selectivity on pecan and walnut-shell AC supports are similar and higher than that of peat. The wood AC support shows the poorest C5+ selectivity during 94 h of testing. At 310 ºC, C5+ selectivity increases for both the pecan-shell and peat AC supports, with the pecan-shell AC support having the better C5+ selectivity.

CONCLUSIONS

An Fe-Cu-K catalyst supported on peat AC shows high initial activity, but deactivates rapidly. Catalyst stability is improved significantly by addition molybdenum to produce Mo-Fe-Cu-K/AC with 6% Mo loading.

Carbon-support type affects both catalyst activity and selectivity. Pecan-shell and peat activated carbon supported catalysts are the most active and have better C5+ selectivity. The catalyst with the walnut-shell AC support has good C5+ selectivity, but is not as active as catalysts with peat and pecan-shell AC supports. The catalyst using a wood AC support is the least active and has the lowest C5+ selectivity. Good catalyst performance with peat and pecan-shell activated carbons may relate to their pore structures since both have significant mesopore and macropore volumes.

PAPERS PRESENTED OR PUBLISHED

"Effect of Type of Activated Carbon Support on Catalytic Behavior of Mo-Fe Catalysts for Fischer-Tropsch Synthesis in a Fixed-Bed Reactor," W. P. Ma, E. L. Kugler and D. B. Dadyburjor, Pittsburgh-Cleveland Catalysis Society Meeting, June 18, 2004

"Effect of Type of Activated Carbon Support on Catalytic Behavior of Mo-Fe Catalysts for Fischer-Tropsch Synthesis in a Fixed-Bed Reactor," W. P. Ma, E. L. Kugler and D. B. Dadyburjor, CFFS Annual Meeting, Roanoke, WV, August 1-4, 2004

Wen-Ping Ma, Edwin L. Kugler, and Dady B. Dadyburjor, "Effect of Mo loading and support type on oxygenates produced during Fischer-Tropsch Synthesis Over Fe-Mo-Cu-K catalyst supported on Activated Carbon", Fuel Chemistry Division Preprints, 2005, in press.

FUTURE WORK

We plan to focus our Fischer-Tropsch work on characterizing Fe-Mo-Cu-K/AC catalysts. Both fresh and spent catalysts are being characterized with regard to their surface area and pore volume distributions, crystalline phases present (x-ray diffraction), physical aggregation (electron microscopy), and chemical environment of catalytic metals (EXAFS). Future reaction studies will focus on minimizing CH4 selectivity while improving C5+ selectivity.

REFERENCES

[1] Dry M. E. Catal. Lett. 1991, 7: 241.
[2] Eilers J., Posthuma S. A., Sie S. T. Catal. Lett. 1991, 7: 253.
[3] Venter J. J., Kaminsky M., Geoffroy G. L., Vannice M. A. J. Catal. 1987, 103: 450.
[4] Steen E. van, Prinsloo F. F. Catal. Today 2002, 71: 327.
[5] Kugler, E.L., Feng, L., Li, X., Dadyburjor, D.B. Studies in Surface Science and Catalysis. 2000, 130A: 299-304.
[6] Li, X.G., Feng, L.J., Liu, Z.Y., Zhong, B., Dadyburjor, D.B., Kugler, E.L. Ind. Eng. Chem. Res. 1998, 37, 3853.
[7] Donnell T.J., Satterfield C.N., Appl. Catal. A 1989, 52: 93.

Table 1. Properties of Activated Carbon Catalyst Supports

AC Type	BET S.A. (m2/g)	Meso- plus Macro-pore Volume (cm3/g)	Micropore Volume (cm3/g)	Ave Pore Size (Å)
Peat	606	0.26	0.22	59.2
Wood	970	0.14	0.44	66.3
Pecan	1016	0.36	0.36	51.0
Walnut	892	0.18	0.32	38.6

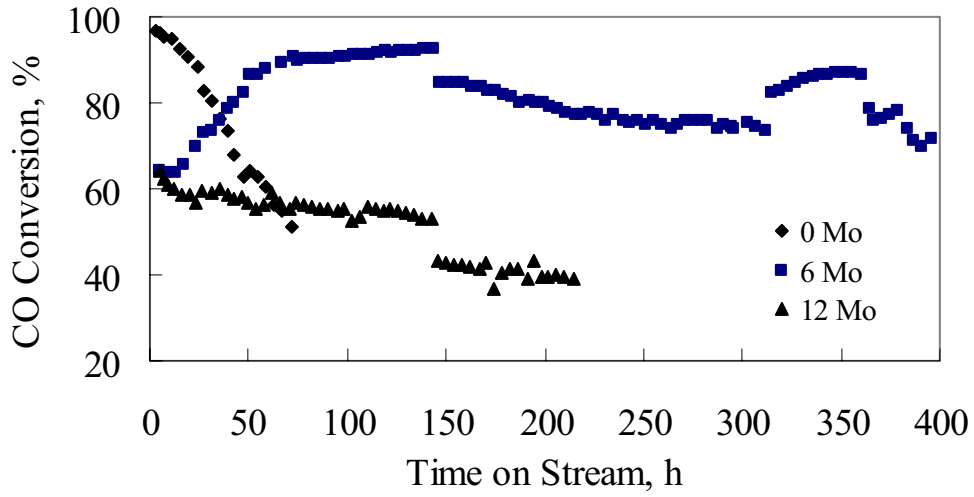

Figure 1. Effect of Mo addition on CO conversion for a Fe-Cu-K/Peat-AC catalyst. Reaction Conditions: 300 psig, 3Nl/g-cat/h, $H_2/CO = 0.9$ and

0 Mo: 0-72h, 320 ºC

6 Mo: 0-144 h and 313-360h, 320 ºC; 145-312 h and 361-396h, 310 ºC,

12 Mo: 0-143 h, 320 ºC; 144-215 h, 310 ºC.

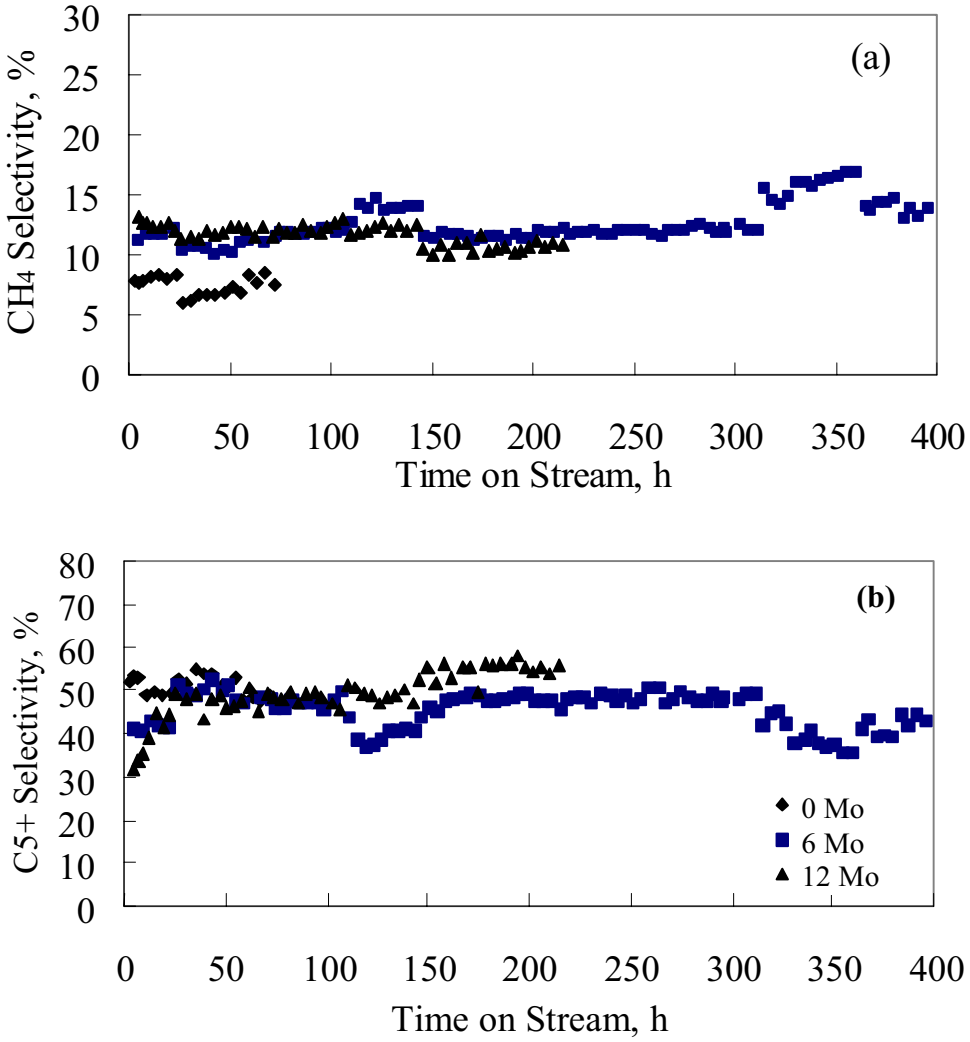

Fig. 2. Effect of Mo loading on (a) methane selectivity and (b) C5+ selectivity for Fe-Cu-K/Peat-AC catalyst
Reaction Conditions: 300 psig, 3Nl/g-cat/h, $H_2/CO = 0.9$ and
0 Mo: 0-72h, 320 ºC,
6 Mo: 0-144 h and 313-360h, 320 ºC; 145-312 h and 361-396h, 310 ºC,
12 Mo: 0-143 h, 320 ºC; 144-215 h, 310 ºC.

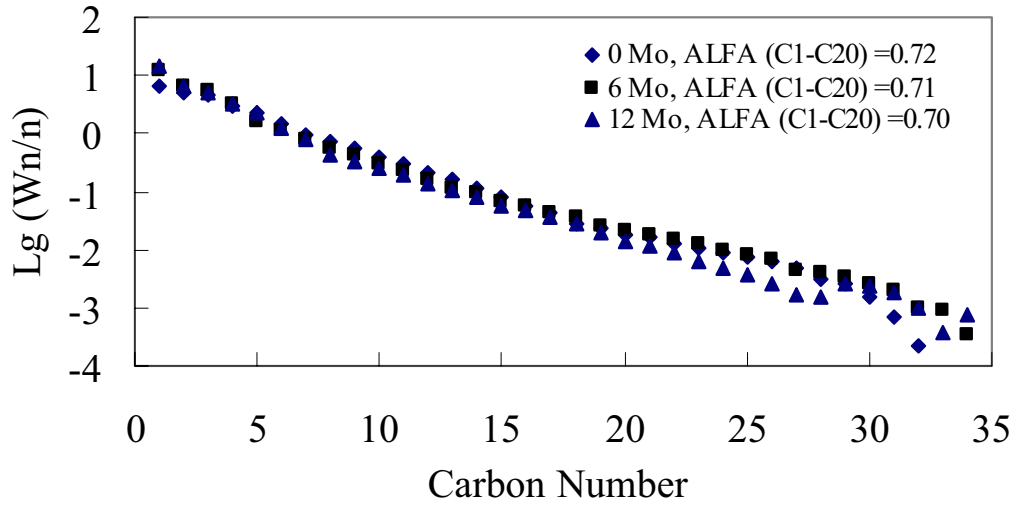

Fig. 3 Overall hydrocarbon distribution on Mo-Fe-Cu-K/AC catalysts (320 ºC, 300 psig, 3Nl/g-cat/h, H_2/CO = 0.9, 47-73 h).

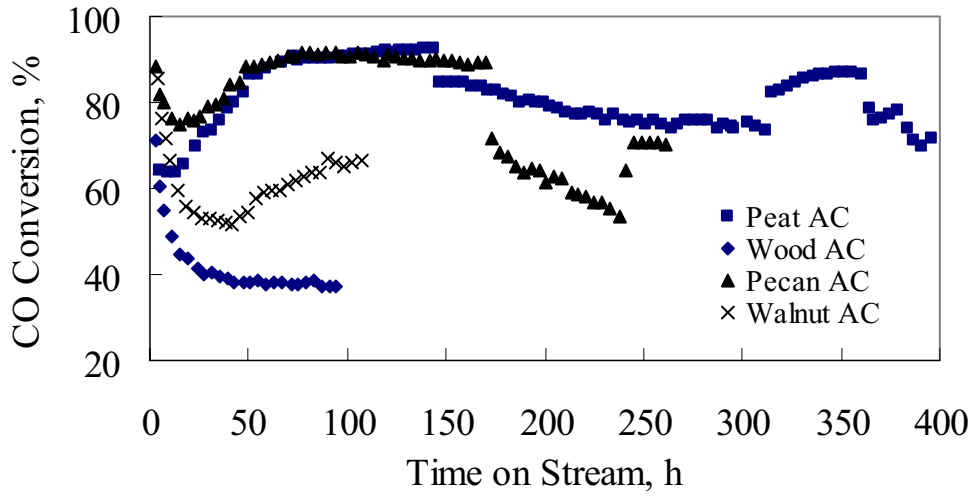

Fig. 4. Effect of carbon support type on CO conversion for Mo-Fe-Cu-K catalysts
Reaction conditions: 300 psig, 3Nl/g-cat/h, H_2/CO = 0.9 and
Peat AC: 0-144 h and 313-360 h, 320 ºC; 145-312 h and 361-396 h, 310 ºC,
Wood AC: 0-94 h, 320 ºC,
Pecan-Shell AC: 0-170 h and 238-262h, 320 ºC; 170-238 h, 310 ºC,
Walnut-Shell AC: 0-107 h, 320 ºC

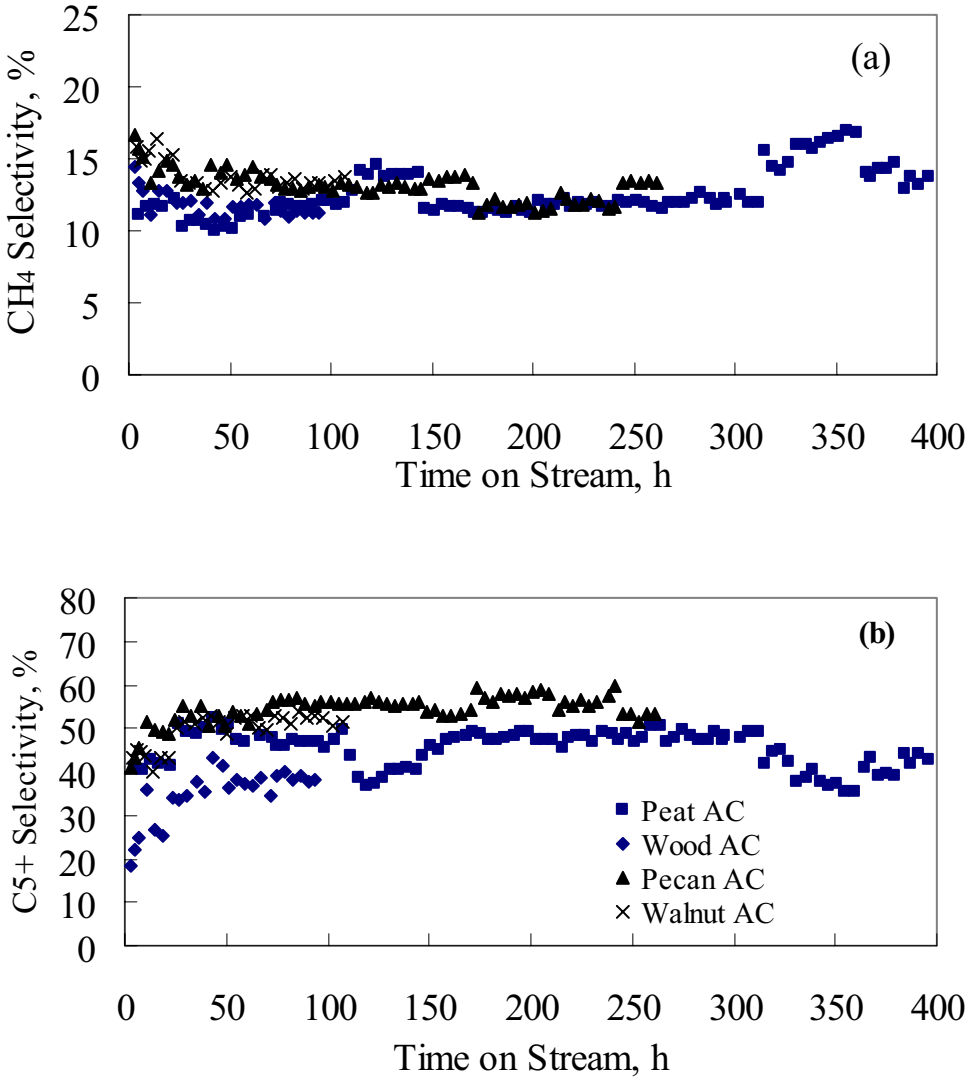

Fig. 5. Effect of carbon support type on (a) methane selectivity and (b) C5+ selectivity for Mo-Fe-Cu-K catalysts
Reaction conditions: 300 psig, 3Nl/g-cat/h, $H_2/CO = 0.9$ and
Peat AC: 0-144 h and 313-360 h, 320 ºC; 145-312 h and 361-396 h, 310 ºC,
Wood AC: 0-94 h, 320 ºC,
Pecan-Shell AC: 0-170 h and 238-262h, 320 ºC; 170-238 h, 310 ºC,
Walnut-Shell AC: 0-107 h, 320 ºC.

Production of Light Olefins and Chemicals from Syngas

James A. Guin, Xiwen Huang, Luckner Jean
Auburn University, AL 36849

Introduction

There are many incentives to promote technology development in the conversion of natural gas and coal to valuable products due to vast worldwide reserves. Production of light C2- C4 olefins via C-1 chemistry is attractive due to its great significance in the production of clean transportation fuels, as well as chemical intermediates for a number of important industrial and consumer products. We have studied two routes for the production of these materials from syngas: (1) Conversion of syngas first to methanol and then methanol conversion to olefins. Here we have been focusing on the development of various modified SAPO series catalysts for the MTO process, and have found that, many modified SAPO catalysts synthesized in our lab demonstrated excellent reactivity (methanol conversions up to 100%) and selectivities to C2-C4 olefins. We are currently studying the ways to improve the SAPO yields, lifetime, and selectivities by metals addition, in cooperation with Dr. Ernst's group at Utah, and by manipulating the SAPO particle sizes. (2) Conversion of syngas to olefins in a single reactor using a hybrid catalyst system consisting of a methanol synthesis catalyst followed by a SAPO catalyst in the same reactor. The hybrid catalyst system is composed of a commercial methanol synthesis catalyst C-79 ($CuO/ZnO/Al_2O_3$) and a SAPO catalyst using both follow-bed and mixed bed systems for syngas conversion. In our previous six months report, we showed our hybrid catalyst syngas reaction system for conversion of syngas to olefins and we compared the CO hydrogenation behavior on SAPO-34, C-79 methanol synthesis catalyst alone, and the hybrid C-79/SAPO-34 catalyst systems. We showed that CO conversions and C2-C4 light olefins selectivity could be significantly increased by employing the hybrid catalyst system as compared to either catalyst alone. In this report, additional study of process variables such as temperature, pressure, CO/H_2 ratio on the C-79/SAPO-34 catalyst system performance is reported.

Experimental Procedure

Catalyst preparation and pretreatment. SAPO catalyst samples prepared by Dr. P. M. Adekkanattu as reported in our previous publications [5,6] were used in the current study. A commercial MeOH catalyst, C-79, was obtained from SUD-CHEMIE Company with the composition: 55-70% CuO, 20-35% ZnO, 1-15% Al_2O_3. Pretreatment and reaction conditions for the syngas conversion were detailed in the previous report (1). In related SAPO studies, we have carried out methanol conversion experiments on several Co SAPO catalyst samples, and have prepared several different catalyst particle size samples by water separation (settling), and grinding. SEM measurements have been made for several SAPO samples to verify particle sizes.

Reaction and Analysis Procedure. The CO hydrogenation reaction is performed in a continuous-flow system with a fixed-bed stainless steel reactor as detailed earlier (1). The flow of H_2, N_2 and syngas is controlled by two mass-flow controllers (Brooks 5850E). The reactant gases are well mixed and preheated by passing through a static mixer and pre-heater. The reactor is situated in a furnace with three heating zones controlled by three temperature controllers located in an electronics unit. The system is designed to allow safe experimentation with carbon monoxide and hydrogen and the reaction is allowed to continue 24-48 hrs depending on the SAPO catalyst deactivation rate, with analysis of products by GC (FID) every 1~2 hrs. Also, a standard quartz tube reactor is being used for MTO reactions with GC analysis.

Results and Discussion

Pressure Effects: It is well known that mid-range or high pressure (>300psi) is favorable for the methanol synthesis process. Methanol catalyst C-79 showed little activity under low pressure operation. On the other hand, the activity of the SAPO catalyst could decrease with the increases in the reaction pressure. Therefore, for the GTO process, which is an integration of these two processes, an interesting effect of pressure on the reaction behavior and product distribution might be expected. Figure 1 illustrates the CO conversions under three different pressures (50psi, 150psi, 300psi) with constant reaction temperature and syngas flowrate and ratio. It can be observed that the CO conversion to hydrocarbons is significantly increased under higher reaction pressure, which is a result of the pressure effects on the methanol synthesis process. The CO conversion is as high as 14% under 300 psi reaction pressures at steady state compared to less than 2% CO conversion at 50psi. The pressure effect on the C2-C4 olefins productivity has been investigated also. The results shown in Figure 2 show that the maximum C2-C4 olefins productivity can reach 6000 ppm at high reaction pressure of 300psi, while only less than 1000 ppm C2-C4 olefins is obtained at low pressure. Theoretically, we believe there could exist an optimum pressure due to the mixed effect of the pressure on the combined methanol synthesis/olefins production processes.

Syngas Ratio Effects. The syngas ratio (H_2/CO) can impose a significant influence on the CO hydrogenation process reactivity and product selectivity. Based on the economic considerations, it would be preferred to use a lean syngas ratio (less than 2) since less than stoichiometric ratios from reformed methane are often obtained. For this purpose, three H_2/CO ratios were investigated to study its effects on the CO conversion and olefins selectivity at 233 ºC and 300psi over hybrid catalyst C-79/SAPO-34. Results shown in Figure 3 establish that an increased syngas ratio (H_2/CO) could lead to a higher CO conversion. For example, the CO conversion is around 20% when syngas ratio H_2/CO is 2 while CO conversion decreases to around 8% with the syngas ratio set at 0.5. Increases in the H_2 feed seem to enhance the process reactivity due to the enhanced hydrogenation process. This can be confirmed from the results shown in Figure 4, where the ethylene relative selectivity significantly decreases under high syngas ratio due to the enhancement in the hydrogenation process. The relative ethylene selectivity, which is defined as the ratio of olefin weight at given carbon number to the total hydrocarbon weight at that given carbon number, is as high as 40% at low syngas ratio, compared to below 10% ethylene selectivity at high syngas ratio. More alkane products are obtained at high syngas ratio compared to low syngas ratio due to the increased hydrogenation of alkenes.

Syngas Flowrate Effects. Different syngas flowrates were employed to investigate the syngas space velocity effects on the CO conversion. In this experimental setup, three syngas flowrates (30sccm, 50sccm, 75sccm) were studied with constant temperature 233 ºC and constant pressure of 300psi. The results shown in Figure 10 illustrate that there is a noticeable effect of syngas space velocity on the CO conversion. The CO conversion is obviously higher at low flowrate (30sccm) than that at high flowrate (50sccm) due to the increase in the syngas residence time. Figure 6 shows the syngas flowrates effects on the DME selectivity, from which we can observe that an increase in syngas flowrate can lead to an improvement in the DME production, 50% of the total products are DME when the syngas flowrate is 75sccm with less olefins production. A possible reason for this can be explained based on the chemistry of MTO process. The main

reaction steps of MTO can be summarized as: methanol is first dehydrated to dimethyl ether (DME).The equilibrium mixture formed, consisting of methanol, DME, and water, is then converted to light olefins. In case of high syngas flowrate (low residence time), the intermediate DME could be swept out of the reactor without undergoing the conversion step into light olefins, resulting in the decreased C2-C4 olefins production. However, the results do not suggest that reducing the syngas flowrate as low as possible is a plausible strategy because much longer residence time could adversely increase olefins hydrogenation. A proper selection of syngas flowrate will be crucial for the high C2-C4 olefins productivity in the GTO process.

Comparison of Follow bed reactor and Mixed-bed reactor for Syngas Reactions. CO hydrogenation was also studied in both follow-bed and mixed-bed reactors. In the mixed-bed reactor, 1 g methanol catalyst C-79 and 0.5 g MTO catalyst SAPO-34 were well mixed to form one single catalyst bed, while C-79 catalyst and SAPO-34 were separated by about 7" in the follow-bed arrangement. Figure 7 gives the comparison of C2-C4 olefins productivity in follow bed reactor and mixed-bed reactor, from which we can observe that although the CO conversions to hydrocarbons are roughly similar in both reactor catalyst setups, there is a considerable difference in the C2-C4 olefins productivity between these two different catalyst bed configurations. In the follow bed reactor, the C2-C4 olefins productivity is obviously higher than that in mixed-bed reactor. The maximum C2-C4 olefins productivity is around 6000ppm in the follow-bed reactor while only 1500ppm in mixed-bed. In mixed-bed reactor, the olefins hydrogenation is probably enhanced due to high H_2 concentration, whereas in contrast, in the follow-bed reactor, most of H_2 is first consumed by methanol synthesis process, there is less opportunity for olefins produced from MTO process to be hydrogenated, which eventually results in high olefins productivity.

MTO Reactions. Results from experiments in the quartz tube reactor compared well with experiments conducted earlier and confirmed the earlier findings. The CoSAPO-34 catalyst did not yield very high conversions of MeOH, and thus other SAPO samples are being utilized in additional studies and appear to have much better activities. Catalysts such as SAPO-44, 47, and 56 as synthesized have particle sizes of 50, 300, and 120 μm, respectively however, grinding studies show that the crystallite size distribution, as evidenced by the SEM pictures in Figure 8, can be dramatically altered which should yield interesting effects in the MTO conversions.

Conclusions

Hybrid catalysts consisting of methanol synthesis catalyst C-79 and MTO catalyst SAPO-34 were employed for the syngas conversion to light olefins process. The experimental results demonstrate that the CO conversions and C2-C4 light olefins selectivity can be significantly increased by employing hybrid catalyst in a follow-bed reactor compared to either catalyst alone. Syngas pressure introduces a notable effect on the CO conversion and C2-C4 light olefins productivity. Moderate increases in reaction pressure lead to higher C2-C4 olefins productivity. Syngas ratio also imposes an obvious effect on the olefins selectivity, whereby high syngas ratio (H_2/CO) decreases the olefins selectivity due to the enhanced hydrogenation. Low syngas flowrate favors the increases in CO conversion. The olefins productivity was significantly improved in follow-bed catalyst set-up than that in mixed-bed configuration. Earlier results from MTO reactions have been confirmed in additional experimental runs, and effects of particle size on the MTO conversions and catalyst lifetime are ongoing.

Papers Published or Presented

1. P. Dutta, A. Manivannan, M. S. Seehra, P. M. Adekkanattu, and J. A. Guin, "Determination of the Electronic State and Concentration of Nickel in NiSAPO Catalysts by Magnetic Measurements", Catalysis Letters, 94, (3-4), 2004, 181-185.
2. S. Wang and J. A. Guin, "Synthesis of Gasoline Additives from Methanol and Olefins over Sulfated Silica", Studies in Surface Science and Catalysis, (Natural Gas Conversion VII), 147, 2004, 439-444.

Future Work

We plan to study the effects of several additional process and catalytic variables including crystallite size and metals impregnation on the performance of several SAPO catalysts in methanol conversion. Some SAPO's will be impregnated with metals by Dr. Ernst's group at Utah. We will also study the development of a novel highly dispersed bimetallic nanoparticle catalysts using mesoporous supports such as SBA's to improve catalytic activity and selectivity in hydrocarbon dehydrogenation processes for hydrogen production. We will continue the MTO experiments to optimize the effects of particle size on the conversion, product selectivities, and catalyst lifetimes for several SAPO.

References

1. J. A. Guin, X. Huang, L. Jean, "Selective Synthesis of Light Olefins from Syngas on Hybrid Catalysts Composed of Methanol Synthesis and SAPO catalysts": CFFS 6-month report, 2004.
2. C. D. Chang, W. H. Lang and A. J. Silvestri: J. Catalysis, 56 (1979) 274.
3. C. D. Chang, R.F. Socha: J. Catalysis, 90, (1984) 84.
4. K. Fujimoto, H. Tominaga. J. Catalysis: 87 (1984), 136.
5. D. R. Dubois, et al.: Fuel Proc. Technol. 83(2003), 203-218.
6. D. L. Obrzut, et al.: React. Kinet. Catal. Lett. 80(1), (2003), 113-121.

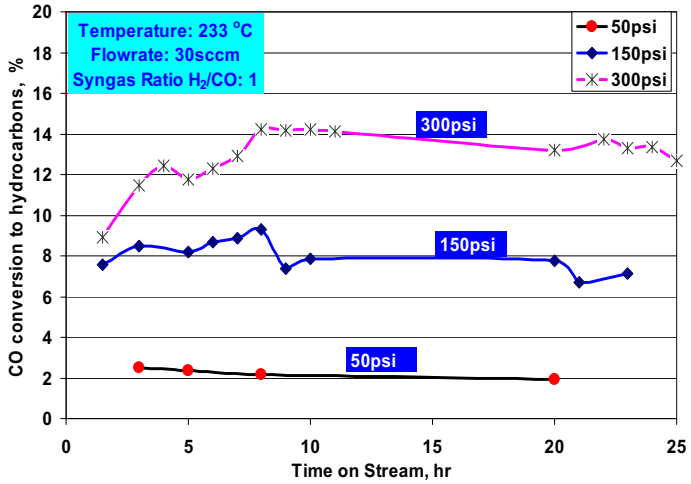

Fig. 1 Pressure effects on CO conversions to hydrocarbons

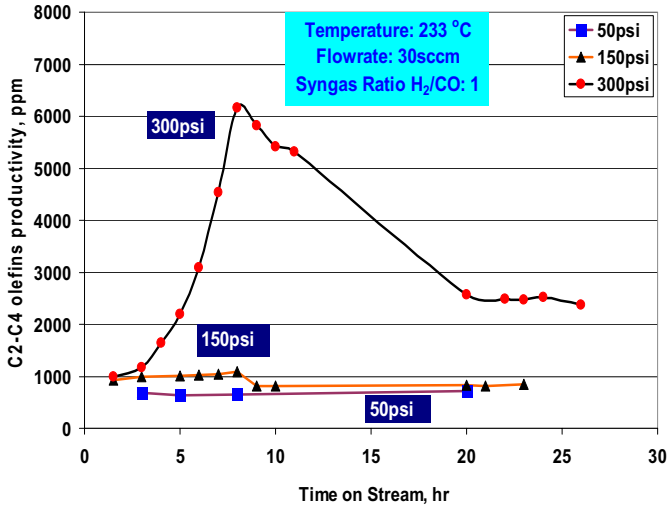

Fig. 2 Pressure effects on C2-C4 olefins productivity

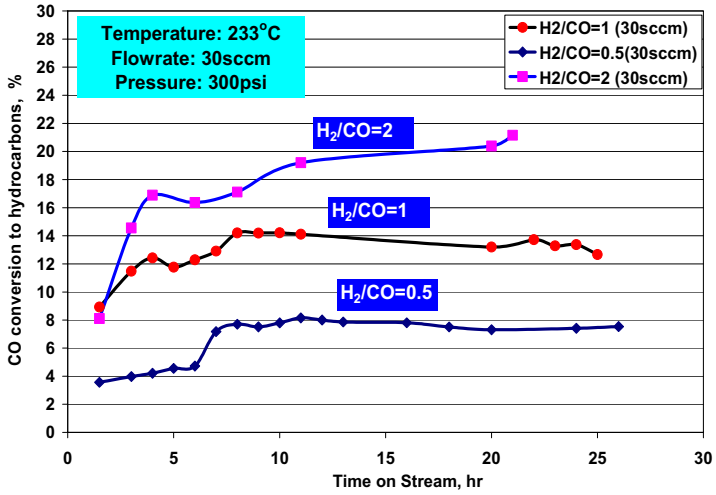

Fig. 3 Syngas ratio effects on CO conversions to hydrocarbons

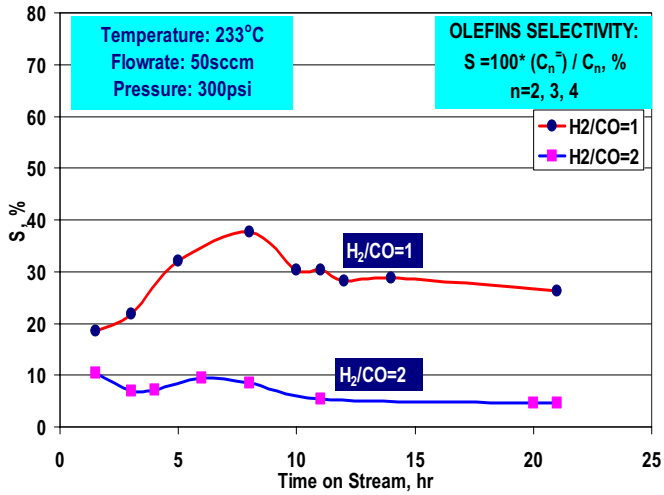

Fig. 4 Syngas ratio effects on ethylene selectivity

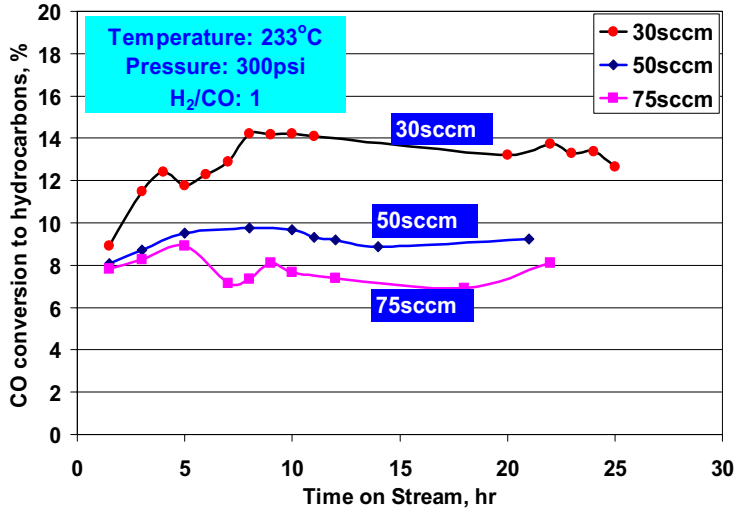

Fig 5 Flowrate effects on CO conversions to Hydrocarbons

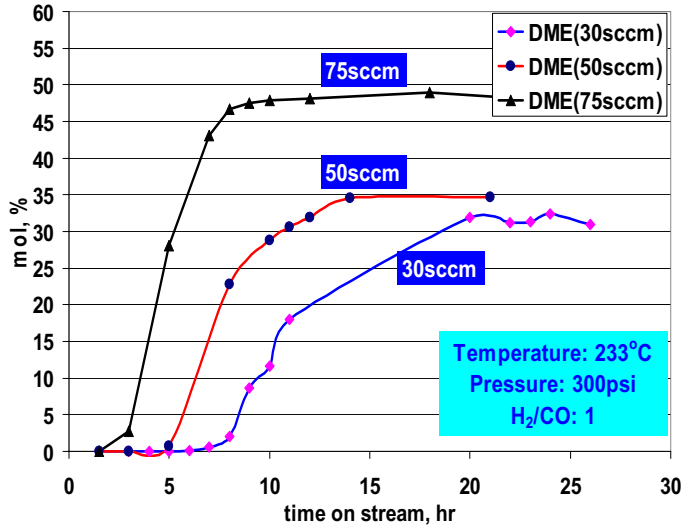

Fig. 6 Flowrate effects on DME selectivity

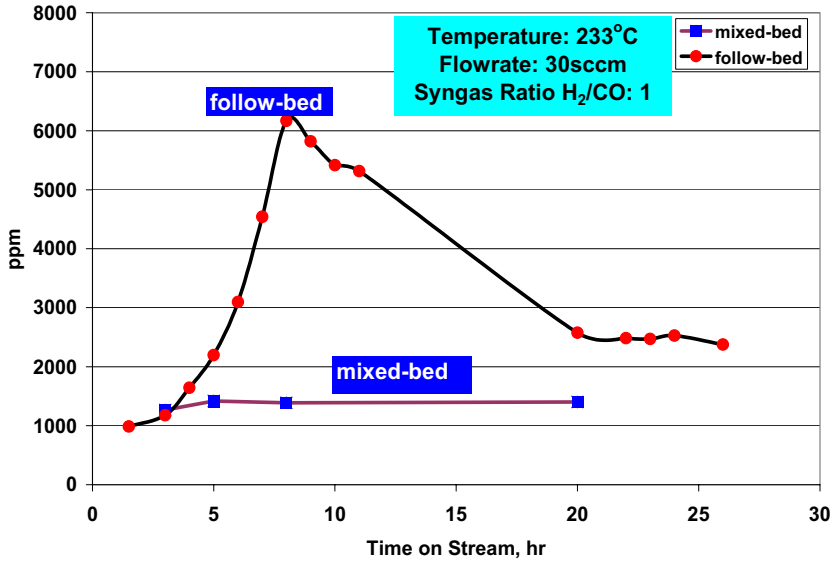

Fig. 7 C2-C4 olefins productivity in follow bed and mixed-bed reactors

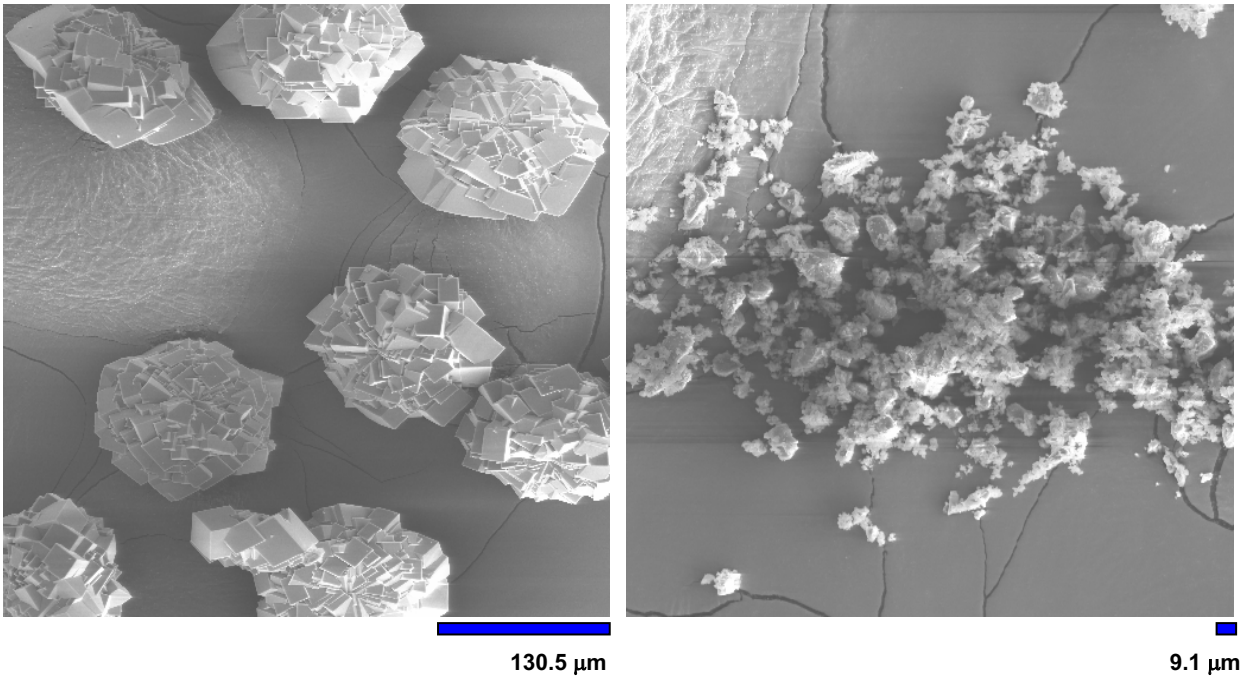

Fig. 8 NiSAPO-44 (Left -- Sample particles original size, Right -- Sample particles after grinding for 10 min)

Hydrogen production by catalytic dehydrogenation of high hydrogen content liquids using Ni-Cu/SC-CNT catalysts

Yuguo Wang, Naresh Shah, Frank Huggins and Gerald P. Huffman
University of Kentucky

Introduction

We have previously investigated the decomposition of methane, ethane, and propane into pure hydrogen and carbon nanotubes using the nanoscale, binary Fe-based catalysts supported on high surface area alumina (M-Fe/Al_2O_3, M=Mo, Pd or Ni) catalysts[i, ii, iii, iv] At temperatures ≤500 °C, the catalytic decomposition of ethane and propane produced carbon nanotubes with a stacked-cone nanotube (SCNT) structure (Figure 1). The high density of open carbene sites at the surface of the SCNT suggests that they may make very good catalyst supports.

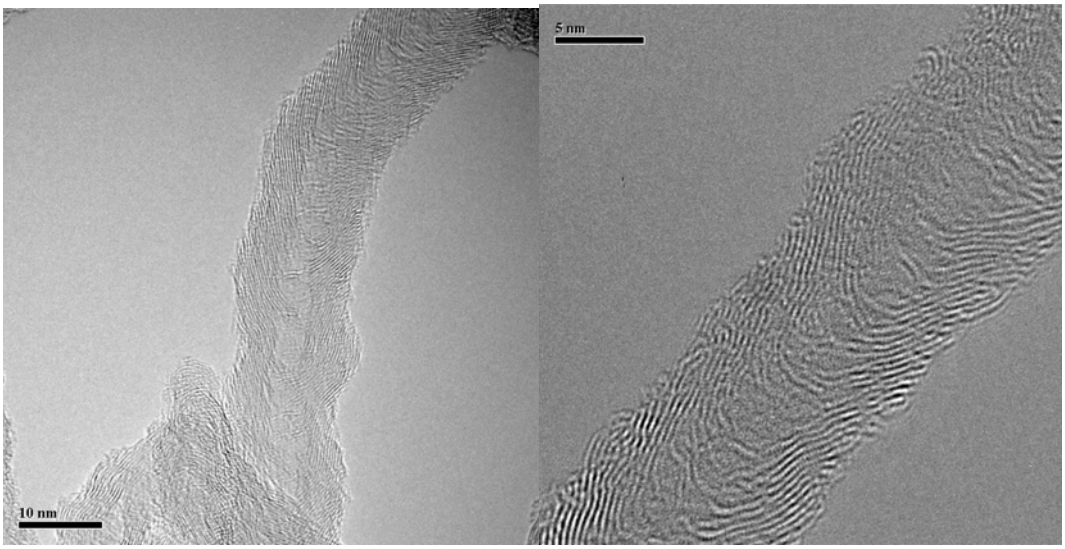

Figure 1. HRTEM images of SCNT produced by dehydrogenation of ethane (left) and propane (right) with a Pd-Fe/Al_2O_3 catalyst at 500 °C and 475 °C, respectively.

For vehicles powered by PEM fuel cells, it is desirable to be able to produce pure hydrogen "on-board" from a liquid fuel. Previously, we have reported that partial dehydrogenation of cyclohexane to benzene and pure hydrogen, or of methylcyclohexane to toluene and pure hydrogen is readily accomplished using a catalysts consisting of only 0.25 wt.% Pt supported on SCNT. v Here we report new results for the same reactions using a much more economical, non-precious metal, binary Ni-Cu alloy catalyst supported on SCNT.

Experimental Procedure

SCNT produced by ethane decomposition at 500 °C over a (0.5 wt.%Pd-4.5 wt.%Fe)/Al_2O_3 catalyst were used as catalyst supports for the work reported in this paper. The SCNT were purified by dissolving the high surface area γ-alumina in boiling concentrated NaOH solution for about 2.5 hours. The x-ray diffraction (XRD) patterns in figure 2 show that this purification process not only removes most of the Al_2O_3 catalyst support but also the amorphous carbon. The SCNT has a BET surface area of 211 m2/g before treatment in boiling NaOH and a BET surface area of 280 m2/g after the treatment.

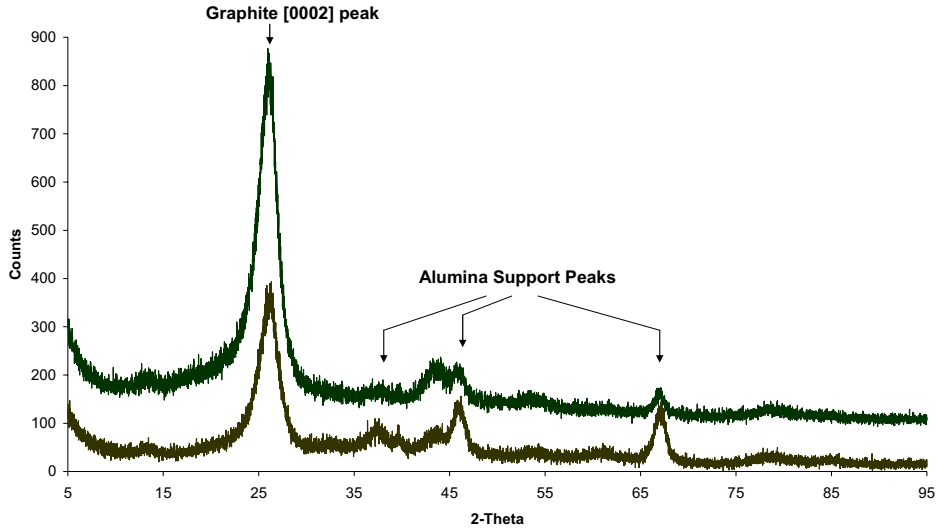

Figure 2. XRD patterns show significant reduction in the peaks due to the alumina support after purification (top) by boiling SCNT produced by catalytic ethane decomposition in concentrated NaOH.

To select the best atomic ratio of Ni to Cu in the binary catalyst, a series of Ni-Cu/Al_2O_3 catalysts were prepared with using incipient wetness method. As shown in Figure 3, the activity of these catalysts reached a plateau between approximately 40% and 60% Ni. The purified SCNT were then impregnated with $Ni(NO_3)_2$ and $Cu(NO_3)_2$ solution to prepare a catalyst consisting of 10 wt.% Ni-Cu(60 at.% Ni – 40 at.% Cu)/SCNT

Dehydrogenation experiments for cyclohexane and methylcyclohexane using this catalyst were carried out in a fixed bed, plug-flow, stainless steel reactor. Cyclohexane and methylcyclohexane with purities of over 99.5% were purchased from Alfa Aesar. For each run, 0.5 gram of catalyst was used. Prior to reaction, the catalysts were reduced in flowing hydrogen (50 mL/min) for 2 h at 500 °C. No methane was produced during this treatment, indicating that the graphitic layers of the SCNT do not undergo any gasification reaction under these reduction conditions. After reduction, the reactor was flushed with an inert gas until the GC showed no residual hydrogen peak (~ 15 min.). Liquid cyclohexane or methylcyclohexane were then pumped into the reactor using a syringe pump at a flow rate equivalent to 5 mL/min of gas flow. Since the free energy of the cyclohexane dehydrogenation reaction becomes negative at temperatures over 295 ºC, the reactions were carried out at a reactor temperature of 315 ºC at atmospheric pressure. The products of the reaction were analyzed online by two GCs with on-line serial sampling valves. The reactor exit stream was first analyzed by a GC with a FID detector for the analysis of hydrocarbon products via a heated transfer line. An online condenser then trapped benzene/toluene and unreacted cyclohexane/methylcyclohexane from the gas stream before analysis by a second GC with a TCD detector for the hydrogen and lower hydrocarbons contents.

Results and Discussion

Dehydrogenation of cyclohexane by Ni-Cu/SCNT catalysts

To decrease the cost, it is highly desirable to develop catalysts that use non-precious metals. Sinfelt et alvi found that Ni-Cu/Al_2O_3 alloy catalysts are very good dehydrogenation/hydrogenation catalysts. Figure 3 shows that the activity of these catalysts for

hydrogen production from dehydrogenation of cyclohexane plateaus between 40 and 60% Cu. Figure 4 shows that 10 wt% of a (60 at.% Ni – 40 at.% Cu alloy precipitated on a SC-CNT support has higher activity and longer catalyst life time than a pure Ni/SCNT catalyst. However, its activity is quite a bit lower than that of the Pt/SCNT catalyst. The HRTEM image in figure 5 shows that Ni-Cu alloys particle sizes are in the range 20-30 nm. This particle size is much bigger than the 1 to 2 nm Pt particles supported on SCNT that were previously investigated.[iv]

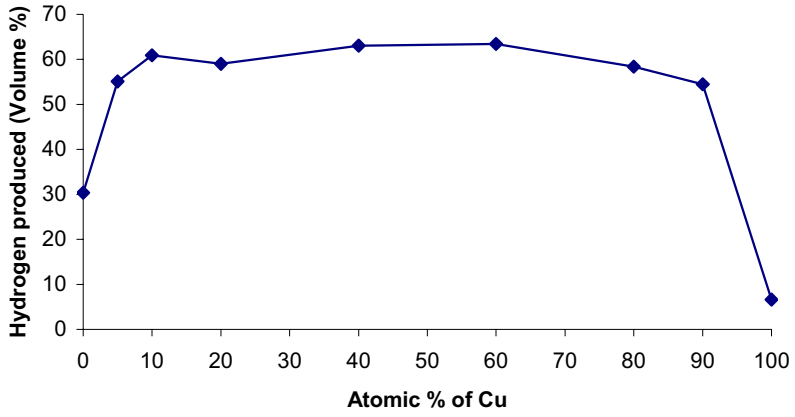

Figure 3. Comparison of catalyst activity for dehydrogenation of cyclohexane at 315 °C by different Ni-Cu/Al_2O_3 catalysts.

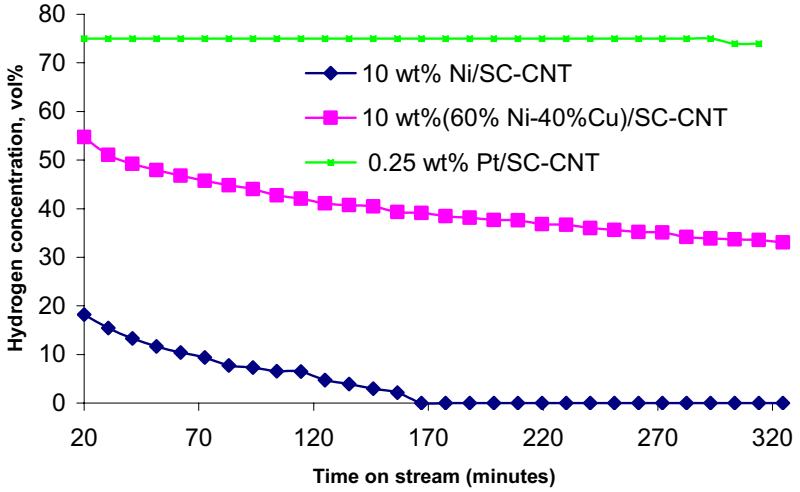

Figure 4. Comparison of catalyst activity for dehydrogenation of cyclohexane at 315 °C.

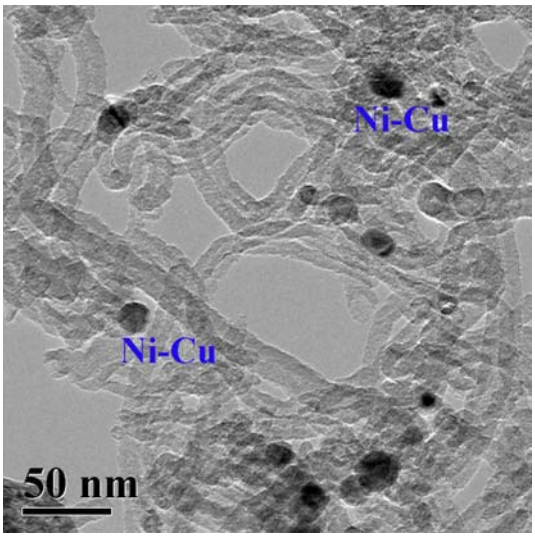

Figure 5. HRTEM picture of used 10 wt% Ni-Cu (Ni at.60% - Cu at.40%)/SCNT.

Conclusions

The results of catalytic partial dehydrogenation experiments to convert cyclohexane or methyl cyclohexane to hydrogen and benzene or toluene, respectively, were reported in our six-month report and a recent publication.[v] Using catalysts consisting of 0.25 to 1.0 wt% Pt supported on stacked-cone carbon nanotubes (SCNT), 100% conversion and selectivity was obtained at approximately 300 ºC and excellent time-on-stream (TOS) was observed. Catalytic partial dehydrogenation of cyclohexane using a more economical Ni-Cu/SCNT catalyst has now been attempted. Although the Ni-Cu catalyst shows 100% selectivity to hydrogen and benzene, it initial conversion of cyclohexane is only about 75%, which declines to about 50% during 5-6 hours TOS. TEM indicates that much smaller Ni-Cu alloy particles need to be produced in order to increase the activity of the Ni-Cu/SCNT catalysts to a level comparable to that of the Pt/SCNT.

Publications and presentations in 2004

1. Y. Wang, N. Shah, and G.P. Huffman, "Production of pure hydrogen and novel carbon nanotube structures by catalytic decomposition of propane and cyclohexane", *ACS Fuel Chemistry Division Preprints*, **48(2)** (2003) 900-901.
2. Yuguo Wang, Naresh Shah, and Gerald P. Huffman, "Pure hydrogen production by partial dehydrogenation of cyclohexane and methylcyclohexane over nanotube supported Pt and Pd catalysts", Energy & Fuels, 18 (2004) 1429-1433.
3. Yuguo Wang, Naresh Shah, and Gerald P. Huffman, "Simultaneous production of hydrogen and carbon nano-structures by decomposition of propane and cyclohexane over alumina supported binary Fe-based catalysts", Catalysis Today (2004) in press.

References

[1] Shah, N.; Panjala, D.; Huffman G. P. *Energy & Fuels*, **2001**, *15(6)*, 1528.
[2]Shah, N.; Wang, Y.; Panjala, D.; Huffman, G. P. "Production of Hydrogen and Carbon Nanostructures by Non-oxidative Catalytic Dehydrogenation of Ethane and Propane" *Energy & Fuels,* **2004** *18(3),* 727-735.

[3] Shah, N.; Pattanaik, S.; Huggins, F. E.; Panjala, D.; Huffman, G. P. *Fuel Processing Technology,* **2003**, 83(1-3), 163-173.
[4] Wang Y.; Shah, N.; Huffman G. P. "Hydrogen production by decomposition of propane and cyclohexane over alumina supported binary catalysts", *Catalysis Today*, In press.
[5]Wang Y.; Shah, N.; Huffman, G. P., "Pure Hydrogen Production by Partial Dehydrogenation of Cyclohexane and Methylcyclohexane over Nanotube-Supported Pt and Pd Catalysts", *Energy & Fuels*, **2004**, *18(5)*, 1429-1433.
[6] Sinfelt at., *J. Catal.*, **1972**, *24*, 283.

Catalytic Production of Hydrogen and Carbon Nanotubes from Methane Using a Fluidized-bed Reactor

Shankang Ma, Naresh Shah, Yuguo Wang, and Gerald P. Huffman, University of Kentucky

Introduction

Previously, we have developed alumina supported binary catalysts, (M-Fe)/Al_2O_3 (M=Pd, Mo, or Ni), that are very active for catalytic dehydrogenation of lower alkanes to produce pure hydrogen and carbon nanotubes (CNT).[1,2] However, all experiments were done in a fixed-bed reactor. Experiments had to be discontinued when the reactor back pressure was greater than 5 psig due to the build-up of CNT. A new reactor has been developed in which the reactor can be operated both in fixed-bed mode and fluidized-bed mode. Here, the results from the initial tests of this reactor for continuous methane dehydrogenation using a (0.5%Mo-4.5%Fe)/Al_2O_3 catalyst are reported.

Experimental procedure

In the new reactor design (Figure 1), quartz frit is used to hold 1.5g of as-prepared (0.5%Mo-4.5%Fe)/Al_2O_3 catalyst powder (75-150 microns). The diameter of the reactor tube is 22 mm.

The methane dehydrogenation experiments to produce hydrogen were carried out in the new reactor operating under both the fluidized-bed and fixed-bed mode. Ultra high purity methane was used both as reactant and as fluidizing media. Methane went in from the bottom of the reactor tube and reacted with catalyst at 700˚C. The hydrogen produced and the unreacted methane exited at the top of the reactor.

The reactions were carried out at methane flow rates from 15ml/min (fixed-bed reactor mode) to 115ml/min (fluidized-bed reactor mode) at atmospheric pressure. The products of the reaction were analyzed online by a GC with a TCD detector.

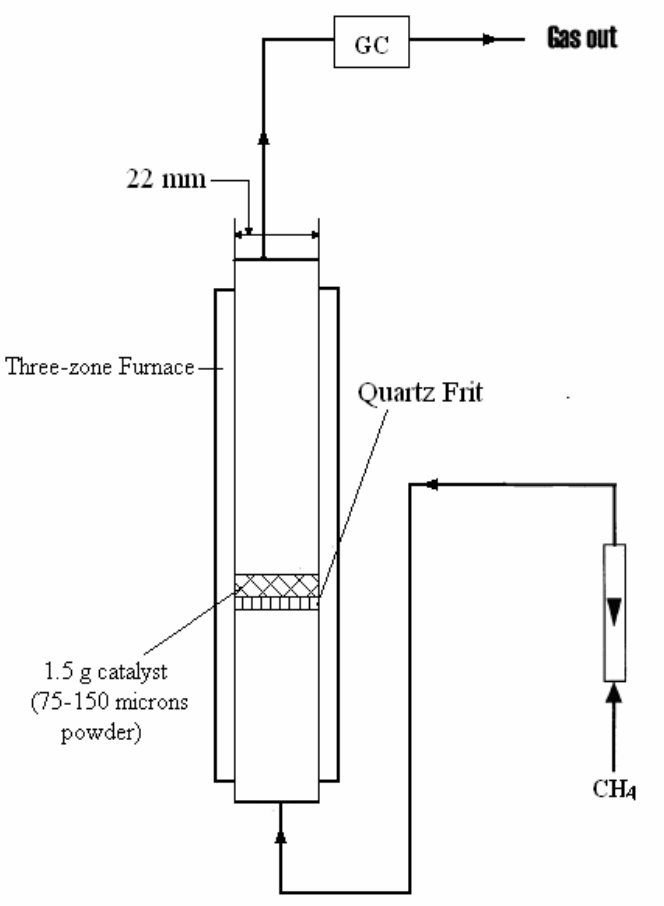

Figure 1. Fluidized-bed Reactor

Results and discussion

Figure 2 shows that when methane flow rate was 15ml/min, it took approximately 80 minutes to reach maximum hydrogen production in the exit stream. Then, after approximately 500 minutes of nearly steady-state reaction, hydrogen production started to drop. As the methane flow rate was increased, the time needed to reach maximum hydrogen concentration in the exit stream became less. Also, hydrogen production dropped at a much higher rate when the methane flow rate was higher. Presumably, the reaction was in a fluidized or partially fluidized bed mode at the higher methane flow rates. The majority of the carbon produced was in the form of parallel walled multiwalled nanotubes (MWNT), irrespective of the methane flow rate and reactor mode.

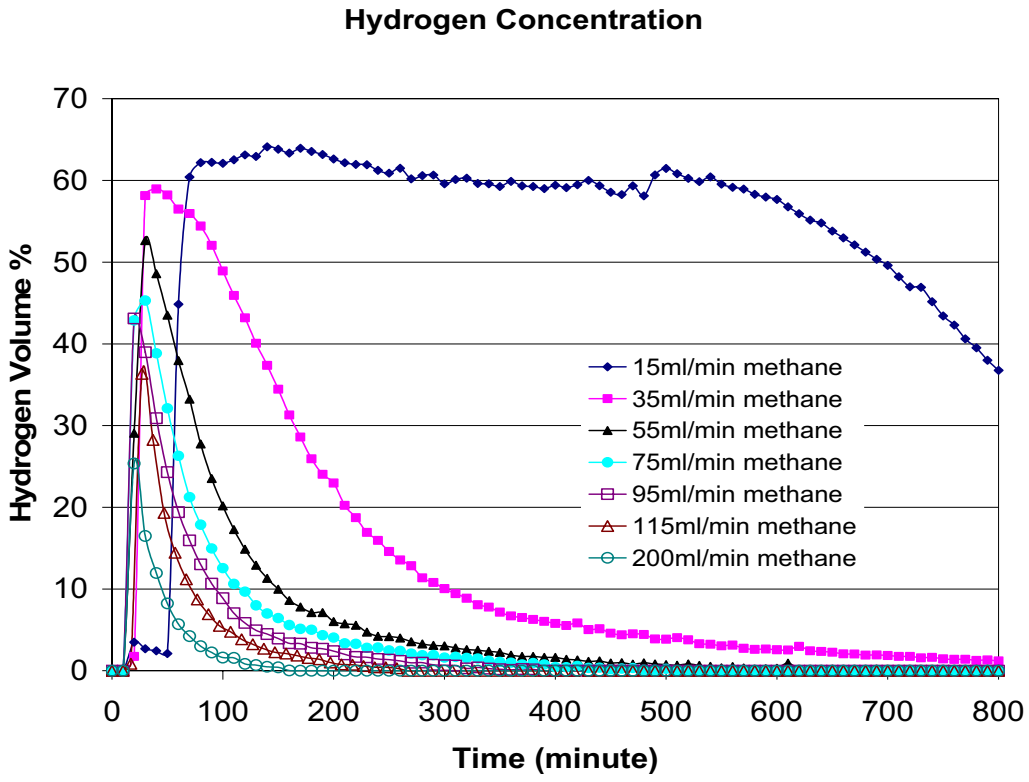

Figure 2. Time on stream hydrogen production at different methane flow rates

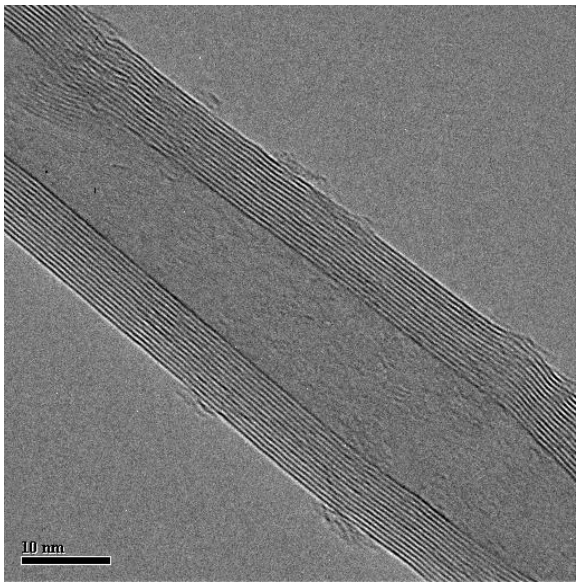

Figure 3. HRTEM image of SC-CNT produced

The GC measures only the concentrations of hydrogen and methane in the reactor exit stream, and the total amount of hydrogen produced is actually the area under the time on stream curves shown in figure 2, multiplied by the flow rate. As shown in table 1, with an increase in the methane flow rate, the total amount of hydrogen produced in a run decreased, and the efficiency of the reactor decreased. Reactor efficiency was very low when reactor mode was in fluidized-bed mode. One reason for this drop in the reactor efficiency could be that methane molecules passed rapidly over the catalyst without any decomposition reaction. In other words, methane acted as a carrier or fluidizing media, rather than as a reactant.

Table 1. Efficiency comparison at different reactor mode

	Methane Flow Rate (ml/min)	Linear Velocity (m/s)	Total Methane Input (ml) in 800 minutes	Total Hydrogen Produced (ml) in 800 minutes	Efficiency (H_2/CH_4)
Fixed Bed	15	2.37	12000	9210	77%
	35	5.52	28000	4830	17%
	55	8.68	44000	3350	8%
	75	11.84	60000	3110	5%
Fluidized Bed	95	14.99	76000	2830	4%
	115	18.15	92000	2000	2%
	200	31.57	160000	1790	1%

Conclusions

The fluidized-bed reactor mode did not show any advantage for methane dehydrogenation reaction under the current experimental conditions. Usually, the fluidized reactor mode is used to improve mass and heat transfer in a reactor. In our case, there is no mass transfer or heat transfer limitation in the fixed-bed mode and by fluidizing the bed, more methane just passes through the reactor without any reaction to produce hydrogen.

Future work

We propose to run this reactor under mixed-mode conditions as shown in Figure 4. The majority of methane dehydrogenation reaction will be run at high efficiency fixed-bed reactor mode during the production cycle. At regular intervals, methane flow rate will be increased to fluidize the bed to carry out short maintenance cycle operations.

Presentations and publications in 2004

1. N. Shah, Y. Wang, and G.P. Huffman, "Production of pure hydrogen and carbon nanostructures by catalytic non-oxidative dehydrogenation of ethane and propane", Energy & Fuels, 18 (2004) 727-736.
2. Gerald P. Huffman, Naresh Shah, Yuguo Wang, Frank E. Huggins, and Bradley Bockrath, "Catalytic Dehydrogenation of Hydrocarbons to Produce Pure Hydrogen and Carbon Nanotubes", Invited presentation at the 29th Int. Conf. on Coal Utilization and Coal Systems, April 18-20, 2004 Clearwater, FL; published in conference proceedings.
3. Gerald P. Huffman, Naresh Shah, Yuguo Wang, and Frank E. Huggins, "Catalytic dehydrogenation of hydrocarbons: alternative one-step process to produce pure hydrogen and carbon nanotube byproducts", ACS Fuel Chemistry Division Preprints, 49(2) (2004) 731-732; invited presentation at the ACS Presidential symposium: Fuels for the Furture: Leading the Way with Chemistry, ACS National Meeting, Philadelphia, PA, August 24, 2004.

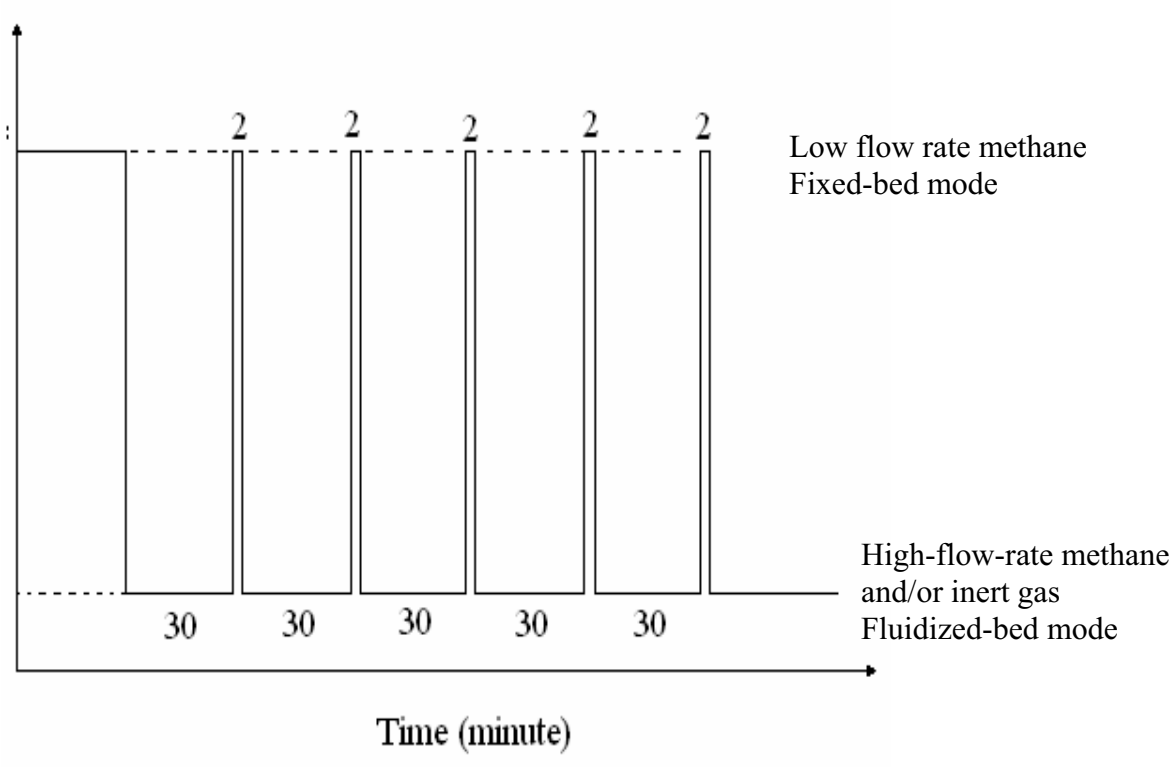

Figure 4. Proposed mixed-mode experimental procedure

Production of Hydrogen in Supercritical Water

J. Gadhe, C.B. Roberts, Ram B. Gupta*

Introduction

This work focuses on reforming reaction under supercritical water conditions to produce H_2. There are various advantages of carrying out reforming under supercritical water conditions which have been mentioned in the literature (references 1-4). The density of supercritical water is higher than that of steam which leads to a higher space-time yield. Higher thermal conductivity and temperature promotes the endothermic reforming reaction. The hydrogen gas is produced at a high pressure which can then be stored/used directly, thus avoiding compression cost.

Methanol is a good feedstock for the reforming reaction because of higher energy density. It has been reported in the literature that when a mixture of methanol and water vapor is passed over catalysts such as copper, it is decomposed into gases. The main components of the product gases are hydrogen, carbon dioxide, methane and carbon monoxide, as follows.

No.	Reaction		□H°@298°C (kJ/mol)
1.	Methanol decomposition	$CH_3OH \leftrightarrow CO + 2H_2$	+91.7
2.	Water-gas shift reaction	$CO + H_2O \leftrightarrow CO_2 + H_2$	-41
3.	Combined reaction of 1 and 2	$CH_3OH + H_2O \leftrightarrow CO_2 + 3H_2$	+50.7
4.	Methanation of CO	$CO + 3H_2 \leftrightarrow CH_4 + H_2O$	-211
5.	Methanation of CO2	$CO_2 + 4H_2 \leftrightarrow CH_4 + 2H_2O$	-223

The main objective is to maximize the reaction number 3. The reactor used in this study is a tubular reactor made of nickel alloy (Inconel 600). The inner wall of the reactor acts as catalyst for the reforming reaction. The advantage of this reactor configuration is its simplicity and compactness.

Experimental

An apparatus was designed for carrying out methanol reforming under supercritical water conditions. Various parts and equipment were acquired and assembled. The flow diagram for the process is shown below in Figure 1.

A typical experimental procedure is as follows. Distilled water is pumped through the system and desired pressure is achieved by adjusting the back pressure regulator. After stabilization, the furnace is switched on with a temperature set point. Once it reaches the desired temperature, flow is switched to methanol/water mixture. The steady state is marked by a constant gas flow and temperature at the reactor outlet. The feed flow rate is read from the pump display and confirmed by the drop in the level in the feed tank. Gas analysis is repeated at least 3 times. Gas flow is read from the flow meter. Liquid flow rate after the phase separator is measured by noting the mass collected in a specified time. It is later analyzed for TOC. The liquid is diluted so as to have the TOC readings in the range of the instrument (0 to 10000 ppm). Molar gas flow rates are calculated based on the total gas flow and confirmed by carbon balance. After the experiment flow is switched back to distilled water and the reactor is well flushed.

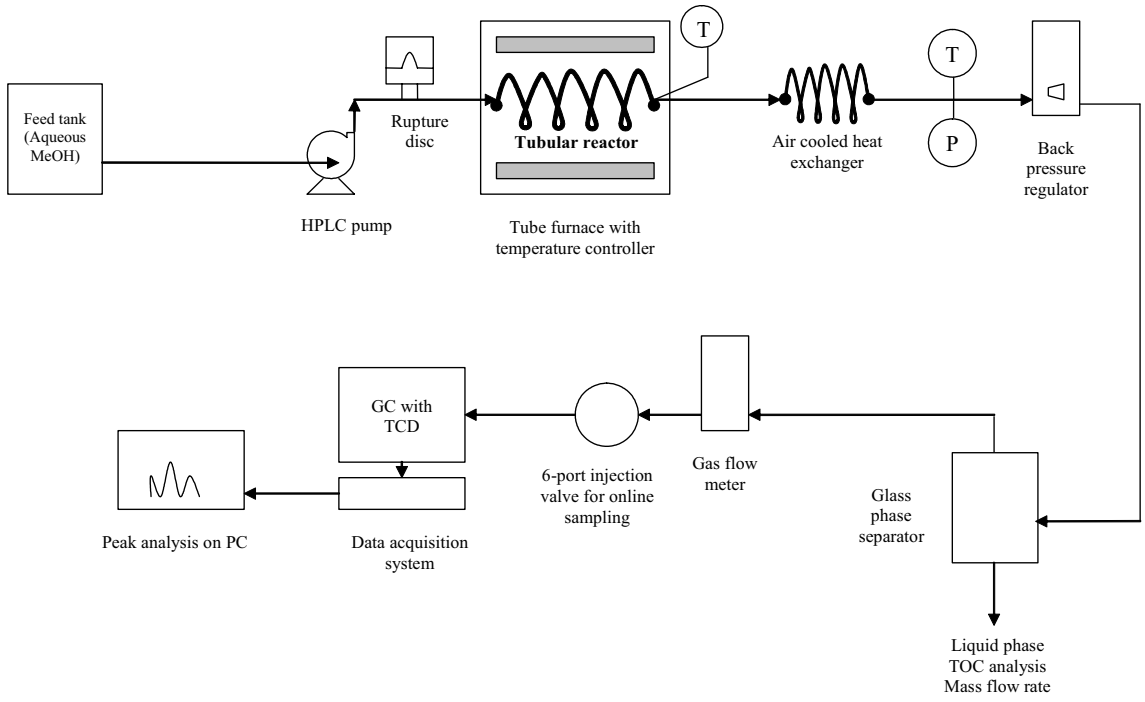

Figure 1: Experimental apparatus used for methanol reforming in supercritical water

Results and Discussion

Hydrogen was produced by reforming of methanol in supercritical water tubular reactor. A series of experiments were conducted to study the effect of various parameters such as pressure, temperature, steam-to-carbon ratio and residence time. Residence time is varied by changing the reactor length as well as by changing the feed flow rate. Both experimental results and equilibrium calculations show that as pressure increases, methanation of CO and CO2 is favored which results in the loss of significant amount of H_2. In addition, methane formation is favored at high temperatures, low steam-to-carbon ratio and high residence time. It is therefore important to reduce the loss of H_2 by minimizing the methanation reactions. Here, three strategies for suppressing methane formation are examined: (1) small residence time by having low reactor length or high feed flow rate, (2) addition of small amount of K2CO3 in the feed, or (3) utilization of the surface catalytic activity of the reactor made of Ni-Cu alloy. All three strategies resulted in the significant reduction in the methane formation and enhancement in the hydrogen production.

Conclusions

Methanol reforming in supercritical water favors the formation of CH4 which is accompanied by a substantial loss of H_2. Factors favoring the methanation reaction include low steam-to-carbon ratio, high temperature, high residence time and high pressure. CH4 production can be reduced greatly by lowering the low residence time so that the equilibrium is not reached. Methanation can also be reduced by the addition of small amounts of K2CO3 or KOH in the aqueous methanol feed. Reactor made of Ni-Cu tubing prevents the formation of CH4 even at higher pressures.

Papers presented or published

Gadhe, Jayant B.; Gupta, Ram B., "Hydrogen Production by Methanol Reforming in Supercritical Water: Suppression of Methane Formation," submitted to Industrial Engineering Chemistry Research, August 2004.

Future work

Various experiments will be conducted to study the additional effect of operating parameters such as temperature, pressure, feed concentration, feed flow rate, and catalyst addition. Kinetic and heat transport modeling of the reactor will also be performed.

It is well known that product removal from the reaction gases will drive the reaction towards hydrogen formation at higher pressures. This breaking of thermodynamic barrier requires the use of hydrogen selective membranes. However, the use of membrane under the harsh supercritical conditions is challenging due to the disability of the membrane to withstand higher pressures. To deal with this a membrane reactor of the following configuration is made in-house.

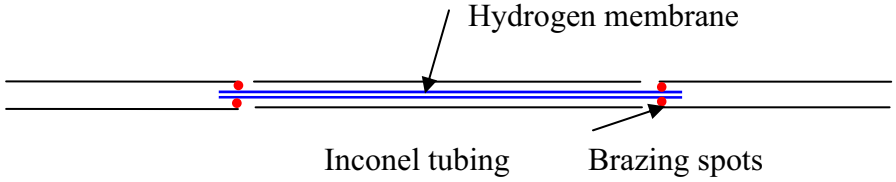

Experiments are also planned with the above membrane reactor.

References

1. Taylor, Joshua D.; Herdman, Christopher M.; Wu, Benjamin C.; Wally, Karl; Rice, Steven F. Hydrogen production in a compact supercritical water reformer. International Journal of Hydrogen Energy (2003), 28(11), 1171-1178.
2. Boukis, N.; Diem, V.; Habicht, W.; Dinjus, E. Methanol Reforming in Supercritical Water. Industrial & Engineering Chemistry Research (2003), 42(4), 728-735.
3. Kruse, Andrea; Dinjus, Eckhard. Hydrogen from methane and supercritical water. Angewandte Chemie, International Edition (2003), 42(8), 909-911.
4. Boukis, N.; Habicht, W.; Franz, G.; Dinjus, E. Behavior of Ni-base alloy 625 in methanol-supercritical water systems. Materials and Corrosion (2003), 54(5), 326-330.

Hydrogen Production by Aqueous-phase Reforming of Ethylene Glycol and Polyethylene Glycol

B. Liu, Y. Zhang, J.W. Tierney and I. Wender
Department of Chemical Engineering, University of Pittsburgh

Introduction

Production of hydrogen by steam-reforming of hydrocarbons requires a complex combination of multiple processes to achieve low carbon monoxide levels (e.g., 10–100 ppm) to be used in PEM fuel cells. An important step toward a simple process for the production of hydrogen containing low levels of CO is made possible by the discovery that hydrogen can be produced by catalytic reforming of ethylene glycol (EG) in liquid water at temperatures near 220 ºC [1-4]. This process has the advantage that the reforming of the oxygenated hydrocarbon and the water–gas shift (WGS) reaction are both thermodynamically favorable at the same low temperatures, thus making it possible to conduct both reactions in one reactor. The process eliminates the need to vaporize water and glycol and leads to low levels of carbon monoxide. Our work started in May 2004 with a focus on EG, a chemical which can be derived from synthesis gas. Polyethylene glycol will also be evaluated.

Experimental

Thermodynamic calculations:

The aqueous-phase reforming of one mole of EG produces five moles of hydrogen

$$C_2H_6O_2 + 4H_2O = 5H_2 + 2CO_2$$

The result of thermodynamic equilibrium calculations using ASPEN PLUS for aqueous reforming of EG and ethanol are shown in Fig. 1, where percent of EG converted is plotted versus temperature at a pressure of 450 psi. The change in conversion of EG is dramatic, rising from 4.6% converted at 166˚C to 99.8% at 169˚C. The almost complete conversion of EG is due to the removal of products (H_2 and CO_2) from the liquid phase in which the reaction is taking place while EG, which has a low vapor pressure (27 psi at 220˚C), remains almost completely in the liquid phase. A high total pressure is needed to keep the water from vaporizing.

Catalyst preparation:

Alumina-supported platinum catalysts were prepared by incipient wetness impregnation with aqueous solutions of tetraammineplatinum nitrate (Pt (NH4)4(NO3)2), followed by drying in an oven at 100 ºC for 12 h. Then the catalysts, with a composition of Pt (1 wt %) and Al2O3 (99 wt %), were calcined at 260˚C for 2 h. and then sieved to a 120–230-mesh size (particle diameters between 63 and 125 μm).

Experimental setup:

Preliminary work on the aqueous-phase reforming of EG was carried out in a batch system using a horizontal shaking 27 ml microautoclave. After 0.5 g catalyst was loaded, the reactor was purged with H_2 and pressurized to 300 psi at room temperature to test for leaks.

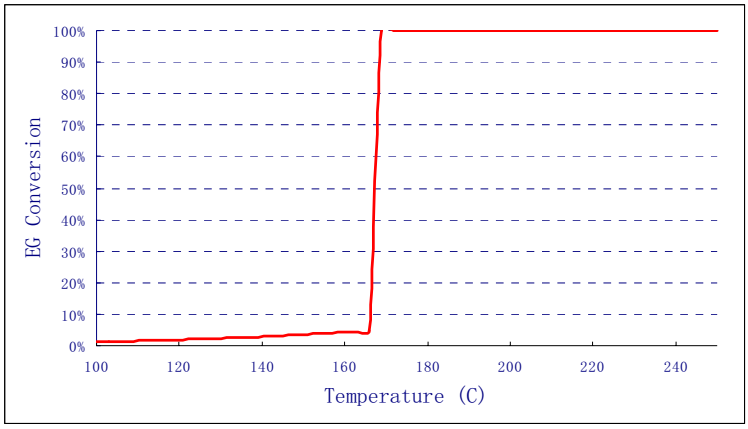

Figure 1 Equilibrium conversion of ethylene glycol by reforming at 450psi

The reactor was then purged four times with H_2 to remove air and then immersed into a fluidized sand bath and heated to the final reduction temperature of 250 ºC. It was then purged with H2 and pressurized to 400 psi at 250 ºC for 30 minutes to reduce the catalyst. After reduction, the system was cooled to room temperature. The system was purged with He four times to remove H_2. A 15ml liquid solution of 10 wt% EG in deionized water was introduced into the reactor with a pump. Argon was added to insure that the final pressure would be great enough. The reactor was then immersed into a fluidized sand bath and heated to the final reaction temperature. The reactor was shaken horizontally at 200 cycles per minute. The reaction was terminated by removal from the sand bath and immediately cooling with running cold water. Before opening the reactor to collect the liquid product, the gas product was sampled and analyzed by GC (HP6890). The liquid product was analyzed by another GC (HP5890).
A continuous system for the aqueous-phase reforming of EG is being built (Fig. 2)

Results and Discussion

Aqueous-phase reforming of 10 wt% EG solutions was carried out in the microautoclave at 210˚C and a final pressure of 470 psi. Conversion of EG was 15%, and the gas contained 70% H_2, 22% CO2, 8% argon. CO was not detected, and small amounts of gaseous alkanes (methane and ethane) were found. Liquid-phase products included CO_2 and small amounts of alcohols (methanol and ethanol), organic acids (acetic and glycolic acids), and aldehydes (acetaldehyde and glycolaldehyde). The microautoclave is not well suited for this reaction since the final pressure depends on the extent of reaction and sampling is difficult. A continuous flow reactor is better suited for obtaining kinetic data and evaluating catalysts than a batch reactor because pressure can be controlled, and online analysis carried out easily.

Conclusions

Preliminary experiments on the aqueous-phase reforming of EG in a batch system have shown that significant amounts of hydrogen are produced with minimal CO and other by-products. This method for producing hydrogen appears promising.

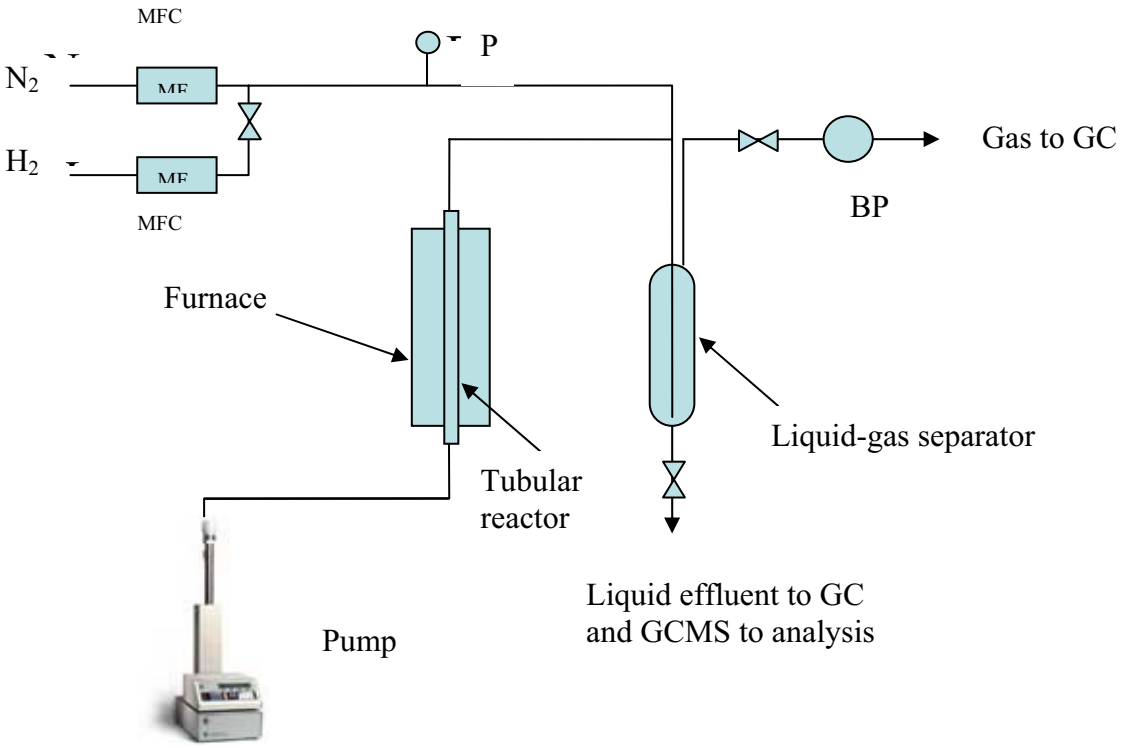

Figure 2. Sketch of the continuous system for aqueous-phase reforming of EG

Future Work

Future work will be done using a continuous reactor with online analysis for aqueous-phase reforming of EG and polyethylene glycol. The system is currently being constructed and tested. Catalysts and operating conditions will be varied to obtain high conversion and selectivity with small amounts of by-products. Related materials such as ethanol, 1-propanol, 1,2-propanediol and glycerol may also be tested.

References

1. U. Bossel, B. Eliasson, Energy and the Hydrogen Economy, 2003.
2. R. R. Davda, J. W. Shabaker, G. W. Huber, R. D. Cortright and J.A. Dumesic, Applied Catalysis B: Environmental 43 (2003), 13–26.
3. J. W. Shabaker, G. W. Huber, R. R. Davda, R. D. Cortright and J. A. Dumesic, Catalysis Letters 88 (2003), 1–2
4. J. W. Shabaker, R. R. Davda, G. W. Huber, R .D. Cortright and J. A. Dumesic, Journal of Catalysis 215 (2003), 344–352.

METHANE AND METHANOL REFORMING TO PRODUCE HYDROGEN WITH COBALT TUNGSTEN CARBIDE CATALYST

Huifang Shao, Wenping Ma, Edwin L. Kugler, Dady B. Dadyburjor
Department of Chemical Engineering, West Virginia University, Morgantown, WV

INTRODUCTION

Many industrial processes use methane as a primary feedstock for producing a mixture of carbon monoxide and hydrogen, called synthesis gas. The methane can arise from natural gas, from coal seams or as an unneeded product during Fischer-Tropsch (FT) synthesis. The syngas serves as the feedstock for a variety of downstream processes, such as methanol synthesis, FT synthesis or ammonia synthesis [1,2]. The use of syngas from FT methane to produce FT products represents a useful way to recycle the unneeded methane from FT. There are three ways to produce syngas from methane:

steam reforming $CH_4 + H_2O \rightarrow CO + 3H_2$
partial oxidation $CH_4 + \frac{1}{2}O_2 \rightarrow CO + 2H_2$
dry reforming $CH_4 + CO_2 \rightarrow 2CO + 2H_2$

Dry reforming is one focus of this research. The second reactant, CO_2, is often present in natural gas, in which case dry reforming is potentially of value in converting "stranded" natural gas reserves to liquid products. In any case, CO_2 is abundant and is a greenhouse gas, so methods of removing it by reaction (as opposed to temporary storage by sequestration techniques) are of value.

Nickel-based catalysts are traditionally used for methane reforming. But this type of catalyst can deactivate rapidly by coke deposition, where coke is formed via methane decomposition and CO disproportionation (Boudouard reaction).[3, 4] Noble metal catalysts (Rh, Ru, Pd, Pt, Ir) exhibit high reactivity and low coke formation in the reforming process, but are expensive.[5] Metal carbides exhibit intermediate activity and intermediate stability. We have shown that bimetallic carbides can improve both activity and stability, and that coke deposition is apparently a requirement for the formation of a stable, active state. We have also shown that carbides with very similar bulk properties do not exhibit the same behavior in the reactor. Hence surface properties are required to be investigated. In this research, we have developed techniques to prepare the bimetallic carbide catalyst in house.[6, 7]

A second focus of this research is methanol conversion to hydrogen. Methanol, a renewable resource, is viewed as an important source of hydrogen since it has a high hydrogen-to-carbon ratio and can be transported easily as a liquid fuel.[8,9] As in the case of methane reforming, there are three important reactions for producing hydrogen from methanol:

decompostion: $CH_3OH \rightarrow CO + 2H_2$
partial oxidation: $CH_3OH + \frac{1}{2}O_2 \rightarrow CO_2 + 2H_2$
steam reforming: $CH_3OH + H_2O \rightarrow CO_2 + 3H_2$

Steam reforming of methanol is viewed as a desirable way to produce hydrogen-rich gas since it minimizes coke formation.[10]

EXPERIMENTAL

The unsupported cobalt tungsten carbide catalyst is now prepared in our own laboratory. The detailed procedure has been described in an earlier report. The final form of the catalyst is very dependent upon the ratio of CO2 to CO in the reducing gas used in the final step of preparation. Hence, different forms of catalyst were prepared, with CO2/CO ratios of 0.1, 0.2 and 0.75. The last value results in catalysts similar to the Co6W6C obtained commercially, while the first two values result in improved catalysts.

Typically 300 mg of the catalyst sample is used for each run. The empty reactor is initially loaded with quartz wool at the center such that the tip of the thermocouple just touches the catalyst bed when loaded. After this, the downstream end of the reactor is filled with fine quartz chips (approx. 1/16 in), and the bottom is sealed with some quartz wool. Then the catalyst is poured with a funnel from the top of the reactor, followed by tapping to ensure that all the catalyst is set in the reactor center. Next, the thermocouple is inserted into the reactor, and the top fitting is connected. Finally, some more quartz chips are added from the side opening of the reactor to fill the upstream of the reactor. The loaded reactor is then mounted in the furnace enclosure. The system is then checked for leaks by flowing an inert gas (argon) at a pressure of 60 psig.

The catalyst pretreatment is then started. The catalyst is first reduced by flowing hydrogen at 60 cc/min for one hour, followed by one hour of flushing with argon. The reaction starts once the pretreatment is finished.

Earlier we have reported the results when the catalysts were tested for reactivity and stability at 850 ºC. To investigate further the performance of the catalysts during the present period, the reactions were carried out at a range of increasing and decreasing temperatures. The temperature profile was designed as follows:

700 ºC → 600 ºC → 850 ºC → 700 ºC → 600 ºC → 500 ºC → 700 ºC

Thus the performance of the catalysts could be obtained at intermediate temperatures, high temperatures, intermediate temperatures after exposure to high temperatures, low temperatures after exposure to high temperatures, then back to intermediate temperatures to test for catalyst stability. To ensure that the properties of the catalyst had stabilized at each temperature, each temperature stage was maintained for 20 hours. The other reaction conditions still remained the same as before:

P = 36 psig (3.4 atm), PCH4 = PCO2 = 1atm

CH4 : CO2 : Ar = 1 : 1 : 1.4, WHSV = 9000 scc / hr / g-catalyst

The catalysts used for methane reforming were characterized by SEM and XRD to compare the bulk components of the catalyst before and after reaction.

For methanol steam reforming, the liquid feed was introduced to the top of the catalytic reactor by an HPLC pump. The total feed rate of liquid methanol and water was fixed at 0.05cc/min, while the ratio of methanol to water was changed. Helium was used as an internal standard for GC analysis while argon was added as a sweep gas to aid kinetic analysis. The methanol and water mixture provided by the HPLC pump was vaporized at the top of the reactor. As in the case of methane reforming, 0.3g of catalyst was used for each experiment. The catalyst was reduced with flowing hydrogen at 400 ºC for one hour, followed by flushing with argon while heating to 850 ºC. Afterwards, the catalyst is activated by methane at 850 ºC for one and one-half hours.

RESULTS AND DISCUSSION

Variable-temperature tests were carried on for each of the three catalyst samples, which were prepared with different ratios of CO2 to CO. The conversions, yields, ratios of hydrogen to carbon monoxide and carbon balance were measured and these are shown in Tables 1 through 3. Qualitatively similar performances were noted for all three.

When the reaction temperature was first raised to 700 ºC, the conversions and the yields were negligibly low. The values increased dramatically as the reaction temperature went up to 850 ºC. Afterwards, the reaction temperature was lowered step by step: 700 ºC →600 ºC →500 ºC, and the values of conversion and yield decreased correspondingly. However, the values of conversions and yields at 700 ºC this time were much higher than those obtained in the first step. Later, the reaction temperature was brought back to 700 ºC, and the values were almost at the same level as those at the second 700 ºC. Clearly, the catalyst cannot be activated if it is at a temperature of 700 ºC or lower at the very beginning. In comparison, the reactivity increases greatly once the reaction temperature reaches 850 ºC. After that, the catalytic activity can be maintained at a relatively high level even if the temperature is lowered again.

Figures 1 through 6 are SEM and XRD results for the fresh and spent catalyst. Only one material was used for these characterizations, made using the CO_2 to CO ratio of 0.75. Before the reaction, the fresh catalyst was shown to be Co_6W_6C. The bulk component of the spent catalyst is WC and Co when the reaction temperature is 850 ºC. But much cobalt tungsten oxide is found as the reaction temperature is 700 ºC. From the SEM images, the structure of the catalyst is more compact when the reaction is run at the higher temperature (850 ºC). Also, carbon deposits, including whisker carbon and carbon tube, can be seen on the surface of the spent catalyst run at 850 ºC. Further, EDAX confirms that a large amount of oxygen exists in the spent catalyst reacted at the intermediate temperature (700 ºC). The existence of the cobalt tungsten oxide probably decreases the amount of the active catalyst and inhibits the desired reaction, which might be the reason that why the reactivity of the catalyst was fairly low in this situation. The specific mechanism of this phenomenon needs to be investigated in future work.

Methanol steam reforming was screened with the same cobalt-tungsten carbide catalyst over a wide range of methanol-to-water ratios. Excessive methanol lead to coke deposition and catalyst deactivation; excessive water led to low reaction rates. After several tests, it was found that the reaction could proceed well with high conversion and low coke formation with a 1-to-1.2 methanol-to-water mole ratio. This mixture contains 60 wt% methanol.

Table 4 shows the effect of temperature on methanol steam reforming using methanol-water in a 1 : 1.2 ratio. The test started at 450 ºC with the temperature being increased in 100 ºC steps to 850 ºC and then decreasing to 450 ºC. The pressure drop in the reactor increased until the temperature reached 650 ºC, which may have been caused by coke formation. After that, the pressure drop in the reactor almost vanished, a condition that remained the same until the end of the test. The reaction products were H_2, CO, CO_2 and CH_4. The selectivity to hydrogen remained high at all reaction temperatures.

CONCLUSIONS

From the above results, the conclusion could be drawn that this bimetallic carbide catalyst was required to be activated at a higher temperature (850 ºC) before exhibiting good reactivity for methane dry reforming. After that, the catalyst maintains high reactivity and good stability over a long period even at lower temperatures. The SEM images and XRD spectra demonstrate the different appearance of the catalyst after it is treated at different temperatures (700 ºC and 850 ºC).

The same catalyst was used for methanol steam reforming and showed nearly constant, high selectivity to hydrogen from 450 to 850 ºC .

PAPERS PRESENTED OR PUBLISHED

1. M.V. Iyer, L.P. Norcio, E.L. Kugler, M.S. Seehra and D.B. Dadyburjor, "Catalysts for synthesis gas formation from reforming of methane," Topics in Catalysis 29 (3-4) 195-198 (2004).

2. H. Shao, E. L. Kugler and D. B. Dadyburjor, "Catalysts for Hydrogen Production from Methane," Fuel Chemistry Preprints 49, 702-705 (2004)

3. "Bimetallic Eta-Carbides and Related Materials as Catalysts for Production of Synthesis Gas from Methane," Seminar presented by D.B. Dadyburjor at Department of Chemical Engineering, University of Akron, April 8, 2004.

4. "Effect of Temperature on Dry Reforming of Methane using Bimetallic Carbide Catalyst," H. Shao (speaker), E. L. Kugler and D. B. Dadyburjor, Pittsburgh-Cleveland Catalysis Society Meeting, Pittsburgh, PA, June 18, 2004

5. "Effect of Temperature on Dry Reforming of Methane using Bimetallic Carbide Catalyst," H. Shao, E. L. Kugler and D. B. Dadyburjor (speaker), CFFS Annual Meeting, Roanoke, WV, August 1-4, 2004

6. "Catalysts for Hydrogen Production from Methane," Paper presented by D. B. Dadyburjor at American Chemical Society Meeting, Philadelphia, PA, August 22-26, 2004

7. "Bimetallic Carbide Catalysts for Methane Reforming," H. Shao, E. L. Kugler and D. B. Dadyburjor (speaker), AIChE Annual Meeting, Austin, TX, November 8-12, 2004

FUTURE WORK

New work has begun on steam reforming of methanol to produce hydrogen. This new avenue will be pursued and may be expanded to include ethanol. The use of carbide catalysts of different compositions is being considered. These materials can be prepared by replacing W with Mo and/or substituting Ni for Co. The reactivity and stability of the new catalysts will be investigated for alcohol reforming.

REFERENCES

1. J. B. Claridge, A. P. E. York, A. J. Brungs, C. Marquez-Alvarez, J. Sloan, S. C. Tsang and M. L. H. Green, "New Catalysts for the Conversion of Methane to Synthesis Gas: Molybdenum and Tungsten Carbide", Journal of Catalysis, 180: 85-100, 1998
2. S. Wang and G. Q. Lu, "Effects of Promoters on Catalytic Activity and Carbon Deposition of Ni/γ-Al2O3 Catalysts in CO2 Reforming of CH4", Journal of Chemical Technology and Biotechnology, 75: 589-595, 2000
3. T. Osaki, T. Mori, "Role of Potassium in Carbon-Free CO2 Reforming of Methane on K-Promoted Ni/Al2O3 Catalysts", Journal of Catalysis, 204: 89-97, 2001
4. J. H. Bitter, K. Seshan, and J. A. Lercher, "Deactivation and Coke Accumulation during CO2/CH4 Reforming over Pt Catalysts", Journal of Catalysis. 183: 336-343, 1999
5. J. R. Rostrup-Nielsen and J-H. B. Hansen, "CO2-Reforming of Methane over Transition Metals", Journal of Catalysis, 144: 38-49, 1993
6. E. L. Kugler, L. E. McCandlish, A. J. Jacobson, R. R. Chianelli, "Eta Phase Materials, Methods of Producing the Same, and Use Thereof as Catalysts for Alcohol Synthesis, Hydrocarbon Synthesis, Hydrocarbon Hydrogenation and Hydrocarbon conversion Reactions", US Patent 5,138,111, Aug 11, 1992
7. R. S. Polizzotti, L. E. McCandlish, E. L, Kugler, "Multiphase Composite Particle Containing a Distribution of Nonmetallic Compound Particles", US Patent 5,338,330, Aug 16, 1994
8. P.H. Matter, D.J. Braden and U.S. Ozkan, Steam reforming of methanol to H_2 over non-reduced Zr-containing CuO/ZnO catalysts, Journal of Catalysis 223, 340, 2004
9. Shabaker J.W. Davda R.R., Huber G.W., Cortright R.D. and Dumesic J.A., Aqueous-phase reforming of methanol and ethylene glycol over alumina-supported platinum catalysts, Journal of Catalysis, 215, 344, 2003
10. Cortright R.D., Davda R.R. & Dumesic J.A., Hydrogen from Catalytic Reforming of Biomass-derived Hydrocarbons in Liquid Water, Nature, 418: 964-967, 2002

Table 1. Conversion, Yield, Product Ratio and Carbon Balance with the catalyst made using $CO_2/CO=0.75$

Temperature (ºC)	Conversion of CH_4 (%)	Conversion of CO_2 (%)	Yield of CO (%)	H_2/CO Ratio	Carbon Balance (%)
700	3.63	5.37	2.03	0.223	97.52
600	2.84	2.88	0		97.14
850	78.77	73.67	63.73	1.113	87.54
700	29.01	35.93	27.72	0.788	95.21
600	9.15	13.86	8.92	0.489	97.38
500	4.32	5.59	2.19	0.315	97.23
700	Not available				

Table 2. Conversion, Yield, Product Ratio and Carbon Balance with the catalyst made using CO2/CO=0.1

Temperature (ºC)	Conversion of CH_4 (%)	Conversion of CO_2 (%)	Yield of CO (%)	H_2/CO Ratio	Carbon Balance (%)
700	4.45	7.71	3.99	0.127	97.88
600	1.63	1.61	0		98.38
850	72.09	68.45	66.75	0.989	96.50
700	28.43	34.13	26.42	0.795	95.10
600	9.15	13.29	9.01	0.467	97.76
500	4.12	4.55	2.24	0.307	97.86
700	27.66	34.50	27.05	0.759	95.92

Table 3. Conversion, Yield, Product Ratio and Carbon Balance with the catalyst made using CO_2/CO=0.2

Temperature (ºC)	Conversion of CH_4 (%)	Conversion of CO_2 (%)	Yield of CO (%)	H_2/CO Ratio	Carbon Balance (%)
700	3.84	4.14	1.88	0.233	97.89
600	2.46	1.43	0		98.06
850	80.53	76.84	67.58	1.079	88.92
700	29.55	35.51	28.35	0.799	95.78
600	8.83	12.49	8.56	0.473	97.88
500	4.35	4.63	2.25	0.297	97.76
700	27.69	33.83	26.77	0.774	95.97

Table 4. Effect of Temperature on Product Composition, CH_3OH:H_2O = 1 : 1.2

T(ºC)	Gas components				$H_2/(CO+CO_2)$
	H_2%	CO%	CH_4%	CO_2%	
450	64.26	17.93	6.36	11.46	2.19
550	63.86	15.10	7.36	13.68	2.22
650	67.49	21.29	1.78	9.44	2.20
750	68.09	19.08	1.85	10.98	2.28
850	68.37	19.60	1.99	10.03	2.31
750	67.68	19.51	2.29	10.51	2.26
650	66.72	25.30	3.26	4.72	2.24
550	64.62	27.18	3.86	4.33	2.05
450	68.81	31.19	0	0	2.21

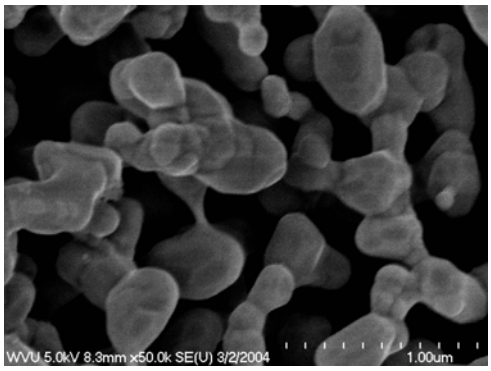

Fig 1 SEM image of fresh catalyst

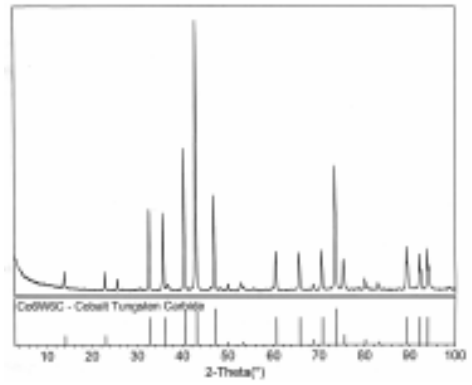

Fig 2 XRD spectrum of fresh catalyst

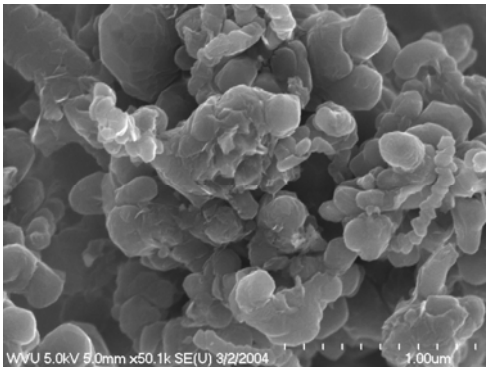

Fig 3 SEM image of spent catalyst run at 850 ºC

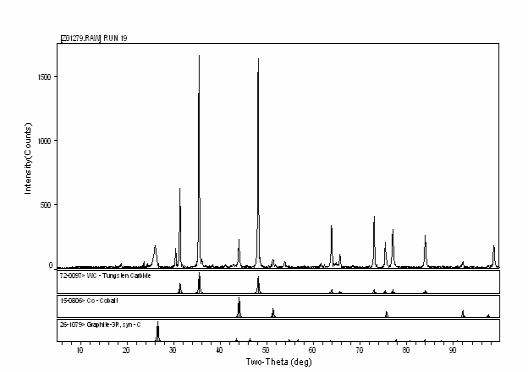

Fig 4 XRD spectrum of spent catalyst run at 850 ºC

Fig 5 SEM image of spent catalyst run at 700 ºC

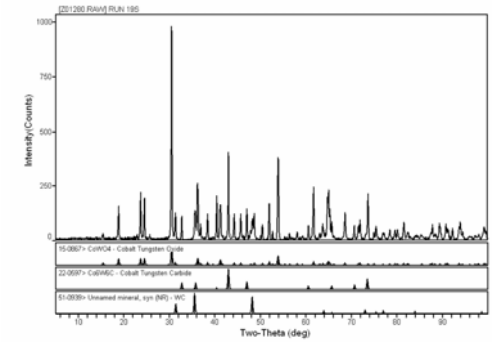

Fig 6 XRD spectrum of spent catalyst run at 700 ºC

Spectroscopic Characterization of C1 and H_2 Chemistry Catalysts

Frank Huggins, Naresh Shah, Artur Braun, and Gerald P. Huffman
Consortium for Fossil Fuel Science and Department of Chemical & Materials Engineering,
University of Kentucky

Introduction

Many of the reactions of interest to C1 chemistry and hydrogen generation from coal and other fossil fuels involve catalysis. This project provides support for those researchers within the Consortium who desire to understand the reaction mechanisms and active species involved in the various reactions under investigation in the Consortium program.

In earlier reports, we described results from 57Fe Mössbauer and/or X-ray absorption fine-structure (XAFS) investigation of key metal species involved in three different experimental investigations. These included:

1. Catalyst dehydrogenation of methane and other light alkane hydrocarbons to yield hydrogen and carbon nanotubes (P.Is. Shah, Wang, and Huffman, U. KY.);
2. Catalytic dehydrogenation of cyclohexane and methyl cyclohexane (P.Is. Wang, Shah, and Huffman, U. KY.);
3. Investigation of metallocenes and metallocene-doped aerogels for use in FT synthesis (P.Is. Ernst, Eyring, and Dunn, U. Utah).

In the final six months of this year, work continued on item 3, but using Ru as the metallic species rather than Co and Fe. In addition, work commenced on the following systems:

4. Development of silica-based zeolitic-like F-T catalysts that incorporate Fe or Co (P.Is. Eyring and Kim, U. Utah);
5. Fe, Mo-based water-gas-shift (WGS) catalysts (P.I. Dadyburjor, WVU);
6. Fe, Cr, K-based high temperature WGS catalysts (P.Is. Huffman and Shah, U.KY).

The Principal Investigators supply the catalysts they are preparing (see other individual reports in this Report and recent previous Consortium reports for details of the preparations) to the University of Kentucky and the materials are then analyzed by iron Mössbauer spectroscopy or XAFS spectroscopy, as appropriate. Electron microscopy studies are conducted if needed.

Experimental procedure

Both 57Fe Mössbauer spectroscopy and XAFS spectroscopy are mature, widely-available techniques that have been much applied in catalyst characterization research. Therefore only a very brief description of the methods will be given here.

57Fe Mössbauer spectroscopy is performed at the University of Kentucky using a Halder, GmbH, Mössbauer driving unit and control unit interfaced to a personal computer by means of two Canberra Nuclear MCS/PHA ACCUSPEC data acquisition cards. One radioactive 57Co source in a rhodium matrix is used as the source of the 14.4 keV gamma rays used in the Mössbauer experiment, while a second weaker 57Co source in a palladium matrix is used to collect the calibration spectrum at the opposite end of the driving unit. The Mössbauer spectra are collected on the ACCUSPEC data cards and then transferred to the hard-drive memory in the PC at the end of the data acquisition. The spectra are then analyzed using a least-squares minimization Fortran fitting program that fits the Mössbauer absorption spectrum as combinations of single peaks, quadrupole doublets, and magnetic hyperfine sextets. These three

situations cover the entire range of different types of Mössbauer absorptions from iron in solids. A lorentzian peak-shape is assumed in the least-squares fitting and chi-square is used as the significant statistical parameter in determining the goodness of fit.

XAFS spectroscopy is used to investigate other elements in the catalyst formulations. XAFS spectroscopy is performed at beam-line X-18B at the National Synchrotron Light Source (NSLS), Brookhaven National Laboratory. The X-ray absorption spectra are collected over an energy range that includes one of the characteristic absorption edges of the element of interest. The spectrum is collected as a function of energy by means of the rotation of a Si(111) channel-cut crystal from typically about 100 eV below the absorption edge to as much as 1000 eV above the absorption edge. Spectra are recorded in either absorption or fluorescence geometry, depending on the concentration of the element in the catalyst, using gaseous ionization detectors or solid state detectors such as a PIPS detector or a multi-element germanium detector. The spectral data acquired at NSLS are transferred to the University of Kentucky for detailed analysis. Such procedures are well-described in the literature [1]. Basically, the XAFS spectrum is divided into separate X-ray absorption near-edge structure (XANES) and extended X-ray absorption fine structure (EXAFS) regions, each of which provides complementary information.

Results and Discussion

Characterization of alkane dehydrogenation catalysts (in cooperation with Shah, Wang, Ma, and Huffman, University of Kentucky).

This work involves detailed characterization of iron and other elements (Ni, Pd, Mo) in binary Fe-M (M=Ni, Mo, or Pd) catalysts supported on alumina that are highly active for the decomposition of methane, ethane, and propane to produce pure hydrogen and carbon nanotubes. The basic reaction can be represented by:

$$C_nH_{2n+2} \rightarrow nC + (n+1)H_2$$

However, as described elsewhere [2-4], the reaction is not so simple for hydrocarbons other than methane because the reactions appear to be sequential involving hydrocarbon chain breakage and the formation of methane and other intermediary hydrocarbon (both alkane and alkene) formation, prior to ultimately forming hydrogen and carbon nanotubes.

As described in the six-month report for this year and a recent publication [5], the binary Fe-M catalysts are initially precipitated on the alumina support as nanoscale mixed ferrihydrite particles. During pre-reduction in hydrogen at 700 °C, these particles react with the alumina support to form a spinel phase, $(Fe^{2+})(Fe^{3+},Al)2O4$, that evolves increasingly towards hercynite, $Fe^{2+}Al2O4$, and an austenitic Fe-M metallic alloy phase is in particle regions not in contact with the alumina. These austenitic alloy particles, which are bound to the alumina support by hercynite, appear to be the active catalytic phase for decomposition of methane into hydrogen with simultaneous formation of carbon nanotubes and for conversion of ethane and propane into methane, hydrogen, and carbon nanotubes.

Some additional Mössbauer measurements are in progress relating to these measurements; these are designed to examine the effect of temperature on the catalyst phase assemblages.

Characterization of Pt-based catalysts for dehydrogenation of cyclohexane (in cooperation with Wang, Shah, and Huffman, University of Kentucky)

This project was largely completed in the first six-month period of this year and the results were described in our previous six-month report. As described in that report and in a recent

publication [6], the dehydrogenation of cyclohexane (C_6H_{12}) to benzene (C_6H_6) and hydrogen or methylcyclohexane to toluene and hydrogen has potential for on-board production of hydrogen for use in vehicular fuel cells. An XAFS investigation was conducted on Pd and Pt-bearing catalysts used for dehydrogenation of cyclohexane in order to complement a similar investigation carried out in the previous year on iron-based catalysts for the same reaction. With a commercial catalyst consisting of 1% Pt supported on alumina or 0.25% Pt supported on stacked cone nanotubes (SCNT), this reaction goes virtually to completion at temperatures around 300 ºC. Significant differences were observed between Pt/alumina and Pt/SCNT for this reaction in only Pt metal was observed in the former, while the latter involved both PtO2 and Pt metal.

Investigation of metallocenes and metallocene-doped aerogels (in cooperation with Ernst and Eyring, University of Utah).

At the University of Utah, significant effort is being expended in developing new catalysts for Fischer-Tropsch (FT) synthesis based on silica aerogels doped with metallocene compounds. Typical metallocene or "sandwich" compounds that are proposed for such catalysts include not only ferrocene [bis(eta-5-cyclopentadienyl)iron] and cobaltocene, but also closely related analogues in which one or both of the cyclopentadienyl ligands is/are replaced by the more reactive pentadienyl ligand, which thereby lead to facile attachment to the silica via protonation by surface hydroxyl group. The University of Kentucky is providing XAFS and Mössbauer spectroscopic support for the characterization of these compounds and for the proposed aerogel catalysts prepared from them. In the previous six-month report, we described some initial measurements made by XAFS spectroscopy to characterize ferrocene, cobaltocene, and oxidized versions of these compounds. More recently, we have started to examine similar Ru-based catalyst materials submitted by Prof. Ernst and his group at the University of Utah.

Ruthenium K-edge XAFS spectra of the five different Ru-containing materials and metallic Ru foil were obtained at beam-line X-18B at NSLS. The spectra were collected over an energy range from 21,900 eV to 23,100 eV in fluorescence geometry at room temperature using a PIPS detector. The XANES data derived from the XAFS spectral data are shown in Figure 1. The Ru XANES spectra readily distinguish the different types of ruthenium compound that have been used to modify the aerogels. In addition, the Ru XANES data demonstrate that the ruthenium compounds are little changed by their incorporation into the silica aerogel. The RuO_x-doped aerogel exhibits a Ru XANES spectrum similar to that of RuO2; the RuCp2-doped aerogel XANES spectrum is similar to that of RuCp2. This suggests that the incorporation of ruthenium compounds into the aerogels is basically a physical process rather than a chemical process.

In addition to the Ru K-edge data, some preliminary data were also obtained at the Ru LIII absorption edge at about 2,838 eV, over the energy interval from 2,720 eV to 3,038 eV. This edge was accessible on beam-line X-19A, which is designed to be a soft X-ray beam-line over the energy range from 2 to 6 keV. As can be seen by the two Ru L-edge XANES spectra shown in Figure 2, the Ru LIII-edge data are very sharp. Unfortunately, time only permitted us to obtain the two spectra shown.

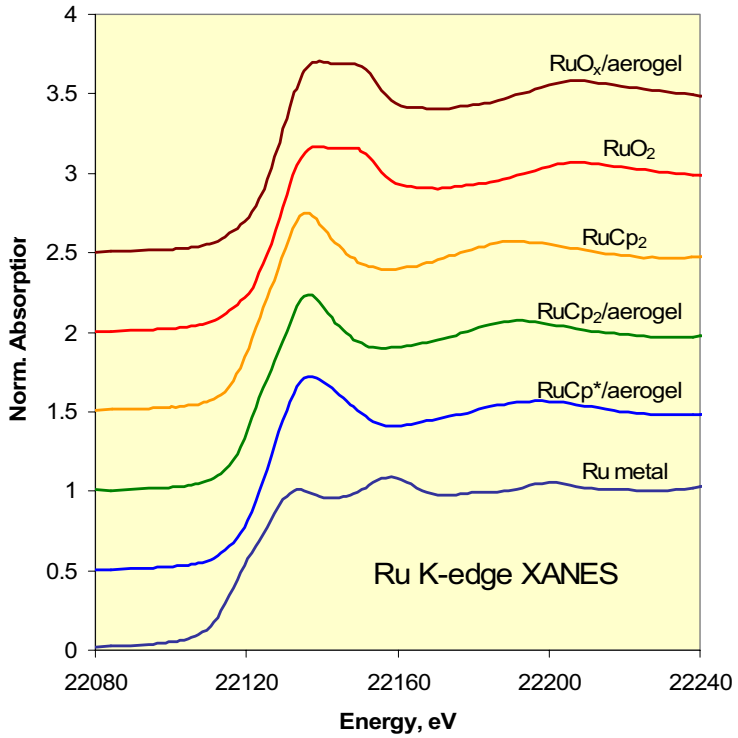

Figure 1: Ruthenium K-edge XANES spectra of three Ru compounds and three Ru compound doped silica aerogel catalysts from Ernst et al., University of Utah.

Further work remains to be done on these catalytic materials. The extended X-ray absorption fine structure (EXAFS) regions of the Ru K-edge XAFS spectra need to be examined and analyzed and additional XAFS data need to be obtained at the Ru LIII-edge. The superior sharpness and resolution of features at the LIII-absorption edge may provide more subtle differences between the bulk and aerogel-doped versions of the same compound than the corresponding K-edge spectra.

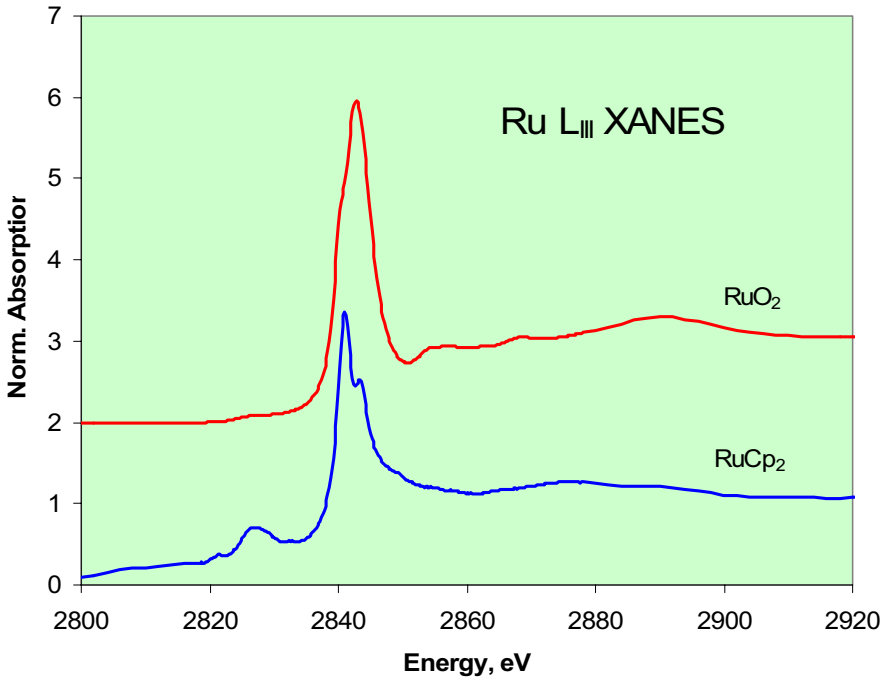

Figure 2: Ru L-edge XANES data for two Ru compounds, RuO2 and Ru(Cp)2.

Development of silica-based aerogel F-T catalysts that incorporate Fe or Co (in cooperation with Eyring and Kim, University of Utah)

Also under development at the University of Utah are catalysts based on mesoporous silica-based aerogels (SBA) doped with Fe or Co ions. As discussed elsewhere in this report, these catalysts have potential for use as Fischer-Tropsch (F-T) catalysts. In this study, two different batches of samples were submitted for Mössbauer and XAFS analyses. The first batch consisted of six samples, as described in Table 1. SBA-15 is a mesoporous silica aerogel, whereas Al-SBA-15 is a similar mesoporous material in which a small amount of Al is substituted for Si. In this latter material, the Si/Al ratio is 60/1. Small amounts of potassium, amounting to 0.5 wt%, are also incorporated in some of the materials. In one instance, the amount of potassium was 3.0%.

Table 1: Composition of Fe-substituted mesoporous silicas.

Identification	%Fe, form	%K, form	Support
Utah 1	20 Fe3+ nitrate	--	100SBA-15
Utah 2	20 Fe3+ nitrate	--	100Al-SBA-15
Utah 3	20 Fe3+ nitrate	0.5 KCl	100SBA-15
Utah 4	20 Fe3+ nitrate	0.5 K2CO3	100SBA-15
Utah 5	20 Fe3+ nitrate	3.0 K2CO3	100SBA-15
Utah 6	20 Fe3+ nitrate	0.5 K2CO3	100Al-SBA-15

Full details of the preparation of these materials are presented elsewhere in this report (q.v. Report by Eyring and Kim). Basically, the SBA substrates are impregnated with ethanol solutions containing the desired amounts of potassium and/or ferric nitrate. The impregnated materials are dried at 100 ºC for 12h, and then calcined in air at 400 ºC for 12 h.

Representative Mössbauer spectra of these materials are shown in Figure 3 and data from all six samples are summarized in Table 2. The spectra appear to consist of two components: a central doublet that can be attributed to ferrihydrite, a non-crystalline iron oxyhydroxide phase, and a magnetic sextet phase, that derives from hematite, a-Fe2O3. In certain formulations, the magnetic component is not present and all of the iron is present as ferrihydrite. Both absorptions typically have to be fit with multiple components in order for the least-squares fitting function to adequately approximate the data. For instance, for the spectrum of Sample 4 shown in Figure 3,

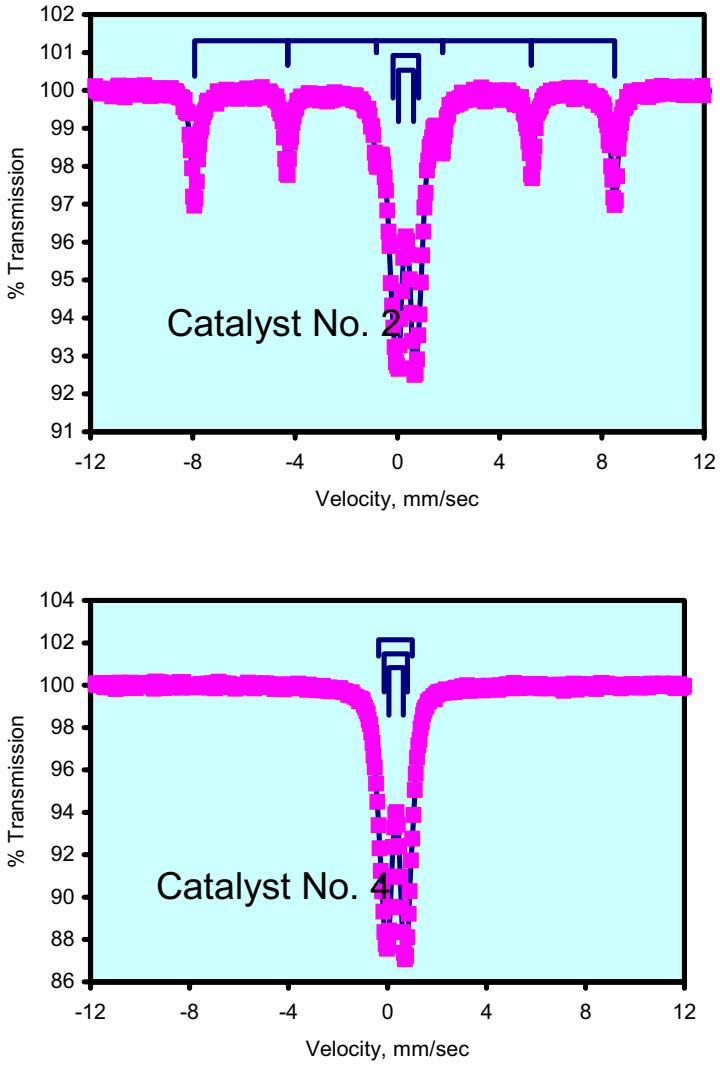

Figure 3: Mössbauer spectra of two Fe-rich catalysts loaded onto mesoporous silica (SBA-15). The spectrum for Catalyst No. 2 contains hematite in addition to ferrihydrite, which is the only phase present in Catalyst No. 4.

the ferrihydrite component has been fit with three separate quadrupole components in order to adequately account for the broadness of the Mössbauer absorption that arises from the lack of order in the ferrihydrite structure that gives rise to a continuous variation in site geometry for the iron atom. Similarly, substitution of Al for Fe in the hematite structure also requires that the spectral features for hematite be least-squares fit by multiple sextets.

The Fe XANES spectra of the same catalysts (Figure 4) look very similar and are typical of ferric oxides or oxyhydroxides; however, subtle differences are apparent as, for example, indicated in Figure 5. In this figure, the pre-edge peak at about 2.5 eV becomes sharper and a little more intense in the order: 1, 2, 6 < 3 < 4 < 5. Typically, such a trend reflects increasing fractions of the iron on tetrahedral sites in the oxide/oxyhydroxide structure or decreasing long-range order. The EXAFS/RSFs shown in Figure 6 reflect the local structure around the Fe atoms in the catalysts. In this figure, the peak at about 1.57 Å represents the nearest neighbor shell of oxygen anions that surround the Fe3+ cation in the oxide/oxyhydroxide structure while the second peak at about 2.75 – 2.85 Å represents the next nearest shell of atoms that coordinate the iron. In all iron oxide or oxyhydroxide structures, the second nearest shell of atoms is invariably other Fe atoms.

Table 2: Tabulation of Results from Mössbauer Experiments

Sample ID	Comp.	IS mm/s	QS mm/s	H0 kGauss	Width mm/s	%Fe	I.D.
Catalyst #1	1 QS	0.34	0.59		0.37	31	Ferrihydrite
20Fe/100 SBA-15	2 QS	0.33	1.01		0.47	33	Ferrihydrite
No K	1H0	0.38	-0.09	508	0.34	36	Hematite
Catalyst #2	1 QS	0.34	0.62		0.38	26	Ferrihydrite
20Fe/Al-SBA-15	2 QS	0.33	1.05		0.43	20	Ferrihydrite
No K	1 H0	0.39	-0.08	507	0.32	47	Hematite
	2 H0	0.46	-0.14	492	0.32	7	Hematite
Catalyst #3	1 QS	0.34	0.56		0.37	47.5	Ferrihydrite
20Fe/0.5K/100 SBA-15	2 QS	0.33	0.94		0.37	37	Ferrihydrite
K as KCl	3 QS	0.32	1.38		0.37	11	Ferrihydrite
	1 H0	0.4	-0.11	507	0.34	4.5	Hematite
Catalyst #4	1 QS	0.35	0.58		0.37	47.5	Ferrihydrite
20Fe/0.5K/100 SBA-15	2 QS	0.33	0.94		0.37	37	Ferrihydrite
K as carbonate	3 QS	0.33	1.36		0.37	15	Ferrihydrite
Catalyst #5	1 QS	0.34	0.59		0.36	45.5	Ferrihydrite
20Fe/3K/100 SBA-15	2 QS	0.33	0.96		0.36	39.5	Ferrihydrite
K as carbonate	3 QS	0.32	1.37		0.36	15	Ferrihydrite
Catalyst #5*	1 QS	0.33	0.60		0.37	46.5	Ferrihydrite
20Fe/3K/100 SBA-15	2 QS	0.31	0.98		0.37	40.5	Ferrihydrite
K as carbonate	3 QS	0.32	1.40		0.37	13	Ferrihydrite
Catalyst #6	1 QS	0.35	0.58		0.37	37	Ferrihydrite
20Fe/0.5K/100Al-	2 QS	0.34	0.95		0.37	30	Ferrihydrite

SBA-15							
K as carbonate	3 QS	0.33	1.38		0.37	10	Ferrihydrite
	1 H0	0.39	-0.07	505	0.33	18.5	Hematite
	2 H0	0.37	-0.1	489	0.33	4.5	Hematite

*Repeat spectrum run at a reduced velocity setting for better resolution. However, the fit is virtually identical to that obtained at larger velocity setting.

It should be noted that the second peak occurs at about 2.75 Å for samples 1, 2, and 6 and at a somewhat longer distance for samples 3, 4, and 5, ~2.85 Å. These two sets of samples correspond to the set of three samples with most hematite and the set of samples with no or very minor hematite, respectively. There is virtually no difference in the intensity of the peak at 1.57 Å exhibited by the six samples; however, the peak at about 2.8 Å exhibits significant variation in intensity, decreasing in the order: 2 > 1 > 6 > 3 > 4 > 5. In both hematite and ferrihydrite, the ferric ion is coordinated by six oxygen anions, and hence, the intensity of the peak at 1.57 Å does not vary significantly. The variation in the peak at about 2.8 Å can be attributed to the hematite/ferrihydrite ratio and to decreasing order in the ferrihydrite structure. The combination of these two factors causes the systematic variation in the height and position of this peak.

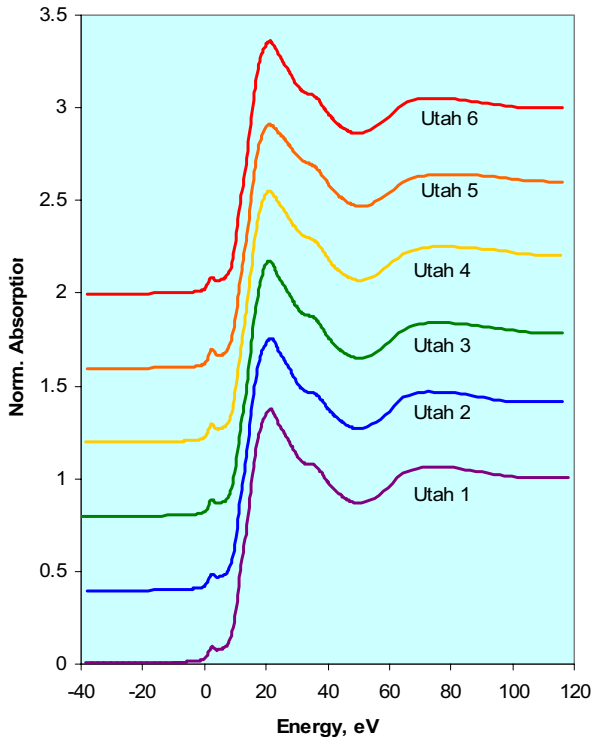

Figure 4: Fe XANES spectra of six 20Fe/xK/SBA Catalysts

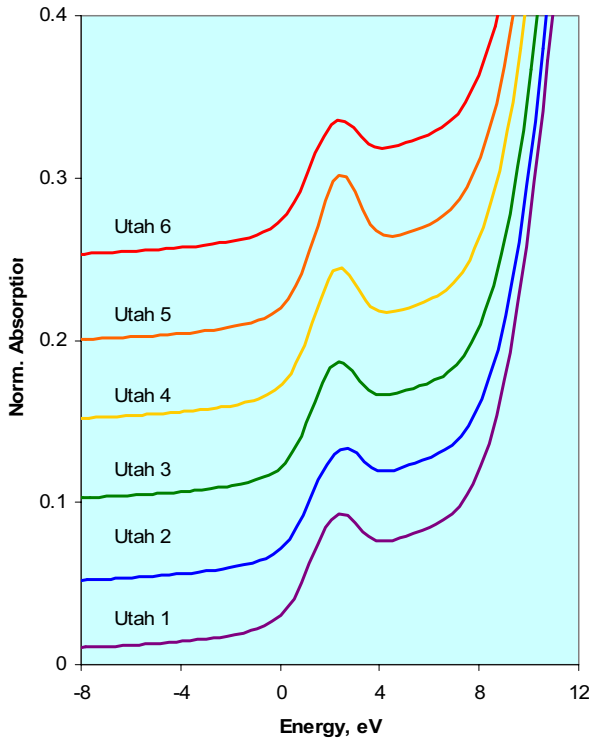

Figure 5: Expansion of pre-edge Fe XANES peak for the six catalyst samples

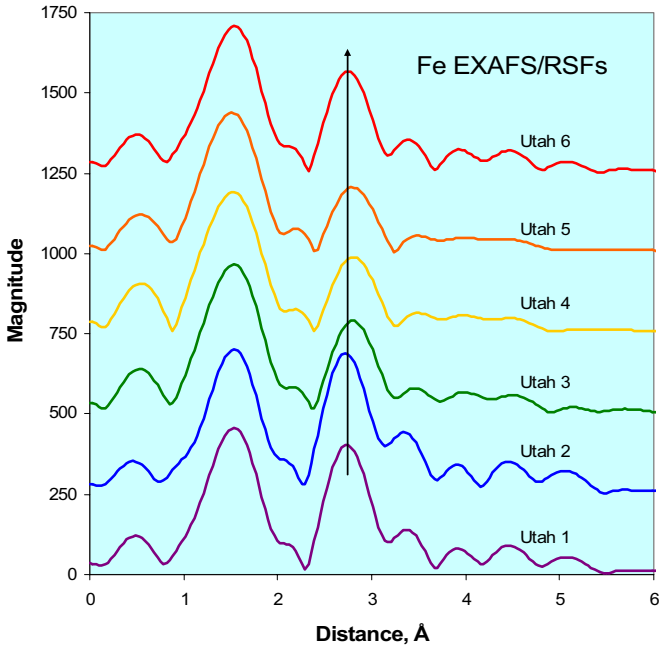

Figure 6: EXAFS/RSFs of the six Utah catalyst samples. The arrow shows the location of the next-nearest neighbor peak in the RSF of hematite. It should be noted that this peak is slightly displaced for Catalysts Nos. 3, 4, and 5, which contain the most ferrihydrite.

Table 3: Data used to construct Figure 7

Sample	Wt %K, form	EXAFS/RSF Peak @ 1.6 Å	EXAFS/RSF Peak @ 2.8 Å	Ratio	Mössbauer %Fe as Hematite
Utah 1	0	4.57	4.04	0.88	36
Utah 2	0	4.52	4.40	0.97	56
Utah 3	0.5, KCl	4.65	2.90	0.62	4.5
Utah 4	0.5, K2CO3	4.41	2.39	0.54	0
Utah 5	3.0, K2CO3	4.39	2.05	0.47	0
Utah 6	0.5, K2CO3	4.51	3.17	0.70	23

As documented in Tables 2 and 3, the six samples show a clear variation in the amount of hematite relative to ferrihydrite and presumably this must be attributed to the presence of potassium in the formulation or variation in the support material. Both the XAFS and Mössbauer spectroscopic data show a correlative trend when the fraction of Fe as hematite derived from the Mössbauer data is plotted against the ratio of the heights of the two major peaks in the EXAFS/RSF plot (Figure 6). The data summarized in Table 3 were used to document this trend, shown in Figure 7. Based on this plot, it would appear that the presence of K in the catalyst formulation has two effects: (i) it enhances the presence of ferrihydrite relative to hematite and (ii) it promotes smaller particles of ferrihydrite. It should be noted that particle size is also important for determining the relative presence of hematite and ferrihydrite [7]; hence, promotion of small particle sizes of ferrihydrite may be the single, most fundamental role of potassium in this formulation.

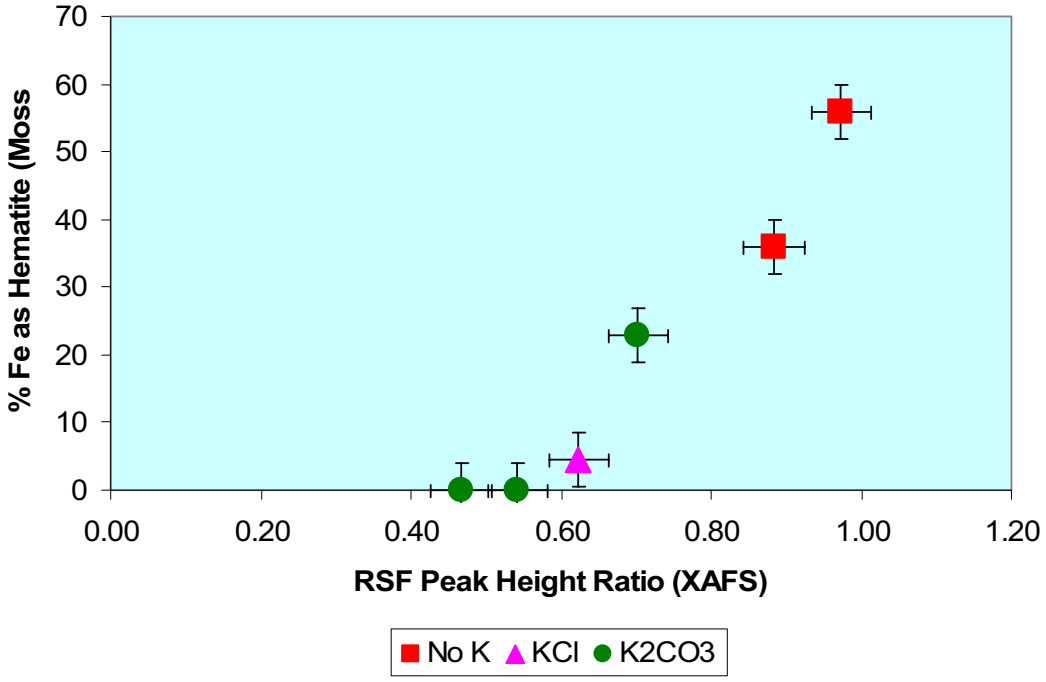

Figure 7: Correlation of %Fe as hematite (from Mössbauer spectroscopy) vs. ratio of EXAFS/RSF peak height (from Fe XAFS spectroscopy).

It would also appear that the presence of Al in the support may have a smaller, opposing effect and promotes the formation of hematite relative to ferrihydrite. It is well-known that Al will substitute readily for Fe^{3+} in most iron oxides, especially hematite. Potassium is usually not incorporated significantly into iron oxides; however, it may be more amenable to incorporation in the less ordered ferrihydrite phase, thereby promoting the formation of this phase.
Most recently, similar catalyst materials, but incorporating Co, have been received from Kim and Eyring (University of Utah). These catalysts were subjected to Co XAFS spectroscopy at beam-line X-18B at NSLS in late October and will be analyzed in the next few months.

Fe, Mo-based water-gas-shift (WGS) catalysts (in cooperation with Dadyburjor, et al., West Virginia University)
Characterization of some novel iron-based catalysts promoted with Mo and supported on alumina, which are under development at West Virginia University for F-T synthesis and water-gas-shift (WGS) applications, has commenced using the spectroscopic and microscopic techniques available at the University of Kentucky. Only a few initial measurements have been made to date using iron Mössbauer spectroscopy and Mo XAFS spectroscopy. The first Mössbauer spectra obtained showed that the catalysts consist of a mixture of iron carbides. Analyses of the Fe Mössbauer and Mo XAFS spectra are in progress and will be complemented by electron microscopy measurements to be made at the University of Kentucky.

Fe, Cr, K-based high temperature water-gas-shift (WGS) catalysts (in cooperation with Huffman, Shah et al., University of Kentucky).
As part of a new investigation into catalysis of the water-gas-shift (WGS) reaction and its potential for producing hydrogen, some basic determinations of high-temperature shift (HTS) catalysts are being made. An iron-based, Cr- and K-promoted catalyst obtained from a commercial vendor has been subjected to iron Mössbauer spectroscopy and Cr K-edge XAFS spectroscopy. The Mössbauer spectrum shows that the catalyst consists of substituted hematite, presumably (Fe,Cr)2O3, whereas the Cr XAFS spectrum showed, somewhat surprisingly, the presence of Cr(VI) species, in addition to Cr2O3 (Figure 8).

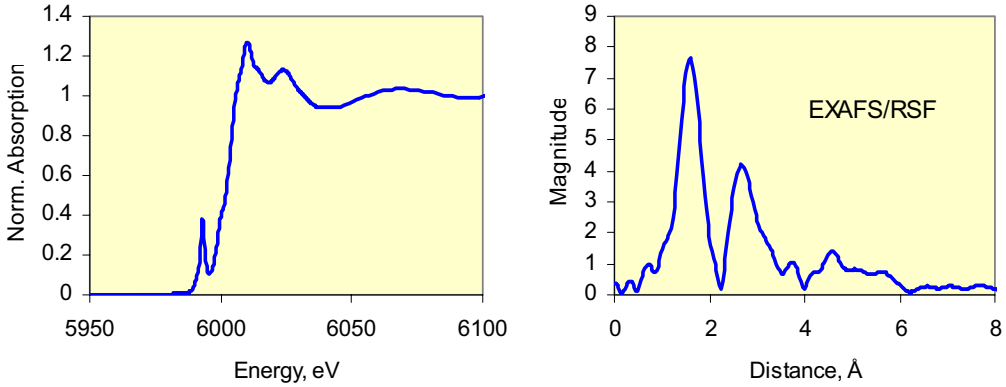

Figure 8: Cr XANES and EXAFS/RSF plots for commercial HTS catalyst. Note the sharp peak at about 5,993 eV indicating the significant presence (~30%) of hexavalent chromium.

Conclusions

Mössbauer and XAFS spectroscopic methods have been used successfully to characterize key elements present in various catalyst formulations under development by Consortium researchers for use in C1 or hydrogen-related reactions.
Mössbauer investigation of binary Fe-M (M = Mo, Ni, and Pd) supported on alumina used in the dehydrogenation of gaseous alkanes implies that austenitic Fe-M-C alloy particles bound to the alumina support by hercynite ($FeAl_2O_4$), are the active phase, whereas formation of cementite (Fe_3C) and other metal carbide phases appear to be associated with catalyst deactivation.
Pt XAFS spectroscopy shows that the Pt speciation is quite different in Pt/Al_2O3 catalysts than in catalysts prepared with Pt supported on stacked-cone carbon nanotubes, despite the observation that both types of catalyst are equally effective in converting cyclohexane to benzene. In the former case, the Pt is essentially all metallic, whereas in the latter case both metallic Pt and Pt oxide are observed.
Six iron containing silica aerogel (SA) catalyst samples prepared by Kim and Eyring at the University of Utah have been examined by iron XAFS and Mössbauer spectroscopies. The iron in the samples is present as a mixture of hematite and ferrihydrite; these two phases vary systematically with the potassium content and the nature of the support in the formulations of the catalysts. The presence of potassium appears to enhance the formation of ferrihydrite relative to hematite (assuming the synthesis of all six materials were otherwise identical), whereas the presence of Al in the SA support material stabilizes hematite.

We anticipate also, based on preliminary measurements reported here, that both Mössbauer and XAFS spectroscopies will be valuable for understanding the chemistry and activity of other novel catalyst systems that are under investigation by the Consortium. Such catalysts include iron, cobalt and ruthenium-containing pentadienyl or cyclopentadienyl compounds placed inside silica aerogels.

Mössbauer and XAFS spectroscopy spectra obtained from Fe, Cr, K-based high temperature water-gas-shift (WGS) catalysts prior to reaction have established that it consists of substituted hematite, presumably $(Fe,Cr)_2O_3$. Surprisingly, the Cr XAFS spectrum showed the presence of Cr(VI) species, in addition to Cr_2O_3.

Papers presented or published (include submitted and in-press papers)

Much of the work reported in this project will be incorporated in papers that describe the reactivity and preparation of the catalysts. Two recent publications are listed below:

1. N. Shah, S. Pattanaik, F. E. Huggins, D. Panjala, G. P. Huffman, XAFS and Mössbauer spectroscopy characterization of supported binary catalysts for nonoxidative dehydrogenation of methane. Fuel Process. Technol. 83, 163-173, (2003).
2. Artur Braun, J. Ilavsky, P.E. Jemian, B. Dunn, E.M. Eyring, F.E. Huggins, G.P. Huffman, Ultra-small angle X-ray scattering of cobalt-doped silica aerogels. J. Appl. Cryst. (2004) in press.

Although not discussed in this report, our group has also conducted extensive high resolution transmission electron microscopy (HRTEM) studies of a number of catalysts prepared by CFFS scientists. Some of this work has been summarized briefly in other project reports included in this annual report (see reports by Seehra et al., West Virginia University and Dunn et al., University of Utah). More detailed summaries of our HRTEM work are included in a number of recent CFFS publications, which are listed below.

3. Alex Punnoose, T. Phanthavady, M. S. Seehra, N. Shah and G. P. Huffman: Magnetic properties of ferrihydrite nanoparticles doped with Ni, Mo and Ir, Physical Review B. 69, 054425 (9 pages), (2004)
4. Alex Punnoose, T. Phanthavady, M.S. Seehra, N. Shah, and G.P. Huffman, "Magnetic properties of ferrihydrite nanoparticles doped with Ni, Mo, and Ir", Phys. Rev. B, 69 (2004), 054425-054434.
5. P. Dutta, A. Manivannan, M. S. Seehra, N. Shah and G. P. Huffman: "Magnetic properties of nearly defect-free maghemite nanocrystals", Physical Review B, in press.
6. Brian C. Dunn, D. J. Covington, P. Cole, R.J. Pugmire, H.L.C. Meuzelaar, R.D. Ernst, E.C. Heider, E. M. Eyring, N.Shah, G.P. Huffman, M. S. Seehra, A. Manivannan, and P. Dutta: Silica Xerogel Supported Cobalt Metal Fischer-Tropsch Catalysts for Syngas to Diesel Range Fuel Conversion, Energy & Fuels, 18, 1519-1521, (2004).
7. Brian C. Dunn, Daniel J. Covington, Paul Cole, Ronald J. Pugmire, Henk L.C. Meuzelaar, Richard D. Ernst, Emily C. Heider, Edward M. Eyring, Naresh Shah, Gerald P. Huffman, M.S. Seehra, A. Manivannan, and P. Dutta, "Silica xerogel supported cobalt metal Fischer-Tropsch catalysts for syngas to diesel range fuel conversion", Energy & Fuels (2004) in press.
8. Brian C. Dunn, Daniel J. Covington, Paul Cole, Ronald J. Pugmire, Henk L.C. Meuzelaar, Richard D. Ernst, Emily C. Heider, Edward M. Eyring, Naresh Shah, and Gerald P. Huffman, "Silica aerogel supported cobalt metal Fischer-Tropsch synthesis", Applied Catalysis A (2004) in press.

Future Work

Similar studies will continue. To complement the investigation of binary ferrihydrite catalysts for alkane dehydrogenation as a function of time-on-stream, a suite of catalysts has been prepared at various temperatures between 525 and 700 ºC after a constant time of 10 hours on stream. These catalysts are currently in the process of being examined by iron Mössbauer spectroscopy. Both XAFS and Mössbauer spectroscopy will continue to be used for characterization of the novel metallocene/aerogel catalysts and the metal–impregnated silica-based aerogel catalysts under development at the University of Utah and of the water-gas-shift catalysts under investigation at West Virginia University. In addition, research at the University of Kentucky will be undertaken to investigate the reactions and modifications of the commercial Fe-Cr-K high-temperature shift catalysts after the WGS reaction. In particular, it is important to establish what happens to the recently discovered Cr(VI) component, which is known to be toxic and carcinogenic to humans.

References

[1] D.C. Koningsberger, R. Prins, (eds.), X-ray Absorption. Principles, Applications, Techniques of EXAFS, SEXAFS, and XANES, J. Wiley & Sons, New York, 1988.
[2] N. Shah, D. Panjala, G.P. Huffman, Hydrogen production by catalytic decomposition of methane. Energy & Fuels, 15, 1528-1534, (2001).
[3] N. Shah, Y. Wang, D. Panjala, G.P. Huffman, Production of hydrogen and carbon nanostructures by non-oxidative catalytic dehydrogenation of ethane and propane. Energy & Fuels, 18 (2004) 727-736.
[4] Y. Wang, N. Shah, G.P. Huffman, Hydrogen production by decomposition of propane and cyclohexane over alumina supported binary catalysts. Catalysis Today (2004) in press.

[5] N. Shah, S. Pattanaik, FE. Huggins, D. Panjala, G.P. Huffman, XAFS and Mössbauer spectroscopy characterization of supported binary catalysts for nonoxidative dehydrogenation of methane. Fuel Process. Technol. 83 (2003) 163-173.
[6] Y. Wang, N. Shah, G.P. Huffman, Pure hydrogen production by partial dehydrogenation of cyclohexane and methylcyclohexane over nanotube supported Pt and Pd catalysts. Energy & Fuels (2004) in press.
[7] Z. Feng, J. Zhao, F. E. Huggins, and G. P. Huffman, Agglomeration and phase transition of a nanophase iron oxide catalyst. J. Catalysis, 143, 510-519, (1993).

Science behind Catalysis in C1 Reactions: Catalyst characterization and determination of Active Species

M. S. Seehra, P. Dutta and A. Manivannan, Physics Department, West Virginia University

Introduction

The objectives of this task are to investigate the structural and electronic properties of catalysts in C1 reactions in order to determine the active species. These catalysts are used by the CFFS researchers in this program to convert C-1 feedstocks into clean liquid transportation fuels and high-value chemicals, and for the efficient production and storage of hydrogen obtained from syngas, hydrocarbons and coals. The catalysts investigated during the past year include the following: Co/SiO_2 and Co/Al_2O_3 used by Roberts et al (Auburn); Co/aerogel and Co/xerogel used by Eyring et al (Utah); Fe-based catalysts (ferrihydrites and maghemites) supplied by Huffman et al (Kentucky) and prepared in our laboratory; and NiO nanoparticles prepared in our laboratory.

Experimental Procedure

For structural investigations of the catalysts, techniques of X-ray diffraction (XRD), FTIR/Photoacoustic spectroscopy and Transmission electron microscopy (TEM) were employed. The electronic states of Co, Fe and Ni in these catalysts were determined from the temperature and magnetic field variations of the magnetization and electron magnetic resonance (EMR) spectra. Theoretical interpretations of these data are essential to determine the nature of the electronic states. The obtained results are then correlated with the yields and distributions of the products in the actual experiments to determine the mechanism of catalysis.

Results and Discussion

Characterization of Co/SiO_2 and Co/Al_2O_3 Catalysts:

The characterizations of the samples of different Co/SiO_2 and Co/Al_2O_3 catalysts, prepared and supplied by Professor Roberts group at Auburn, were one of the major tasks for us during the past year. Results of our studies on the as-prepared and calcined catalysts have been accepted for publication in Catalysis Letters [1]. A follow-up paper on similar studies on these catalysts used in conventional gas-phase (GP) and supercritical hexane phase (SCH) Fischer-Tropsch synthesis (FTS) has been recently completed [2]. These studies are built upon similar work during 2002-2003 on the characterization of Ni/SAPO catalysts prepared by Guin et al (Auburn) for the conversion of methanol to olefins [3, 4]. The goal of our studies was to determine the different states of cobalt (Co0, CoO, Co_3O_4, Co^{2+}, Co^{3+}) in the as prepared, calcined and used catalysts. This allowed us to determine the nature of transformations occurring in the catalysts under calcinations and FT synthesis and then correlate these changes with product selectivities and yields. Since details of these studies will appear in publications soon [1, 2], only a brief summary of the results is given here (see Table 1, Fig. 1 and Fig. 2.).

In the as-prepared catalysts of Co/SiO_2, Co was found to be present as Co^{2+} and Co^{3+} species but not in its usual crystalline forms as Co0, CoO or Co_3O_4. Upon calcinations, the Co^{2+} - Co^{3+} species transformed to crystalline Co_3O_4. Under conventional GP-FTS, Co_3O_4 in sample S1 completely transformed to nanocrystalline Co0 whereas under SCH-FT reaction, in sample S2 Co^0 and some CoO are detected (Table 1). Magnetic experiments showed that Co^0/CoO phase is a composite rather than individual particles indicating that reduction of $Co_3O_4 \rightarrow CoO \rightarrow Co^0$ is not complete.

For the Co/Al_2O_3 catalysts, the reduced but unused catalysts contained primarily Co_3O_4. When this sample is used in the SCH-FTS reaction for 10 days, Co_3O_4 was found transformed to CoO and hcp Co^0, indicating partial reduction of the catalyst. However, when the same catalyst is used in SCH-FTS at the higher temperature of 260 ºC (for seven days), both hexagonal-closed-pack (hcp) Co^0 and face-centered-cubic (fcc) Co^0 are detected without any CoO or Co_3O_4 (Fig. 2). This shows that now the reduction to Co^0 is complete. For the GP-FTS, the reduction of Co_3O_4 to Co^0 was also found to be incomplete.

Table I.

Samples	Particle Size of Co0 (nm)	Magnetic Measurement	EMR	XRD
A1 (15%Co/SiO_2) Fresh	--	paramagnet Co^{2+}	Co^{2+} line	SiO_2
B1(15%Co/SiO_2) Fresh	--	paramagnet Co2+	Co^{2+} line	SiO_2
A1 (Calcined)	--	Co_3O_4	No Co^{2+} line	SiO_2, Co_3O_4
B1 (Calcined)	--	Co_3O_4	Co^{2+} line	SiO_2, Co_3O_4
C1(15%Co/Al_2O_3) Calcined	--	Co_3O_4	Co^{2+} line	Co_3O_4, δ-Al_2O_3
S1 (HSA 15%Co/SiO_2) Used 10 days (GP)	≈ 1	Co0	Co^0 line	SiO_2(quartz, cristobalite, tridymite)
S2 (LSA 15%Co/SiO_2) Used 13 days (SCH)	≈ 11	Co0/CoO	broad Co^0 line	fcc-Co0, CoO, SiO_2 (cristobalite)
A1 (15%Co/Al_2O_3) Used 10 days (SCH)	> 12	Co0/CoO, Co0/Co_3O_4	Co^0 and Co^{2+} lines	hcp-Co^0, CoO, Co_3O_4; γ-Al_2O_3, ε -Al_2O_3
A2 (15%Co/Al_2O_3) Used 7 days	≈ 13	Co0	Co^0 line	hcp-Co^0, fcc-Co^0; γ - Al_2O_3
A3 (15%Co/Al_2O_3) Unused, reduced catalyst	> 12	Co_3O_4	Co^0 and Co^{2+} lines	Co_3O_4;γ- Al_2O_3 ε-Al_2O_3 CoO, hcp Co^0

Comparing the selectivity and yield of the products in the FT reaction for the different catalysts, the following conclusions were reached: (i) In the GP-FTS, the presence of Co_3O_4 (incomplete reduction) yielded higher methane selectivity whereas the presence of Co2+ species yielded lower methane selectivity but higher olefin selectivity. Also the Al_2O_3 supported catalysts gave much higher selectivity towards olefins than Co/SiO_2 [1, 2]; (ii) In the SCH-FTS, because of the single phase SCH medium and rather complete reduction of Co_3O_4 to Co0, both the activity and selectivity of the cobalt catalyst was found to be very stable for up to 15 days time-on-stream. Details of these results are given in References 1 and 2.

Characterization of Co/Aerogel and Co/Xerogel Catalysts:

The samples of Co/aerogel catalysts were prepared by Prof. Eyring's group (Utah) for the FT synthesis. Seven Co/xerogel and three Co/aerogel samples were analyzed in this work using X-ray diffraction and magnetic measurements. Results from xerogel samples on the syngas to diesel-range fuel conversion have recently appeared in print [5]. In contrast to the Auburn samples of Co/SiO_2 and Co/Al_2O_3 which contained Co_3O_4 in the calcined samples, samples of Co/aerogel and Co/xerogel contained CoO and Co^0. However, in the FT reaction, reduction of CoO to Co0 was found to be quite incomplete since the used samples all contained Co2+ ions as detected by EMR spectroscopy. This line is definitely due to Co2+ in cubic symmetry and not due to either CoO or Co0. This incomplete reduction of CoO to Co0 in these catalysts is most likely the cause of the lack of optimum conversion [5]. For more details, see Ref. 5 and its attached supporting materials.

Other Projects:

Our group has been involved in the synthesis of the nanoparticles of the oxides of Fe, Co and Ni and in the characterization of their structural and electronic properties. The motivation for these studies is that these materials are precursors to the catalysts for energy conversion processes and hence understanding their properties in nanocrystalline forms is important. In Fig. 3 we show micrographs of NiO nanorods of approx. 5 nm diameter, some properties of which have been reported in two recent papers [6, 7]. Similarly, in Fig 4, we show the TEM micrograph of maghemite (γ-Fe_2O_3) nanoparticles, structural and magnetic properties of which are detailed in a recent paper [8]. Structural and magnetic properties of 5 nm ferrihydite ($FeOOH.nH_2O$) nanoparticles doped with Ni, Mo. Ir and Si have been reported in three recent papers [9,10,11]. Finally, a paper on the reforming of methane to produce synthesis gas using Co-W-C catalysts has been published in collaboration with Professors Kugler and Dadyburjor [12]. Details of these studies are available in cited papers [6-12] and these are omitted here for sake of brevity.

Conclusions

Investigations of Co-based catalysts have clearly shown the need for multi-technique characterization of the catalysts as used in our work. Since Co^0 is the active catalysts in the FT synthesis, its detection by XRD is often difficult if the particle size is less than 5 nm or if the concentration is less than 3%. However, by magnetic measurements, Co^0 as well as CoO and Co_3O_4 are easily detected by their characteristic and different properties even in small quantities. Also, these studies can distinguish whether these phases are separate entities or as composites of Co0/CoO or $Co0/Co_3O_4$.

Our investigations have shown that reduction of CoO and Co_3O_4 to Co0 is often incomplete, thus affecting the synthesis products and their distributions. These correlations have provided considerable insight into the FT synthesis. The close collaborations of our group with other CFFS researchers have been the key to this success.

Our studies of the Co- and Fe-based nanoparticles have shown that their properties are significantly different from those of their bulk counterparts. This is important since most good catalysts are in nanocrystalline form.

Papers Published

1. P. Dutta, N.O. Elbashir, A. Manivannan, M.S. Seehra, and C.B. Roberts: Characterization of Fischer-Tropsch Cobalt-based Catalytic Systems (Co/SiO_2 and Co/Al_2O_3) by X-ray Diffraction and Magnetic Measurements, Catalysis Letters, in press.
2. N.O. Elbashir, P. Dutta, A. Manivannan, M.S. Seehra, and C.B. Roberts: Impact of Cobalt-based Catalyst Characteristics on the Performance of Conventional Gas-Phase and Supercritical-Phase Fischer-Tropsch Synthesis, Applied Catalysis A (to be submitted).
3. D.R. Dubois, D.L. Obrzut, J. Liu, J. Thundimadathil, A. M. Prakash, J.A. Guin, A. Punnoose and M.S. Seehra: Conversion of Methanol to Olefins over Cobalt, Manganese and Nickel Incorporated SAPO-34 Molecular Sieves, *Fuel Processing Technology* 83, 203 -218 (2003).
4. P. Dutta, A. Manivannan, M. S. Seehra, P. M. Adekkanattu, and J. A. Guin: Determination of the electronic state and concentration of nickel in Ni-SAPO catalysts by magnetic measurements, Catalysis Letters, 94 181-185, (2004).
5. B. C. Dunn, D. J. Covington, P. Cole, R.J. Pugmire, H.L.C. Meuzelaar, R.D. Ernst, E.C. Heider, E. M. Eyring, N.Shah, G.P. Huffman, M. S. Seehra, A. Manivannan, and P. Dutta: Silica Xerogel Supported Cobalt Metal Fischer-Tropsch Catalysts for Syngas to Diesel Range Fuel Conversion, Energy & Fuel,18, 1519-1521, (2004).
6. M. S. Seehra, P. Dutta, H. Shim and A. Manivannan: Temperature dependence of electron magnetic resonance and magnetization in NiO nanorods, Solid State Communications, 129, 721-725 (2004).
7. M.S. Seehra, H. Shim, P, Dutta, A. Manivannan and J. Bonevich: Interparticle interaction effects in the magnetic properties of NiO nanorods, Journal of Applied Physics, (accepted).
8. P. Dutta, A. Manivannan, M. S. Seehra, N. Shah and G. P. Huffman: Magnetic properties of nearly defect-free maghemite nanocrystals, Physical Review B, in press.
9. A. Punnoose, T. Phanthavady, M. S. Seehra, N. Shah and G. P. Huffman: Magnetic properties of ferrihydrite nanoparticles doped with Ni, Mo and Ir, Physical Review B. 69, 054425 (9 pages), (2004)
10. M. S. Seehra, P. Roy, A. Raman and A. Manivannan: Structural investigations of synthetic ferrihydrite nanoparticles doped with Si, Solid State Communications, 130, 597-601 (2004).
11. A. Punnoose, M.S. Seehra, J. van Tol and L.C. Brunel: High-frequency electron magnetic resonance and magnetic studies of ferrihydrite nanoparticles and evidence of a phase transition, Journal of Magnetism and Magnetic Materials (in press).
12. M.V. Iyer, L.P. Norcio, A. Punnoose, E.L. Kugler, M.S. Seehra and D.B. Dadyburjor: Catalysis for synthesis gas formation from reforming of methane, Topics in Catalysis, 29, 197-200 (2004).

Future Work

We will continue to investigate the structural/electronic properties of the catalysts prepared/supplied by the CFFS researchers. A detailed paper on the electronic states of cobalt in Co/aerogel and Co/xerogel catalysts is under preparation. We are also working on the reduction kinetics of single phase CoO and Co_3O_4 particles to determine the manner in which each phase individually reduces to Co0 in H_2 environment. In new in-house projects, we have undertaken the studies of Ni nanoparticles prepared by the sol-gel technique in order to determine how their properties change with change in their particle size and degree of dispersion in SiO_2. We have also initiated the studies of light-metal hydrides as potential hydrogen storage materials. Since these hydrides require special handling and this is a new area for us, high quality glove-box facilities are being developed in our laboratory for this purpose. It is expected that during the coming year, we will have a productive research program in this very important area of national interest.

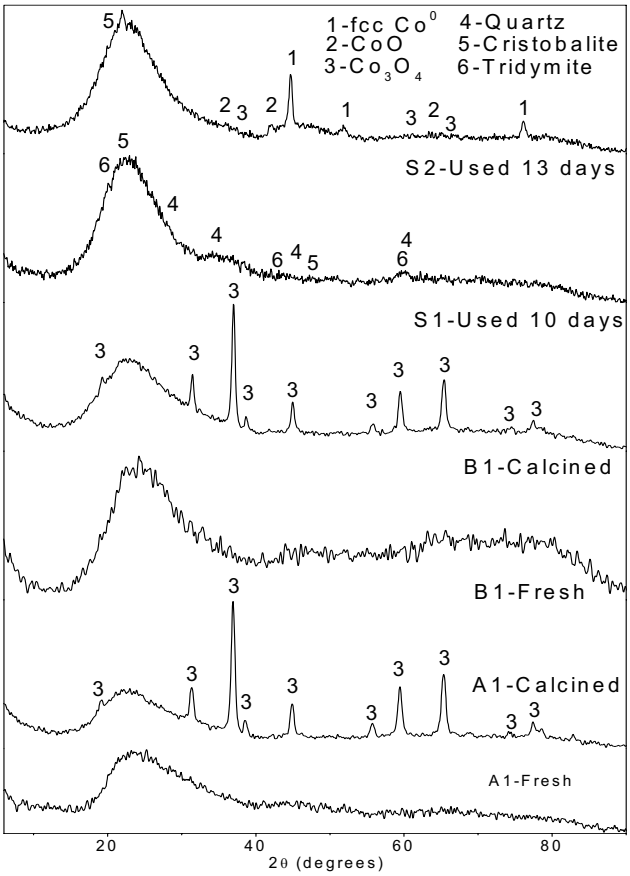

Fig. 1. Room temperature X-ray diffraction patterns of Co/SiO_2 samples of Table 1 (from Refs. 1 and 2). Expected line positions of the various phases are marked.

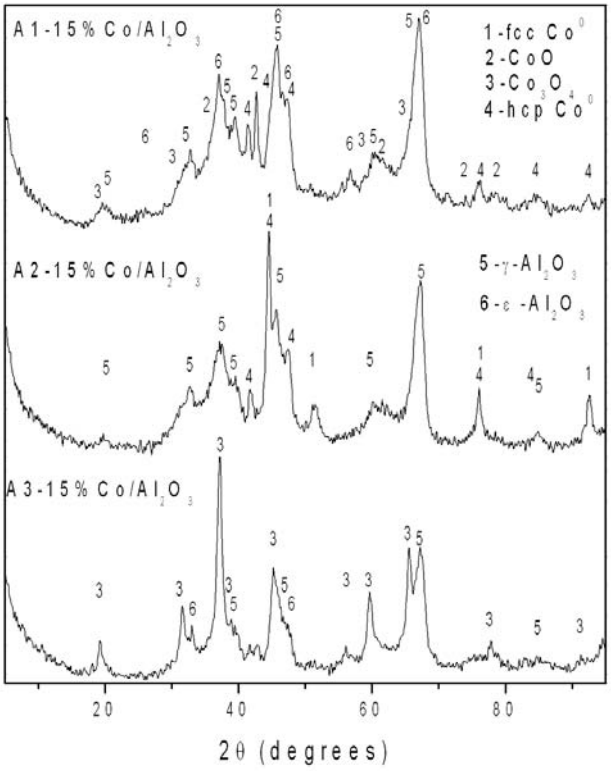

Fig. 2. Room temperature X-ray diffraction pattern of some Co/Al_2O_3 catalysts of Table 1 (from Ref. 2). Expected line positions of the various phases are marked.

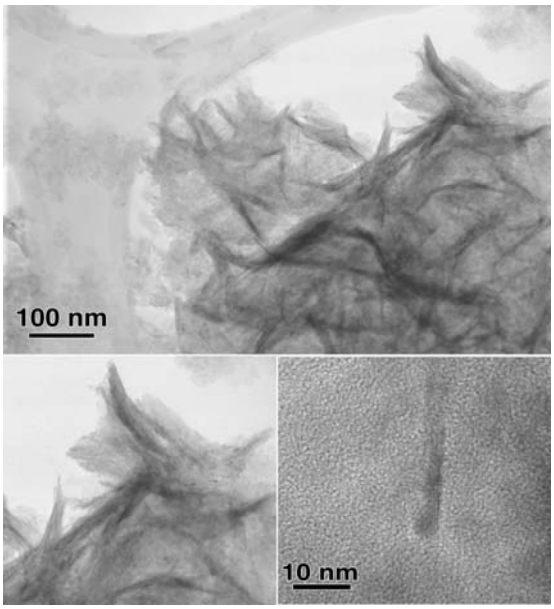

Fig. 3. TEM micrographs of NiO nanorods of diameters ≈ 5 nm (Ref. 7).

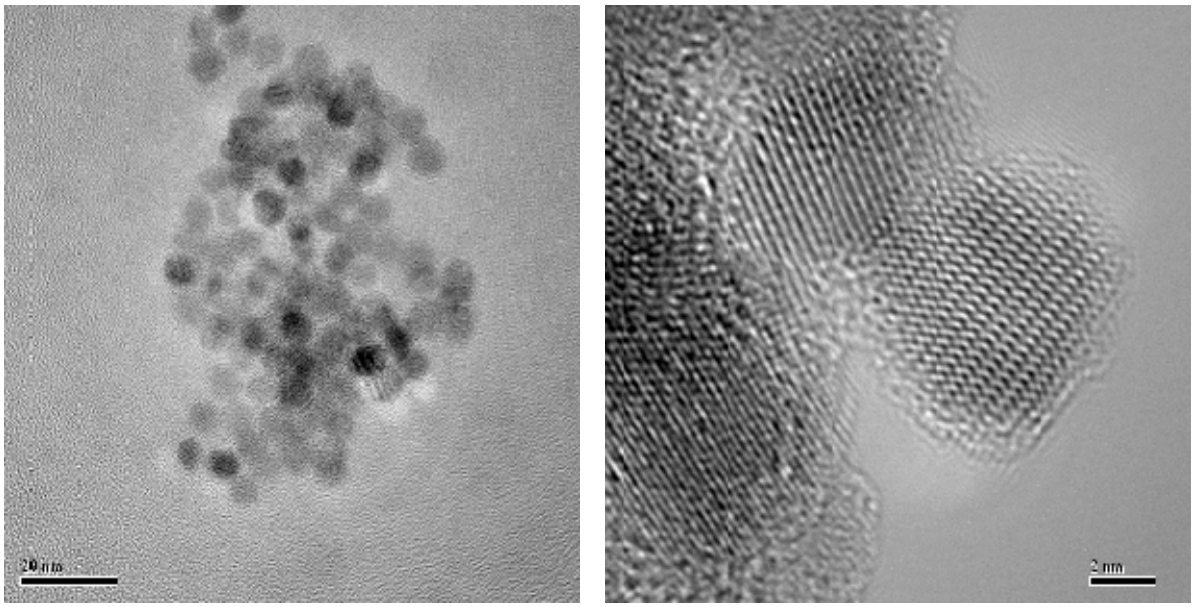

Fig. 4. TEM micrographs of 7 nm nanocrystals of γ-Fe2O3 (Ref. 8). The bar length on the left (right) picture is 20 nm (2 nm).